SMALL SCALE FRACTURE TOUGHNESS TESTING

SMALL SCALE FRACTURE TOUGHNESS TESTING

By

Jon Lereim, Siv.ing

A Thesis

Submitted to the Faculty of Graduate Studies

in Partial Fulfilment of the Requirements

for the Degree

Master of Engineering

McMaster University

April, 1978

ABSTRACT

Small scale tests were utilized in order to obtain characteristic fracture mechanics parameters such as the crack opening displacement (C.O.D.) and the J-integral. Two main types of steels were used (H.S.L.A. and AISI 4340) in obtaining data over a wide range of yield strengths and ductilities. Tests were done to see the effect of both notch geometry and sample geometry in one of the H.S.L.A. steels, and it is verified that the minimum value of C.O.D., at crack initiation in plane strain, is independent of the geometry and plastic zone size. Further the development of a simple single specimen J-integral test method is done during this work. In terms of the data obtained both the minimum C.O.D.$_i$ values and the J_{Ic} values increase with increasing ductility of the materials tested. In the attempt to relate the magnitude of the fracture toughness with microstructural parameters and the limiting processes occuring at the crack tip prior to fracture, the concept of the process zone is discussed. For this study a simple plain carbon steel spheroidized with different carbon contents was examined in addition to the H.S.L.A. and 4340 steels. From the data obtained the minimum C.O.D.$_i$ at crack initiation was found to be approximately equal to the product of the materials plain strain ductility and a characteristic distance scaling with the spacing between large non metallic inclusions or the spacing between the bands of the sulphides.

MASTER OF ENGINEERING (Metallurgy)

McMASTER UNIVERSITY Hamilton, Ontario

TITLE: Small Scale Fracture Toughness Testing

AUTHOR: Jon Lereim, Sivilingeniør (N.T.H., Norway)

SUPERVISOR: Professor J.D. Embury

NUMBER OF PAGES: (xii), 130

ACKNOWLEDGEMENTS

During this study of small scale fracture mechanics testing, I am particularly thankful to my supervisor, Dr. J.D. Embury, for his helpful discussions and guidance. I am also very grateful to Miss Grace Martello for her excellent typing. I would like to thank the technicians who helped me, especially Tom Bryner and Fred Pearson, and also Mr. Mellsop at the Research Center of the Steel Company of Canada.

Further, the author is grateful to N.T.N.F. (Norway) for providing a fellowship (rekrutterings stipend) for parts of this work.

TABLE OF CONTENTS

LIST OF TABLES

LIST OF FIGURES

CHAPTER 1

INTRODUCTION

As a consequence of the development and use of structural materials with higher strength level, the awareness of catastrophic failure and increasing requirements for a safe design, much emphasis has been placed on the development and application of fracture mechanics. In order to determine the intrinsic fracture resistance of a material and its use in the selection of materials and structural design, attention must be given to the load bearing capacity of structures containing flaws.

In the formulation of the stress field around a crack tip or a sharp stress concentrator in the pure elastic case, following Westergaard's analysis (1), a characteristic field parameter K may be defined in terms of the applied stress σ and the crack length a. Thus,

$$K = f(\sigma, a) \tag{1-1}$$

This parameter is included in the expressions for the stress field in the vicinity of a crack tip under different loading conditions, geometries and displacement modes, and represents the intensity of the stress field. The essential point which emerges from linear elastic fracture mechanics, L.E.F.M., is that the fracture resistance can be specified as a critical value of the stress intensity parameter K_c, such that

$$K_c = \sigma\sqrt{\pi a} \tag{1-2}$$

where σ = applied stress, a = flaw size or crack length. If the values of K_c and the applied stress are known, the critical flaw size can readily be calculated, or a suitable combination of the design stress and flaw size can be estimated once K_c is established and considered as a material parameter. However, K_c is dependent on sample geometry up to a certain value of the thickness of the structure or test sample. Above that range, maximum constraint is achieved or plane strain conditions occur at the crack tip. As soon as plane strain conditions are obtained the magnitude of K_c is constant and independent of the specimen size. Therefore, the plane strain stress intensity factor K_{Ic}, which is a lower level of the critical stress intensity factor, will act as a material parameter independent of geometry.

Examining the energetics of the onset of instability at a crack tip prior to crack extension or failure in pure elastic conditions, there is a correlation such as

$$G_{Ic} = \frac{K_{Ic}^{2}(1-\nu^{2})}{E} \qquad (1\text{-}3)$$

where the constant G_{Ic} is the energy release rate or crack driving force in plane strain, E = Young's modulus, ν = Poisson's ratio.

Thus either G_{Ic} or K_{Ic} may be considered as material parameters.

In the original Griffiths analysis is the critical energy release rate equal to the surface energy of an ideal elastic material. However, in metals, the magnitude of the energy release rate is much greater than the surface energy of the material and arises due to the plastic work produced around the crack tip (2)(3). A limiting condition here is that the extent of the plastic flow preceding instability must be much smaller than either the initial crack length, or the thickness of the specimen if this plastic work is to be independent of the sample geometry, and represents a characteristic measure of the fracture resistance. Then the basic linear elastic fracture mechanics may still be valid even for materials which behave in a quasi elastic manner during the fracture testing. On this assumption, the standard K_{Ic} test methods require nearly pure elastic conditions during the testing, where the minimum size limitations are given in terms of the yield stress σ_y and the plane strain stress intensity factor K_{Ic} as

$$B, b, a \geq 2.5 \left(\frac{K_{Ic}}{\sigma_y}\right)^2 \tag{1-4}$$

with B = thickness, b = remained uncracked ligament, a = crack length.

With increasing ratio $(K_{Ic}/\sigma_y)^2$ the minimum size limitations of the test samples and the corresponding testing device increase as in Table (1-I). Thus huge sample size and facilities are needed for examining very tough materials with low or intermediate yield strength. In such cases, the costs will be too high to utilize the standard K_{Ic} testing as a quality control test.

In addition, the sample size may be too large to be representative for the behaviour of the sections actually used in service and also for estimation of the local fracture toughness as in welds and the heat affected zones. Further, the K_{Ic} testing will give a critical parameter prior to crack extension only, and will not be characteristic for any eventual stable crack growth before instability.

There is, consequently, an increasing interest for alternative fracture toughness parameters where the minimum size requirements of of the samples are not so large and which may be easily obtained in laboratory testing. These parameters must be a characteristic measure of the stress and strain field around the crack tip and related directly and quantitatively to the materials fracture toughness, even in cases where considerable amount of plastic yielding may occur.

Data obtained in small scale tests may then represent the corresponding critical values in structures under service conditions.

In the recent literature, three parameters have been suggested which may permit the extension of the concepts of fracture mechanics into the elastic/plastic region, and to cases where general yielding occurs. These parameters are:

1) Critical Crack Opening Displacement (C.O.D.) (4).
2) J-integral (Rice integral) (5).
3) R-curve analysis (6,7).

C.O.D.

It was suggested by several authors, notably by Cottrell and Wells (8)(9), that a critical opening displacement preceding crack extension might be treated as a material parameter under certain defined conditions. For some materials it has been shown that the critical opening displacement at crack initiation from an initially sharp notch or crack, $C.O.D._i$, is a characteristic of the material and is nearly independent of size and geometry of the test samples. However, a minimum sample thickness is required to achieve plane strain conditions which is in accordance with K_{Ic} testing (10). Then the magnitude of the critical $C.O.D._i$ appears to characterize fracture for cases of both localized and general yielding, and several theoretical treatments linking C.O.D.$_i$ to the fracture toughness crack driving force G_c are available (4,9,11,12). All the analyses involve expressions of the form

$$G_c = \sigma \cdot \delta_{crit} \qquad (1\text{-}5)$$

where δ_{crit} is assumed as the critical opening displacement and σ is a characteristic stress for the material. Although there is agreement about the form of expression (1-5), some discrepancy appears concerning the magnitude of the stress σ. In plane strain L.E.F.M., the value of σ is found to be the yield stress of the material, while results from finite element analysis of general yield conditions indicate a value approximately 2x yield stress which is closer to either the U.T.S. or true fracture stress. If the critical C.O.D.$_i$ can be verified as a material parameter, the value obtained in small scale samples may be used as a simple fracture criterion and at least as a comparative fracture toughness parameter for the selection of materials, independent of the exact correlation with the energy release rate.

In order to establish the critical C.O.D.$_i$ as a characteristic of the material and as a quality control parameter, part of the present project has been concerned with an investigation of the influence of sample geometries on the critical C.O.D.$_i$ and factors such as the size of the sample, thickness, width, ratio of notch depth/sample width, notch angle and notch root radius have been considered. In addition, the magnitude of the critical C.O.D.$_i$ can be related to metallurgical factors such as inclusion distribution. Like other mechanical properties of a material, the C.O.D.$_i$ values may depend on content, shape and distribution of inclusions, sample orientation as different yield stress levels, the influence of the factors was considered in the present work.

J-integral

As an alternative fracture criterion, the path independent energy line integral, the J-integral, at crack initiation may be used. The J-integral was first developed by J.R. Rice (5,13), and suggested as a crack initiation criterion in terms of J_{Ic} by Landes and Begley (14).

In any linear elastic behaviour the J-integral may be interpreted as the potential energy difference between two identically loaded bodies having neighbouring crack sizes as (15).

$$J = \frac{1}{B}\frac{\partial U}{\partial a} \qquad (1\text{-}6)$$

where B = thickness of specimen, U = energy and a = crack length.

This expression is equivalent to the energy release rate, i.e.

$$J = G \qquad (1\text{-}7)$$

which is also proposed up to crack initiation in plane strain even when a large amount of plastic deformation occurs in the sample.

Since the plane strain stress intensity factor K_{Ic} is directly related to the energy release rate G_{Ic} as in (1-3), the J-integral may, in theory, be utilized indirectly as a design parameter.

To investigate the use of J_{Ic} as a fracture criterion, any eventual effects of sample size and geometry on the results have been considered in this project, since minimum size requirements can be estimated for standard J_{Ic} testing.

In addition, any correlation between the critical C.O.D.$_i$ and J_{Ic} values, a critical stress, known literature data for K_{Ic}, and toughness in terms of Charpy V-energy are of interest because they permit the correlation of simple small scale laboratory tests and service behaviour.

Test Techniques

The critical C.O.D.$_i$ and J_{Ic} values, which are obtained in small scale tests, may be used as alternative criteria to the standard K_{Ic} if the measurement techniques are relatively simple and the data shows adequate reproducibility and correlation with existing values. There are a number of different techniques of getting the C.O.D. values. Some may have a lack of accuracy, as the paddlemeter by F.M. Burdekin and D.E.W. Stone (4), while others require very sophisticated measuring techniques, eg. laser interferometry, change in electrical potential with crack extension (16)(17).

However, in the literature, two techniques have been described which seem to combine simple testing procedure and acceptable accuracy:

1) Crack profile technique by replicas of silicone rubber (Robinson-Tetelman, 18).
2) Clip gauge displacement (British Draft Standard, 19).

Both techniques have been applied during this work.

In terms of the J-integral testing, no simple technique exists which uses a single specimen test to measure the critical J_{Ic}.

Using a compliance technique, J_{Ic} can be established, but there is a demand for several specimens containing cracks of various lengths.

The method developed by J.R. Rice et. al (20) for measuring J on deeply notched bend type specimen appeared to simplify the test procedures considerably and the result can be expressed as:

$$J = \frac{2U}{Bb} \tag{1-8}$$

where U = area under the load/load point displacement curve up to crack initiation, B = specimen thickness, b = heigh of remained uncracked ligament.

In principle, J_{Ic} can be determined from a single specimen if U, the work done up to crack initiation is measured.

Expression (1-8) was utilized by J.D. Landes and J.A. Begley (21) for determination of J_{Ic} from a J vs. crack extension curve. Still, this method requires at least 4 specimens in obtaining J_{Ic}.

A single specimen procedure is developed by G.A. Clarke et. al (22) where expression (1-8) is used as the analytical tool. The principle by this technique was unloading the sample at successive stages for determination of crack initiation where the change of the slope of the unloaded and reloaded lines occurred, and which requires very sensitive electronic equipment. See Fig. 2.14.

Thus it is clear that the development of simpler single specimen test techniques will extend the use of J_{Ic} as a fracture criterion. The solution to this problem, which is an important part of the present study, led to the development of an alternative test method.

Metallurgical Aspects of the Study

To clearly see the extent and limitations of the use of small tests in fracture, it is essential to test materials with a range of yield stresses which represent both the range where C.O.D.$_i$ and J_{Ic} data have a special advantage and the range where reliable values of K_{Ic}, and other fracture parameters, have already been established. Thus two different types of steels have been used in this study:

1) A High Strength Low Alloy Structural Steel, $\sigma y \approx 500$ MPa of the type proposed for arctic pipeline construction.
2) A High Strength Steel AISI 4340 which can be quenched and tempered to give values of the yield stress in the range 800-1600 MPa.

The HSLA structural steels represent a group of materials which have a combination of very high toughness and intermediate yield strength. Because of the size requirements for standard K_{Ic} testing, relatively few standard K_{Ic} data are available except for low test temperatures. Therefore, the alternative parameters as C.O.D.$_i$ and J_{Ic} are of particular interest for this class of steels.

Variation of tempering temperature in the quenched and tempered AISI 4340 will give a material which changes from quasi brittle to highly ductile behaviour at room temperature. There are a number of fracture data available for this system, and comparison can be made between the data obtained in the present work and the known data obtained from large scale tests.

Microstructural Aspects

The present work indicates that fracture can be described in terms of local events at the crack tip which are independent of the overall spread of plasticity in the sample. Thus the volume in which the critical events at the crack tip occur may be termed the process zone for fracture. This region is one where severe strain gradients occur. In order to develop a physical model it is necessary to delineate the critical events, such as void initiation and growth or strain localization, which occur in the process zone. These events are shown schematically in Fig. 1.1.

By examining the detailed microstructure in the process zone, some correlation may be established between the magnitude of the fracture parameters, the size of the process zone and microstructural features. In terms of a critical opening displacement $C.O.D._i$, one can consider expressions of the form

$$C.O.D._i = \varepsilon_c \times l \qquad (1\text{-}9)$$

where ε_c is some critical strain and l is a gaugelength which both are determined by microstructural parameters.

In order to try to determine some information about the microstructural aspects which limit the fracture parameters, the double notch technique was used (23) both in the structural steels and the high strength steels.

Of importance here is also to get some indication about the type of the critical localized strain and any eventual correlation between the size of the process zone and the larger plastic zone. In addition, some model experiments in terms of C.O.D. measurements and double notch technique were done in spheroidized carbon steels where the carbide spacing and the straining path are known. Then a clearer and more quantitative model of the actual physical limiting processes occurring in the process zone may be established, and the last section of the thesis deals with these types of model studies.

Thus in summary, the present study considers the following aspects of fracture:

a) The development and evaluation of small scale fracture tests.

b) The delineation of the events occurring in the process zone and their quantitative description in terms of microstructural events.

c) The correlation of small scale fracture parameters of known physical basis with existing data on the behaviour of large scale samples and service behaviour.

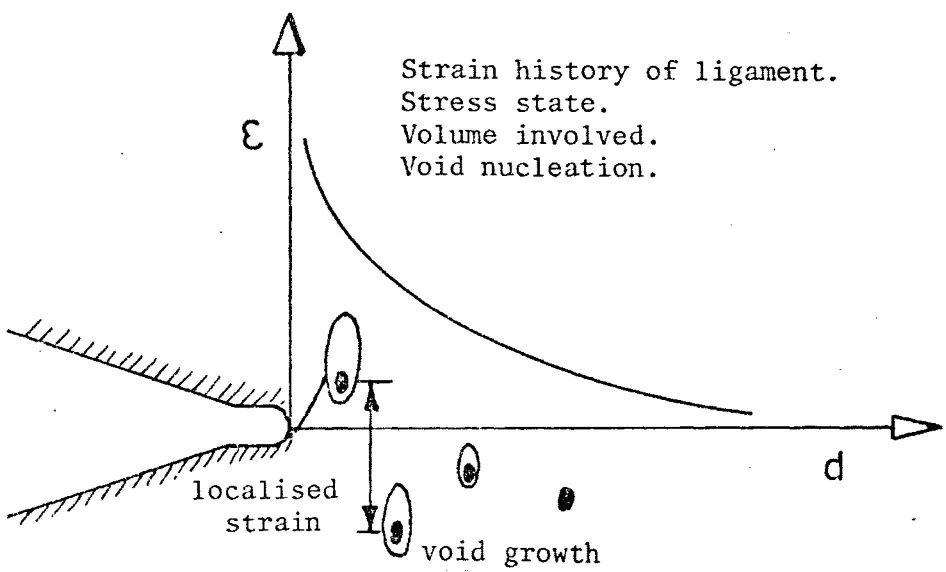

Fig. 1.1 Critical events at the crack tip.

Min. thickness of specimen for elastic plane strain behaviour. (ASTM Standard)

$$B \geq 2.5 \left(\frac{K_{Ic}}{\sigma_y}\right)^2$$

K_{Ic} ($MNm^{-3/2}$)	σ_y (MNm^{-2})	Thickness, B (cm)
50	2500	.1
50	1000	.7
100	1000	2.5
100	500	10.0
200	500	40.0
300	300	250.0

Table 1.1 K_{Ic} Testing

CHAPTER 2

LITERATURE REVIEW

2.1 Introduction

The concepts of fracture mechanics were first developed to describe the behaviour of elastically loaded bodies containing flaws. Thus most of the theoretical work in fracture mechanics has been done assuming linear elastic behaviour. However, as many materials deform in a plastic manner prior to fracture, it is of importance to extend the concepts of fracture mechanics into the inelastic/plastic range. The basic parameter used in fracture mechanics is the plane strain stress intensity factor K_{Ic}, and for materials in which the extent of plasticity is small compared with sample dimensions, basic principles in the linear elastic fracture mechanics (L.E.F.M.) can be extended to the non-linear elastic/plastic range by redefining the effective crack length to include the size of the plastic zone. These concepts are briefly reviewed in section 2.2 together with the limitations of the use of L.E.F.M. in quasi brittle materials due to size requirements for standard K_{Ic} testing.

In terms of the non-linear fracture mechanics in which extensive plastic yielding occurs, and in some cases on a scale comparable with the dimensions of the sample (general yield), a variety of parameters have been used to represent the fracture resistance prior to crack extension and instability. They are:

1) The critical Opening Displacement measured at the original crack tip at the point of crack initiation, $C.O.D._i$.
2) J-integral or Rice integral in terms of J_{Ic}.
3) R-curve analysis or resistance curve analysis.

The present study has been concerned with the determination of the critical $C.O.D._i$ and J-integral values for materials exhibiting various degrees of plasticity including general yielding conditions. Thus these two criteria are reviewed in terms of the basic methods of analysis testing procedures and previously obtained data in sections 2.3.1 and 2.3.2.

Further, in some cases a correlation may be established between the fracture mechanics parameters, obtained both in the elastic and elastic/plastic regimes, and the corresponding toughness determined as the upper shelf level of the energy absorption in the Charpy V-Notch test. These correlations are reviewed in section 2.4.

Finally in order to build up a physical model for the fracture events occurring at the crack tip in section 2.5, the existing literature is reviewed in regard to correlations between the fracture resistance, the scale and distribution of microstructural features, and the magnitude of the local stresses and strains established ahead of the crack tip prior to the onset of instability or crack extension.

2.2 Linear Elastic Fracture Mechanics

In the analysis of the stress field around a crack tip, which was initially developed by Westergaard using the Inglis solution for a sharp elliptical hole (1), the stresses can be expressed in mode I and

II of the deformation as

$$\sigma = \frac{\sigma_{app}\sqrt{\pi a}}{\sqrt{\pi r}} f(\sin\frac{\theta}{2}, \cos\frac{\theta}{2}) \tag{2-1}$$

Similarly for mode III which is pure shear

$$\tau = \frac{\tau_{app}\sqrt{\pi a}}{\sqrt{\pi r}} f(\sin\theta) \tag{2-2}$$

where r = distance from the crack tip

a = initial crack length

θ = angle which gives the orientation with respect to the coordinate system used at the crack tip.

Alternatively equation (2-1) and (2-2) can be expressed as

$$\sigma \ \alpha \ K \times r^{-\frac{1}{2}} \tag{2-3}$$

$$\tau \ \alpha \ K \times r^{-\frac{1}{2}} \tag{2-4}$$

where K is the stress intensity factor.

Thus the stresses ahead of the crack tip are directly related to the materials fracture resistance in terms of the stress intensity factor and to the distance from the crack tip.

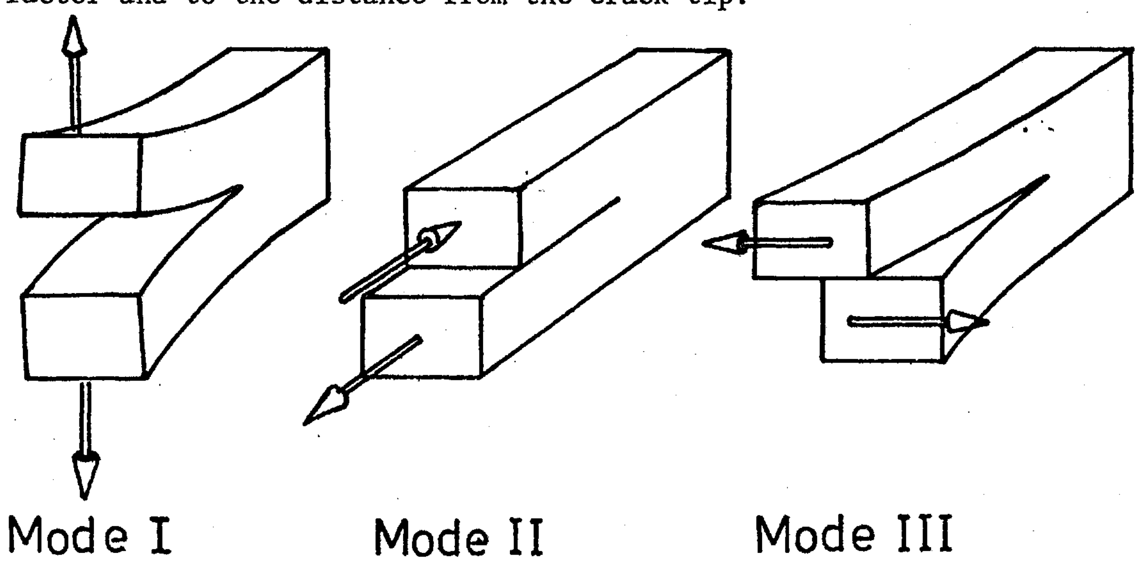

Fig. 2.1

For the behaviour in the crack tip region at the onset of failure, it is of importance to examine the contribution of the different energy terms to the process of crack extension, i.e. to define instability conditions involved in the onset of crack extension.

Assuming quasistatic conditions, the kinetic energy may be ignored, the total energy is given as

$$W = U_o + U + S \tag{2-5}$$

where U_o = elastic energy of an uncracked body

U = strain energy due to the crack

S = surface energy.

From Griffiths formalism based on ideal brittle materials, the different energies are given as

$$U = \frac{\pi}{2} \frac{\sigma^2 a^2}{E} (1-\nu^2) \text{ (plane strain)} \tag{2-6}$$

$$S = 2a\gamma_e \tag{2-7}$$

Consideration of the variation of the total energy W with respect to the crack length leads to the expression

$$\frac{\sigma^2 \pi a}{E} (1-\nu^2) = 2\gamma_e \tag{2-8}$$

where the left side represents the elastic energy release rate, G, and the right side is the materials fracture resistance.

A modification of the Griffith theory was done independently by Irwin and Orrowan (2)(3), which extended the analysis to materials of quasibrittle behaviour.

In that modification the surface energy γ_e, was replaced by the sum of the surface energy and the plastic work γ_p per unit area such that

$$\sigma^2 \frac{\pi a}{E} (1-\nu^2) = 2(\gamma_e + \gamma_p) \tag{2-9}$$

Since $K = \sigma\sqrt{\pi a}$, and the left hand side is equivalent to the energy release rate G in modus I, it gives the following relation

$$G_I = K_I^2 \frac{(1-\nu^2)}{E} \tag{2-10}$$

At instability or 2% crack growth $G_I = G_{Ic}$, $K_I = K_{Ic}$ and equation (2-10) is identical to equation (1-3).

However, in order to keep the size of the plastic zone at the crack tip in quasibrittle materials independent of sample geometry, it is estimated that

$$W, B, a \geq 50\ r \tag{2-11}$$

where r = radius of plastic zone

W = width of specimen

B = thickness

a = crack length

In plane strain conditions see Fig. 2.2 when r is given as

$$r = \frac{1}{6\pi} \left(\frac{K_{Ic}}{\sigma_y}\right)^2 \tag{2-12}$$

a combination of (2-11) and (2-12) then leads to the size requirements as

$$W, B, a \geq 2.5 \left(\frac{K_{Ic}}{\sigma_y}\right)^2 \tag{1-4}$$

As shown in Table 1-1, this leads to very large dimensions of the specimens for materials of high toughness and low or intermediate yield stresses which is the major disadvantage for the applications of the linear elastic fracture mechanics to structural materials.

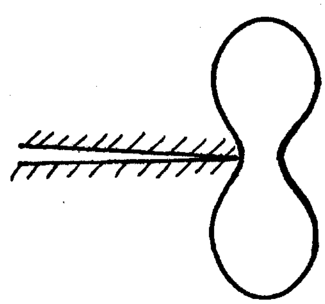

Fig. 2.2

2.3 Elastic Plastic Fracture Mechanics

2.3.1 General

The most widely used small scale test in ductile failure is the Charpy V-Notch impact test which characterizes the total energy absorbed in both crack initiation and growth and is a comparative measure of the toughness of a material using a sample of standard dimensions. The data obtained can, to some extent, be correlated with the stress intensity factor K_{Ic}. However, better defined parameters for the characterization of crack initiation and growth in small scale tests are needed for correlation with the service behaviour. The most promising parameters derived for small scale tests appear to be the critical $C.O.D._i$ and the J-integral which are reviewed in two separate subsections.

2.3.2 The Crack Tip Opening Displacement - C.O.D.

2.3.2.1 The background of C.O.D.

It is estimated that a critical value of the crack opening displacement prior to crack extension is a characteristic measure of the material independent of the size of the structure or test sample, i.e. the variation in constraint and extensive plastic deformation will not affect the critical value of C.O.D. Therefore it is assumed that a certain C.O.D. obtained under some defined conditions may be a sort of measure of the fracture resistance or the fracture toughness.

In an analysis by Burdekin and Stone (4) which is based on the theoretical models of Dugdale and Barrenblatt, where the opening displacement is defined at the points for the original crack tip, is given as

$$\delta = \frac{8\sigma_y a}{\pi E} \ln \left[\sec\left(\frac{\pi\sigma}{2\sigma_y}\right)\right] \qquad (2\text{-}13)$$

For $\sigma/\sigma_y \ll 1$ equation (2-13) may be simplified taking the first term of a series expansion for $\ln [\sec(\frac{\pi\sigma}{2\sigma_y})]$ such as

$$\delta = \frac{8\sigma_y a}{\pi E} \left[\tfrac{1}{2}\left(\frac{\pi\sigma}{2\sigma_y}\right)^2\right] \qquad (2\text{-}14)$$

i.e. $$\delta = \frac{\sigma^2 \pi a}{\sigma_y E} \qquad (2\text{-}15)$$

At a critical value δ_c with a corresponding critical stress at initiation of failure, this is readily shown to be of the form

$$G_c = \sigma_y \times \delta_c \qquad (2\text{-}16)$$

where $G_c = K_c{}^2/E = \sigma^2\pi a/E$

A relationship of the type shown in equation (2-16) may also be derived for a miniature tensile specimen model (24). Assuming that the critical opening displacement at the crack tip is a measure of the critical strain, ε_c, in a miniature tensile specimen of length 1, the C.O.D. is given as $1 \times \varepsilon_c$, equation (1-9). For the unit amount of crack growth and unit thickness of the sample, the energy release rate is given as

$$G_c = \sigma_{flow} \times \text{C.O.D.}_c \qquad (2\text{-}17)$$

where σ_{flow} is the appropriate stress level for the ligament thus depending on the amount of strain, σ_{flow} may be the initial yield stress, U.T.S. or true fracture stress.

An expression similar to (2-17) is found by Levy et al (12) using a finite element method for a non-hardening material in small scale yielding under plane strain conditions such as

$$G_{Ic} = 2.14\ \sigma_y \cdot \text{C.O.D.}_i \qquad (2\text{-}18)$$

Therefore there is strong evidence of having an equation of the form which relates the C.O.D._c directly to the energy release rate generally described in equation (1-5) or given as

$$G_{Ic} = \sigma_c \times \text{C.O.D.}_i \qquad (2\text{-}19)$$

in plane strain, and the critical C.O.D._i may be used as a significant fracture parameter even if it is obtained in a small scale test in general yield conditions.

2.3.2.2 Techniques for C.O.D. Testing

Some of the most relevant techniques applied for C.O.D. testing are reviewed.

1) Paddlemeter

This method is based on rotation of a square paddle at the bottom of a notch as the parallel notch surfaces separate (4). The blade is carried on the end of a shaft, which is in the plane of the crack and is perpendicular to the notch root. The rotation is converted to a linear displacement at a displacement transducer, and the C.O.D. is given in terms of a voltage output. The procedure is simple in principle. However, the obtained C.O.D. values seem to be very sensitive to the positioning of the paddlemeter inside the slotted notch. Further, the method requires a certain minimal thickness of the notch to be able to use the paddlemeter and which may not be representative of a fatigue precrack.

2) Metallographic Sectioning

In this technique the samples are sectioned and polished and the C.O.D. value is obtained on that surface. The obtained value is from off-load condition and may vary from the on-load C.O.D. which is normally measured. In addition, this technique is time consuming.

3) Double Notch Sample

The specimen has two identical notches or cracks which are loaded in the way that the same stress field occurs at both notch tips, and the two stress fields must be independent of each other. The sample will break completely at one of the notches when instability is exceeded, while the remained deformed notch reflects the pattern of displacement and straining up to crack initiation. Then the opening displacement can be measured at the surface or by sectioning to get the mid region value which is maybe in plane strain. Still these values are from off-load conditions.

4) Stretch Zone Measurements

Before crack extension, the crack tip has undergone a considerable amount of intense strain which leads to the blunting of the crack. Alternately, the region is called the stretch zone and may be related directly to the C.O.D. values (25). Measuring the extent of the stretching can be done on a replica of the fracture surface or on the fracture surface itself in a scanning electron microscope. However, it is relatively difficult to determine the exact width of the stretch zone.

5) Clip Gauge Displacement

This is perhaps the most extensively used test method and can be applied on specimens which contain a fatigue precrack (19). The principle is that the displacement V_g at the top of the notch measured by a clip gauge is related to the opening displacement at the bottom of the notch or crack. See Fig. 2.3.

Assuming a linear relationship between C.O.D. and V_g, the expression will be of the form

$$\text{C.O.D.} = \frac{V_g}{1 + \frac{1}{r}\frac{(a+z)}{(W-a)}} \qquad (2\text{-}20)$$

where r is a rotational factor which must be determined by calibration shown in a calibration curve in Fig. 2.4.

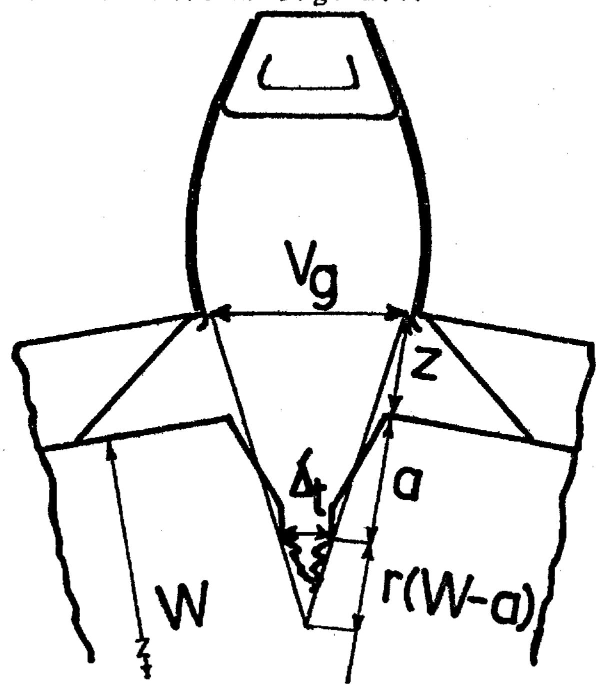

Fig. 2.3 Clip gauge displacement at top of the notch related to C.O.D. at crack tip.

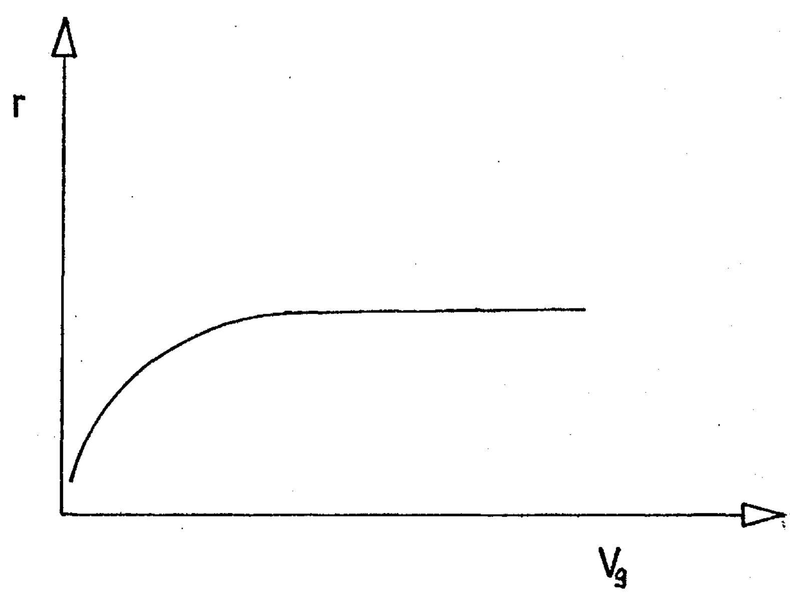

Fig. 2.4 Calibration curve r vs. V_g.

However, the point of crack initiation has to be determined.

A relative simple method (10) which requires several specimens, is by measuring the clip gauge displacement versus crack extension. Make a plot of either the measured V_g or calculated C.O.D. versus crack extension Δa and extrapolate to crack initiation to determine the critical opening displacement. See Fig. 2.5.

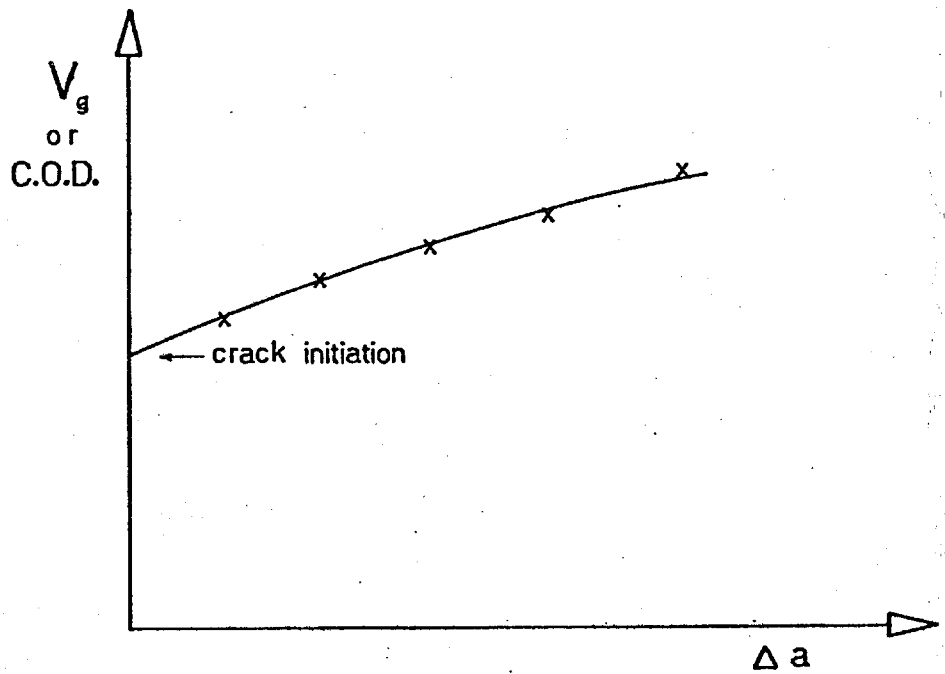

Fig. 2.5 Displacement versus crack extension.

The crack extension can be visualized either by heat tinting the new surface and then broken up, or cooling the sample down to the complete brittle range where it is deformed until failure. Then it is easy to distinguish between the area of the extended crack and the fracture surface which appeared due to the complete failure of the sample (heat tinted versus not heat tinted areas or ductile versus brittle surfaces) and the length of the extension Δa can be measured readily.

The clip gauge displacement can be applied in a wide range of temperatures, limiting by the temperature range of the extensometer used for measuring V_g. In addition the method is useful in detecting the critical displacement when no stable crack growth occurs before fracture. However, consistent data are obtained only if a correct calibration curve is used. The assumption of a constant rotational factor in equation (2-20) may give considerable scatter in the data, especially in the lower range for the displacements.

6) Electrical Potential Method

An electrical potential may be established between two points located on each side of a crack tip, which is applied by several authors (26)(27). When crack extension occurs, a change in resistance is the result and the measured crack potential is changed. If the potential U is plotted versus load, the corresponding critical load at crack initiation is known. See Fig. 2.6.

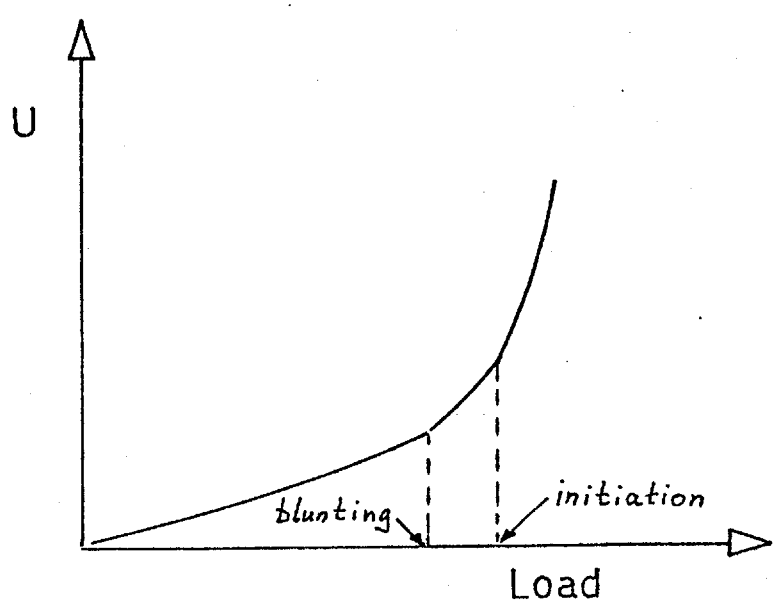

Fig. 2.6 Crack potential versus load.

If a clip gauge technique is used to obtain the C.O.D. values, and the load is plotted versus the clip gauge displacement, the critical opening displacement is readily derived from the obtained critical clip gauge displacement. However, the stretch zone which occurs before real crack growth may give some change in the electrical potential (See Fig. 2.6), and must not be taken into account as a potential for the actual crack extension.

7) Acoustic Emission

In this method the origin of elastic stress waves which arise from an extending crack may be determined by measuring the different arrival times of these stress waves at each of an array of transducers mounted on the component surface (29). However, a serious limitation of this technique is the high gain which must be employed to detect emissions from defects and distinguish this emission from the background noise. By use of measuring the clip gauge displacement on top of a notch, a correlation can be made between this displacement and the acoustic emission. The A-E method is then used to determine the point of crack initiation. The corresponding V_g can be measured, and a critical C.O.D. is derived from the magnitude of the clip gauge displacement.

8) Crack Profile Technique

In this technique plastic silicone rubber is used to replicate the opened notch or crack with any eventual crack growth (See Fig. 2.7) applied by Robinson and Tetelman (18).

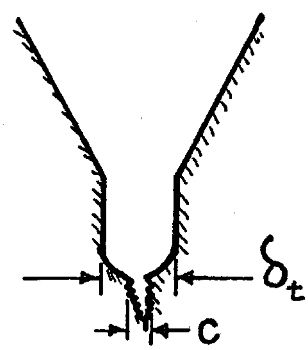

Fig. 2.7 Replicated crack profile.

The casting is sectioned and the profile, similar to Fig. 2.7, is examined to obtain the displacements at the crack tip, and the critical opening displacement at crack initiation can be expressed as

$$C.O.D._i = \delta_t - c - 2r \qquad (2\text{-}21)$$

where δ_t = total displacement

c = width of the extended crack

2r = diameter and slot width.

The value of δ_t ought to be measured at the original crack tip or in the blunted region. If the initial stress concentrator is a pre-crack or a slot with parallel sides, the sides will remain almost parallel even up to maximum load or instability. Thus both the initial C.O.D. and the C.O.D. at maximum load can be determined.

In addition, no extra equipment is needed for obtaining the crack opening displacements. However, the curing time for the silicone rubber increases with decreasing temperature leading to some lower limiting temperature in the estimated range -25°C-40°C for the application of the test method.

Examination of other materials as replicating media may depress the temperature which represents the lower limit.

Further, this test method is of advantage especially for detection of a ductile crack where stable crack growth occurs before instability.

2.3.2.3 Previous results - effects of geometry

As in the case of the stress intensity factor K_{Ic}, the critical C.O.D. values may depend on crack or notch tip geometry. Previous work (10) has shown an effect of slot width or root radius as illustrated in Fig. 2.8.

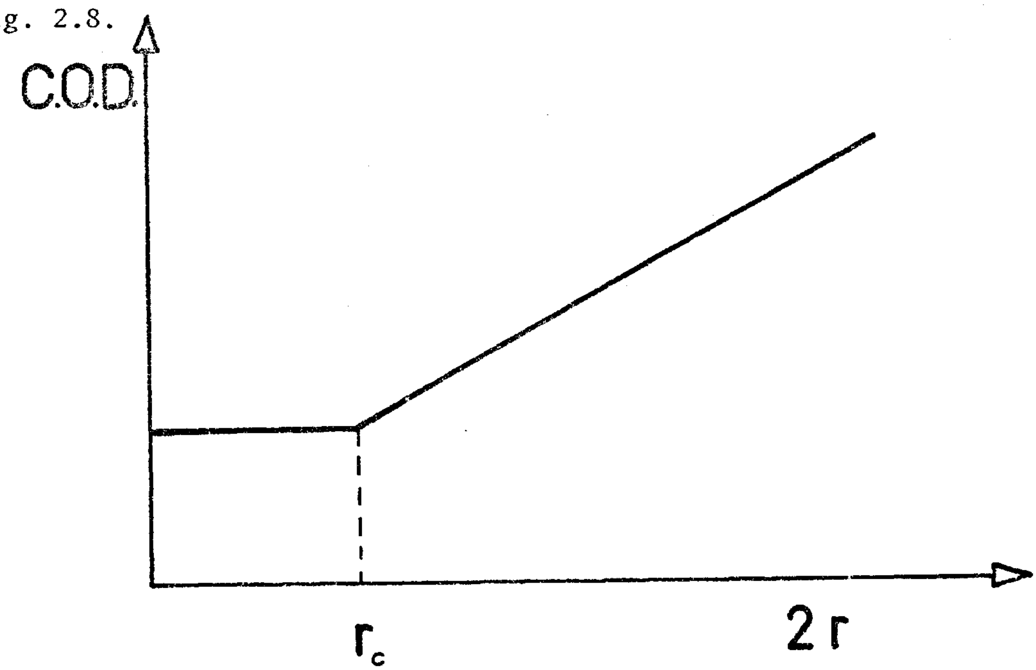

Fig. 2.8 Effect of slot width on $C.O.D._i$

Below, a critical radius r_o, the values at crack initiation seem to be constant and similar to the value obtained for a fatigue precrack. This minimum value is then the critical opening displacement at crack initiation which is considered as a material parameter. However, the displacements at maximum load do not really show the same consistent behaviour as the data established at crack initiation.

The influence of sample geometry has also been considered in the literature.

Above a certain thickness of the sample in a free machining mild steel (10), the data at crack initiation seem to be independent of the specimen thickness and it is assumed that plane strain conditions are obtained in this constant region. The maximum load data again do not behave strictly in the same manner and were more dependent of the geometry.

In Robinson-Tetelman's work where the crack profile technique was used, it was important to measure the critical $C.O.D._i$ in the middle third of the cross section of the sample of standard Charpy V-Notch size for the steels tested. Plane strain in the ductile range occurred in the mid region only.

To obtain consistent results it is estimated that a minimum ratio of notch depth/width of the specimen, a/W, is required to avoid general yielding back to the top surface of the sample, and a resultant drop in the triaxial constraint at the crack tip. J.F. Knott (30) reported that the ratio (a/W) had to be larger than .35 to avoid this effect on the critical $C.O.D._i$.

If the clip gauge displacement method is used to detect the crack opening displacement, yield break through to the top surface will affect the relationship between V_g and C.O.D. (18). Using an estimated standard value for the rotational factor may lead to considerable errors in the C.O.D. values.

In addition, Chipperfield et al (31) made comparison of data obtained in both three point and four point bend test samples, and concluded that C.O.D.$_i$ was identical in both test configurations, while the data obtained during crack extension and maximum load were strongly dependent on the type of loading.

2.3.3 J-integral

2.3.3.1 Principles

In a general term, J.R. Rice (32) has defined a line integral, J, on any curve Γ surrounding the crack tip where the curve is traversed in the counterclockwise direction, beginning along the bottom surface of the crack and ending along the top surface such as

$$J = \int_{\Gamma} [W dx_2 - T \frac{\partial u}{\partial x_1} ds] \qquad (2\text{-}22)$$

where W = the integral of the strain energy density

T = the traction vector normal to the curve Γ, (See Fig. 2) and

ds is the increment of the arc length.

The line integral is defined for a two dimensional deformation field where the first term in equation (2-22) represents the strain energy per unit area of the body inside the integral loop, and the last term represents the work done per unit area by the applied tractions along the integral path.

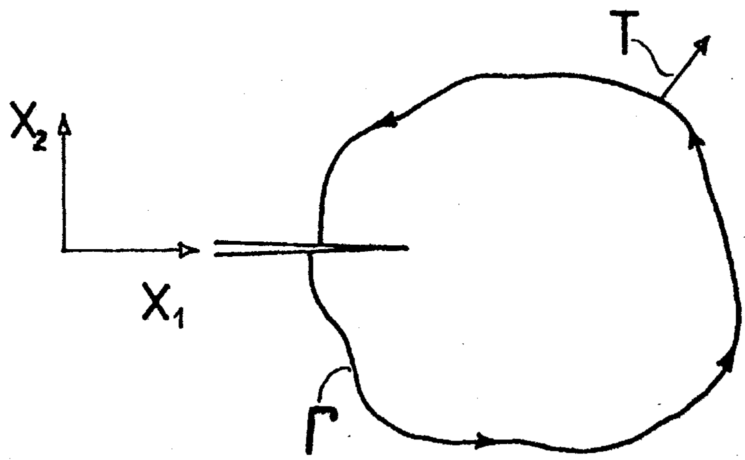

Fig. 2.9 Coordinate system at crack tip and arbitrary line integral contour.

Since the J-integral is found to be path-independent in a non-linear elastic behaviour, the contour may be chosen close to the crack tip. As the crack propagates the amount da, (See Fig. 2.10) and the shape of the crack tip is remained, the traction term of equation (2-22) diminish since the open surface can have no stress normal to it. Thus

$$J = \int_{\Gamma_t} W dx_2 \qquad (2\text{-}23)$$

However, this expression is equivalent to

$$J = - \frac{\partial U}{\partial a} \qquad (2\text{-}24)$$

where ∂U is the change in the total potential energy per unit thickness as the crack propagates the amount da.

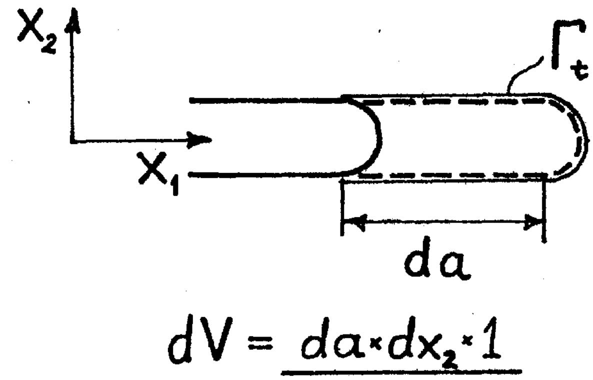

Fig. 2.10 Profile of extended crack of the amount of da.

J is in equation (2-24) expressed with the same function as the energy release rate G in the linear elastic theory, without the restriction to behave in a linear elastic manner.

A limitation for the J-integral, however, is that reversible unloading must be possible. Therefore the value of J cannot be identified with the energy available for crack growth in elastic/plastic materials, although it still can be considered as a measure of the characteristic crack tip elastic/plastic stress-and-strain field (14).

Extensive amount of work is done in order to apply the J-integral as a measure of the stress-and-strain field ahead of a crack tip. The magnitude of J prior to crack extension under plane strain conditions in terms of J_{Ic}, is estimated as a characteristic of the material independent of test piece geometry, referred to Landes and Begley (14,33).

Further, they obtained very good consistency between the data for J_{Ic} from elastic/plastic deformed bend bars and the G_{Ic} measured in a standard ASTM procedure in some Ni Cr Mo V steels. Therefore, J_{Ic} seems to have the same meaning as a fracture parameter in elastic/plastic behaviour as in linear elastic theory where the definitions of J and G are identical.

In the application of J as a failure criterion, J must give some information on the stresses and strains around a crack tip. If the integral line is chosen as a circular path of radius r, $x_2 = r \sin\theta$ and $ds = r d\theta$, a modified form of equation (2-22) appears as

$$J = \int_{\pi}^{\pi} [W \cos\theta - T \frac{\partial u}{\partial x_1}] r d\theta \qquad (2\text{-}25)$$

Both the first and second term of the expression in (2-25) are of the order stress times strain. For J to be path independent, the product of stress and strain must show a 1/r singularity as $r \to 0$ (33,34), i.e.:

$$\sigma_{ij} \times \varepsilon_{ij} \to \frac{\text{a function of } \theta}{r} \text{ as } r \to 0 \qquad (2\text{-}26)$$

In linear elastic behaviour the product of stress and strain may be represented as σ^2/E. As this product is of order 1/r, the corresponding stress field singularity is shown to have an order $1/\sqrt{r}$ which is in accordance with the results for the singularities of the stress fields from Westergaards or Irwin's stress functions (1). Thus the path independent line integral represents a characteristic measure of the crack tip stress and strain field.

2.3.3.2 Measurement techniques

The original test method for determining J_{Ic}, the compliance method, is based on equation (2-24) for the rate of change of potential energy with respect to the crack length (35). Several specimens of the Compact Tension Specimen type (CTS) of different crack lengths are tested, and the work done for a given deflection is plotted versus crack length as in Fig. 2.11b where U, the potential energy or work done is obtained as the area under the load deflection curve up to a given deflection. See Fig. 2.11a.

From the definition of J in equation (2-24), J is then the slope of the curve energy versus crack length as shown in Fig. 2.11b.

These values of J at a given initial crack length a_o may be plotted as a function of the load point displacement u. See Fig. 2.12.

At a critical load point displacement, u_{crit}, at crack initiation, the value J_{Ic} is found.

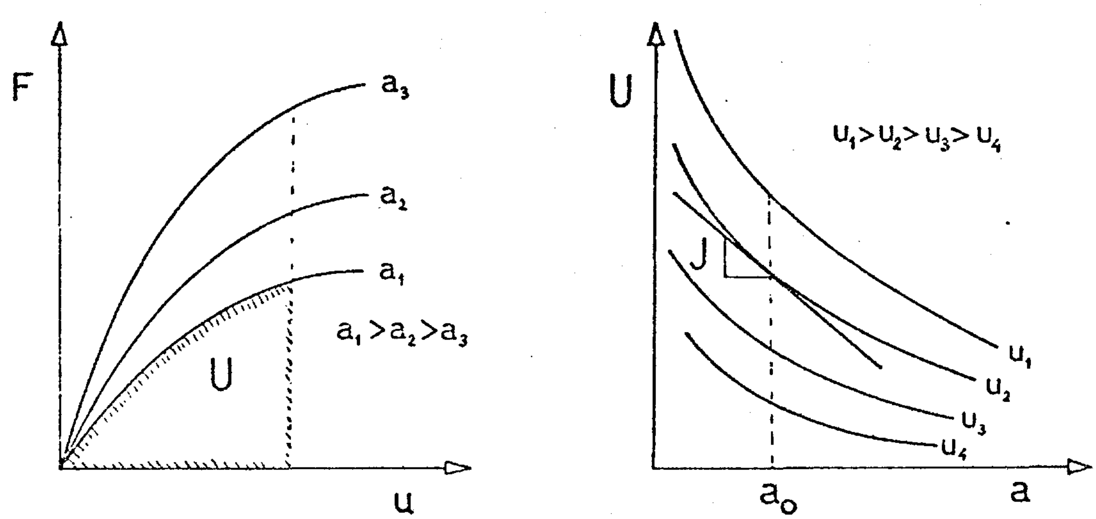

Fig. 2.11a&b Schematic diagram of the principles of the compliance technique.

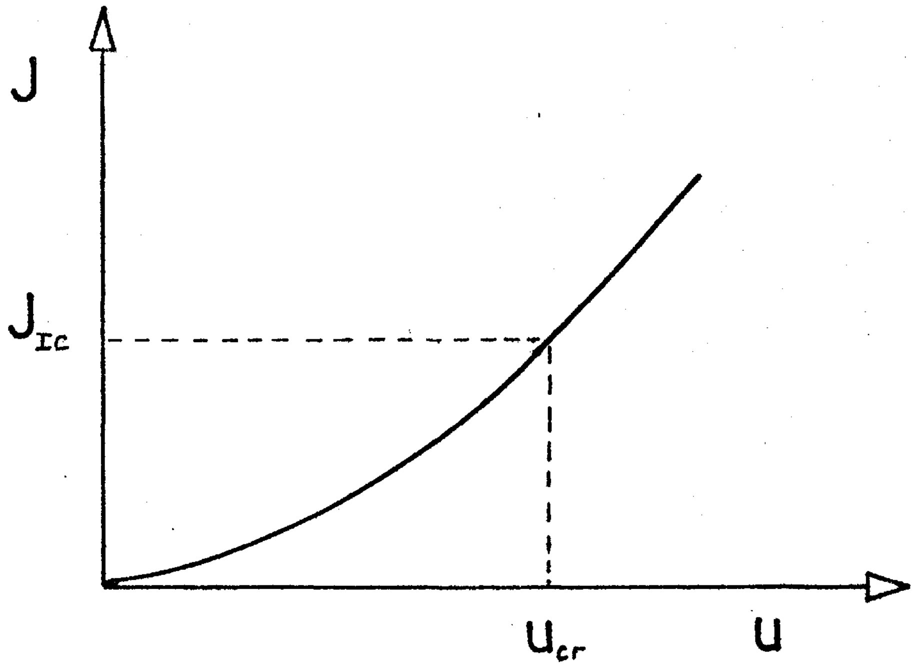

Fig. 2.12 J versus load point displacement u.

Modifying equation (2-24) the definition of J is given by (20)

$$J = \int_{o}^{\delta} \left(- \frac{\partial P}{\partial a}\right)_{\delta} d\delta \tag{2-27}$$

or

$$J = \int_{o}^{P} \left(\frac{\partial \delta}{\partial a}\right)_{P} dP \tag{2-28}$$

In this case J is the rate of change with respect to the crack size a, of the area under the load-load point displacement curves, P versus δ, where P is denoted as force per unit thickness. For a deeply notched test sample subject to bending, equation (2-28) can be expressed in terms of moment per unit thickness, the rotation and the remained ligament ahead of the crack respectively such as

$$J = \int_{o}^{M} \left(- \frac{\partial \theta_{tot}}{\partial b}\right) dM \tag{2-29}$$

where $\theta_{tot} = \theta_{no\ crack}$ and θ_{crack}.

Further it was found (34) that

$$\left(\frac{\partial\theta_{tot}}{\partial b}\right)_M = \frac{2M}{b}\left(\frac{\partial\theta_{crack}}{\partial M}\right)_b \tag{2-30}$$

Substituting (2-30) into (2-29) gives the form

$$J = \frac{2}{b}\int_o^{\theta_{crack}} Md\theta_{crack} \tag{2-31}$$

The area under the curve moment versus rotation gives the work done where the deformations due to the crack only is presented.

If the bending of the deeply cracked sample is done principally by an applied force, P, which undergoes a deflection, δ_{crack} equation (2-31) becomes

$$J = \frac{2}{b}\int_o^{\delta_{crack}} Pd\delta_{crack} \tag{2-32}$$

where again the integral is simply the work done per unit thickness. Equation (2-32) may then be given in the final form, such as

$$J = \frac{2U}{bB} \tag{1-8}$$

where U = area under the load-load point displacement curve.

b = remained uncracked ligament

B = sample thickness.

Therefore, the J-integral may be identified from a single specimen test which is a considerable simplification of the estimation procedure for J-integral testing.

Using equation (1-8) for determination of J is a distant advantage over the original compliance or energy rate method. However, the point of crack initiation has to be accurately defined. Several specimens with the same original crack length of deeply notched samples can be deformed to different values of the load point displacement and then unloaded (21). If any crack advance Δa occurs, it must be quantified in order to get the actual measure of Δa. This can be done by different techniques.

In steel, Landes and Begley proposed using heat tinting with subsequent breaking of the samples in liquid nitrogen. Then Δa can readily be measured and a curve J versus crack advance, Δa, a resistance curve, can be plotted. See Fig. 2.13.

As the crack blunts before real extension, this effect can be shown as the blunting line in Fig. 2.13. The value of J_{Ic} is then found at the intersection between the blunting line and the extrapolated J versus Δa curve.

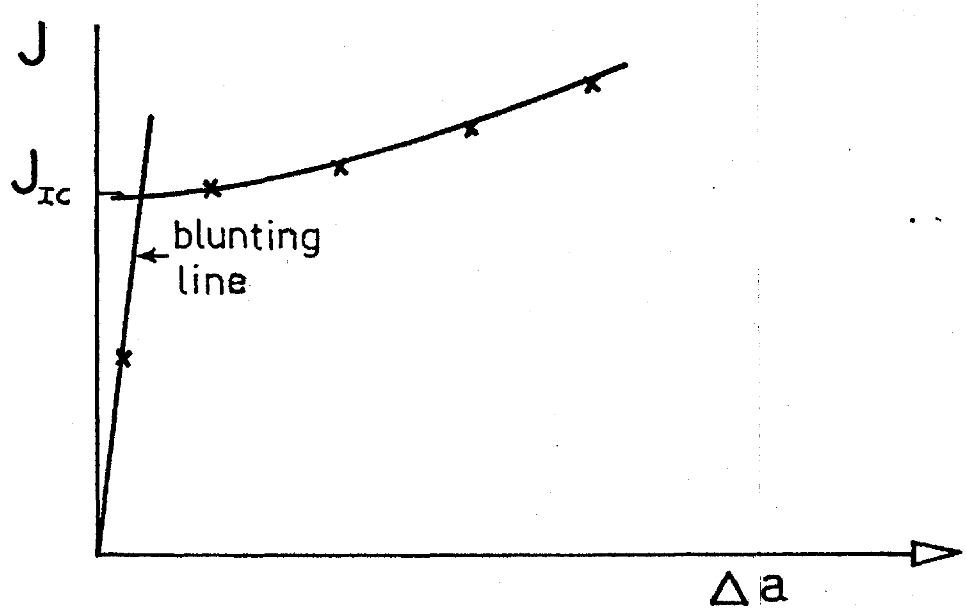

Fig. 2.13 J versus crack extension Δa

To clearly define the crack growth resistance curve, at least four test samples are needed. This method, where both J_{Ic} and the resistance curve are obtained, is presently used as a standard method (21,36,37).

Since J is determined from a single specimen at any displacement, much effort is given determining J_{Ic} from a single specimen test.

A compliance method is developed by G.A. Clarke, et al (22) which in principle is shown in Fig. 2.14 where the elastic compliance is measured by partially unloading and reloading of the sample. This procedure is repeated at different load point displacements shown as straight lines on the load-load point displacement curve in Fig. 2.14.

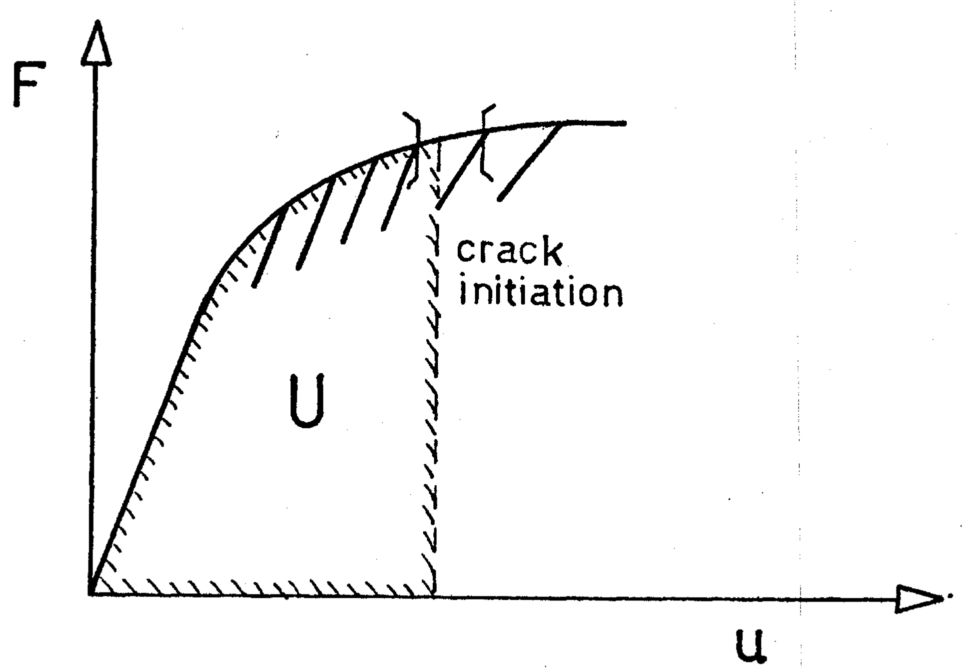

Fig. 2.14 A single specimen compliance method for determination of J_{Ic}.

The point of crack initiation is estimated as the point where the first change of the slope of these unloaded reloaded curves occurs, and that the decrease in slope or the stiffness is due to the crack extension and corresponding reduced remained uncracked ligament ahead of the crack only.

To perform these tests a very sensitive plot is needed of the load-load point displacement curve to obtain the first change in slope which may be affected by elastic backstresses.

A second method for determination of the point of crack initiation in a single specimen is the electrical potential method (38), as used for measuring critical crack opening displacement at crack initiation, described in section 2.3.2.2.

Again J_{Ic} can be obtained when U the work done up to crack initiation is measured.

Other methods of measuring the point of crack extension are similar for those applied to get the critical C.O.D.-values. See section 2.3.2.2.

All these techniques where the point of crack initiation is detected and J_{Ic} obtained from equation (2-32), represent the distinct advantage in J_{Ic} testing in that only a single specimen is required. The real disadvantage is that they all require very sophisticated electronic equipment with a high degree of precision being able to detect the initial point of crack extension.

One of the salient features of the work reported in this thesis is the development of a simple method of obtaining the J_{Ic} value from single specimens for materials with a range of yield stresses. This will be discussed in detail in Chapter 3.

2.3.3.3 Limitations on J_{Ic} testing

One important limitation for a J_{Ic} test method is the estimated size requirements to determine a valid geometric independent J_{Ic}. Paris (39) suggested the size requirements to be expressed in terms of the approximate size of the process zone or the opening displacement prior to crack extension, and in accordance with the standard ASTM K_{Ic} testing, see section 2.2, such as

$$B, b, a, \geq \alpha\, J_{Ic}/\sigma_{flow} \tag{2-33}$$

where B, b, a, are the specimen thickness, uncracked ligament and crack length respectively. The proportionality factor is assumed to be in the order of 25 to 50, and σ_{flow} is often taken as the mean value of the yield stress and U.T.S.

In addition, the use of the current test methods, which are based on equation (1-8) are limited to bend type specimen, i.e. either pure bend specimen or a compact tension specimen.

2.4 Correlation Between Fracture Mechanics Criteria and the Charpy V-Notch Impact Toughness Parameters

As the Charpy V-Notch, CVN, impact test is the most common measure of a materials toughness, it is of interest to correlate the charpy data with the corresponding values of K_{Ic}, C.O.D., J_{Ic} obtained from slow bend tests.

In general, the toughness measured in a Charpy specimen increases with increasing temperature including a brittle region, a transition range and a fully ductile range shown schematically in Fig. 2.15. However, there is a shift in the transition range and the upper shelf level between slow bend and impact testing as in Fig. 2.15.

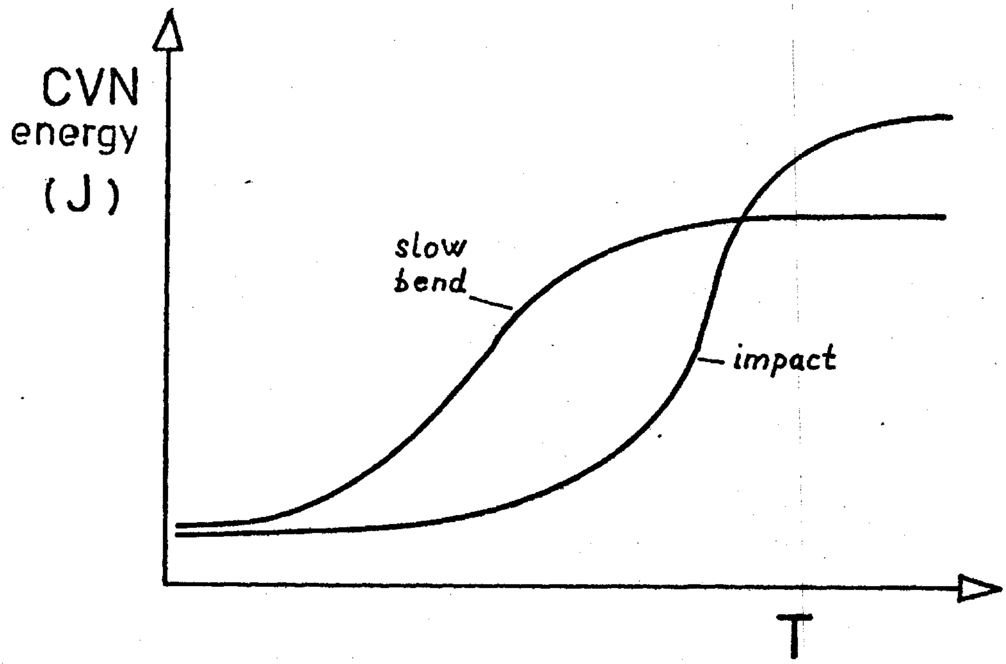

Fig. 2.15 CVN-energy for slow bend and impact test as a function of temperature.

Similar effects are seen on the K_{Ic} behaviour, and a correspondence between K_{Ic}^{*} and CVN energy absorption values obtained at particular test-temperature and strain rate can be expressed as

$$\frac{K_{Ic}^{*2}}{E} = A \times CVN \tag{2-34}$$

where A = a constant of proportionality.

K_{Ic}^{*} is in general not identical with the standard value of K_{Ic} which is obtained under quasistatic testing conditions.

Since the effect of temperature and loading rate on CVN and K_{Ic}^{*} are the same, correlations may be established between the plane strain stress intensity factor K_{Ic} obtained in a slow bend test, and the upper shelf value of the impact CVN data. According to Rolfe, Novak, Barsom (40,41) the correlation between K_{Ic} and CVN_{max} is given such as

$$\left(\frac{K_{Ic}}{\sigma_{ys}}\right)^2 = \frac{5}{\sigma_{ys}} \left[CVN - \frac{\sigma_{ys}}{20}\right] \tag{2-35}$$

where σ_{ys} = yield strength at the upper shelf temperature or room temperature.

This correlation was obtained in steels having yield strengths in the range 750-1700 MPa (110-246 ksi). However, as long as it is an upper shelf correlation, equation (2-35) is assumed to be valid for steels of yield strength < 700 MPa. In agreement with equation (2-35), Maxey et al (42) found from a number of experimental data a relationship between the CVN_{max} shelf value and the energy release rate obtained in a slow full scale K_{Ic} test, such as

$$G_c = \frac{12\ CVN_{max}}{A_c} \tag{2-36}$$

where A_c is the area of the fracture surface of the Charpy V-notch specimen. For G_c expressed in terms of the stress intensity factor K_c equation (2-36) becomes

$$\frac{K_c^2}{E} = \frac{12\ CVN_{max}}{A_c} \tag{2-37}$$

Further, data which may be obtained in small scale tests, as the critical opening displacement, are affected by the temperature and the rate of loading in a manner similar to that described for the K_{Ic} and CVN behaviour. See Fig. 2.16.

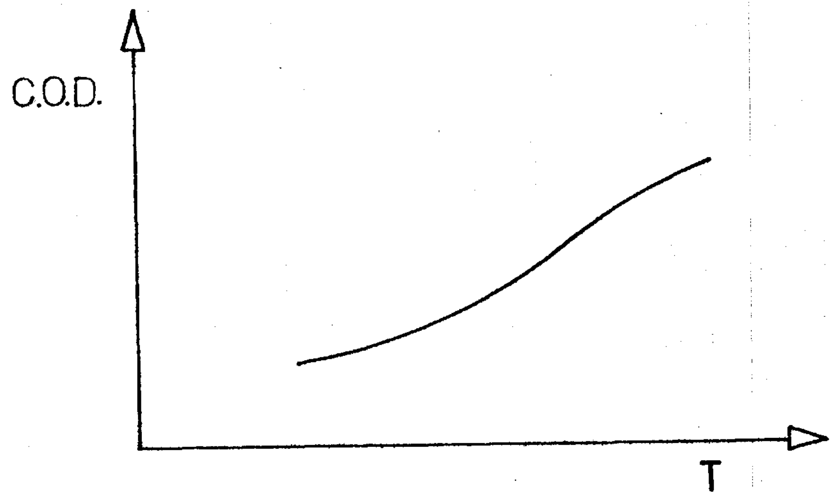

Fig. 2.16 C.O.D. versus temperature.

Also the characteristic of J-integral values in terms of J_{Ic} seem to scale with the magnitude of K_{Ic}^{*} in terms to the effect of test temperature and loading rate. Since the critical C.O.D. and J_{Ic} may be directly related to the energy release rate as in equation (2-5) and (1-7), a correlation between the upper shelf impact CVN value and the critical C.O.D. or J_{Ic} from a slow test may be established. Therefore, a high shelf value of the CVN energy absorption may indicate a correspondingly high C.O.D. or J_{Ic} value.

In the case of delamination, the corresponding data may be somewhat different. If delamination occurs normal to the direction of the movement for crack extension, this may act as a crack arrestor and the absorbed energy will increase due to the change in operative stress scale even if the crack initiates at an early stage.

2.5 Correlations Between Fracture Toughness Parameters, Deformation History and Microstructural Features

In the area of fracture mechanics, one measure of fracture resistance is the energy release rate G_c which can be related to the crack opening displacement δ_{crit} by the expression

$$G_c = \sigma \times \delta_{crit} \qquad (1\text{-}5)$$

where δ_{crit} is the critical opening displacement and σ is some critical stress related to strain attained before failure occurs. As reviewed in section 2.3.1.1, the magnitude of the critical stress is found vary, depending on the level of the yield stress of the material and the type of analytical model used. Equation (1-5) may also be written as

$$G_c = \lambda \times \sigma_x \times \delta_c \qquad (2\text{-}38)$$

where λ is a correlation coefficient of the order $1 < \lambda < 2.6$ in the literature.

For $J_{Ic} = G_c$, and $C.O.D._i = \delta_c$ in equation (2-38). This can be plotted as in Fig. 2.17 where the slope of the curves represent the constant λ (43) and most data fall in between the two lines drawn in the diagram.

However, for high strength materials with relatively small differences between the magnitudes of σ_y, σ_{uts} and σ_f, the precenity of the data points to the lower line in Fig. 2.17 and is often taken as an indication that the most probable critical stress is the yield stress. However, the physical implication of this conclusion must be examined more closely. In a rigid plastic material, the critical stress is simply the yield stress as in the strip yielding model by Dugdale (44), while most other models predict a higher critical stress than the yield stress.

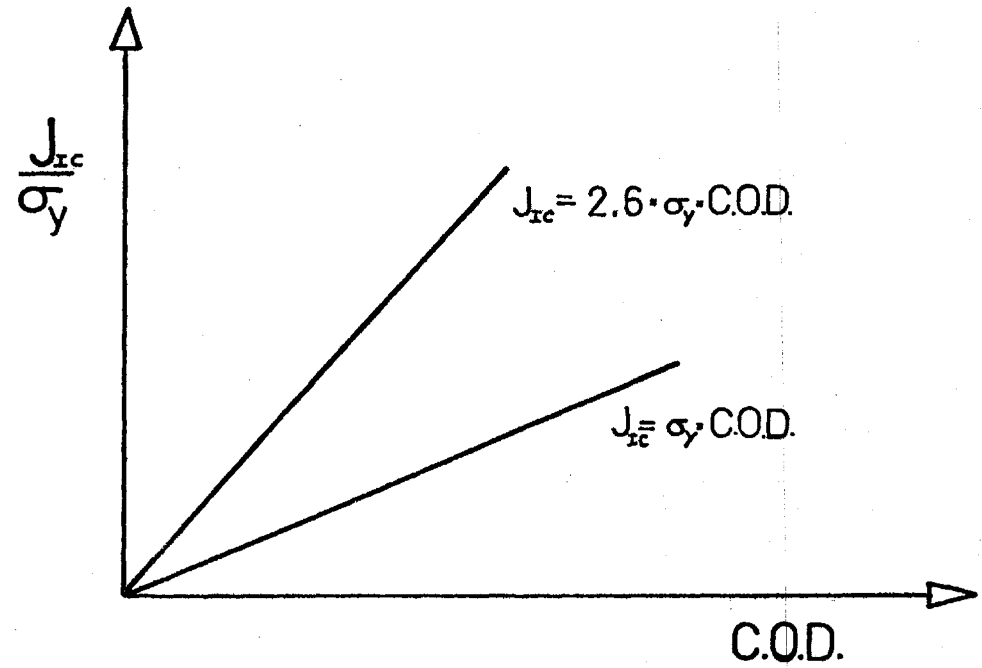

Fig. 2.17 Relationship between C.O.D. and J-integral.

It is of importance to know if the obtained magnitude of the critical stress obtained from a comparison of G_c and δ_{crit} represents the uniform plastic work in the sample, or if it just describes the critical stress level exceeded ahead of the crack tip, and if it can be related to the local deformation history ahead of the crack tip prior to crack growth.

Assuming that the critical stress is related to the local features at the crack tip and that a certain limiting local strain determines the point of crack extension, the critical stress would be the corresponding stress derived from the equivalent stress strain curve as shown in Fig. 2.18.

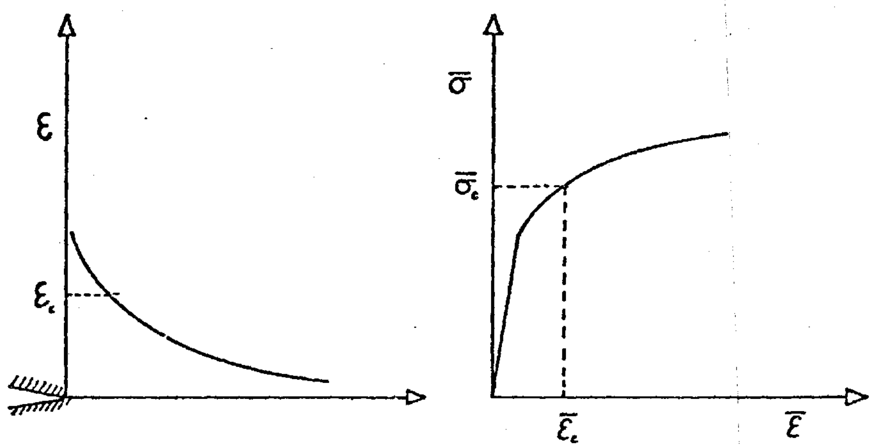

Fig. 2.18 Correlation between a limiting crack tip strain and the equivalent limiting stress.

In terms of the opening displacement at the crack tip, this can be considered in terms of the attained of a critical strain in a tensile ligament of length 1. Thus

$$\text{C.O.D.}_i = \varepsilon_c \times 1 \qquad (1\text{-}9)$$

If the crack tip is considered as a mini tensile model, see section 2.2, the critical strain is assumed of the order of the uniaxial true strain to failure which is in accord with Smith and Knott (10) in their analysis of a free machining mild steel. Therefore the critical opening displacement and the corresponding energy release rate seem to be strongly dependent on the ductility or a critical strain ahead of the crack tip.

In most models of ductile fracture (45), (46), (47) a simple geometric condition can be used to describe the growth and coalescence of voids at inclusions following their nucleation at some critical local stress. The process of growing the voids to the crack tip may have occurred by extensive plasticity at the crack tip, or by some form of localised shear (48)(49)(50) particularly in materials at higher yield stress.

Thus the critical strain level at the cracktip may depend on the material both in terms of the yield stress level, and the amount of eventual void growth before linking with the blunted crack tip. Increasing the yield stress often leads to a decrease in ductility measured as the uniaxial true strain to failure. In addition, as processes of void growth occur, the ductility measured in terms of a critical strain may vary with the stress state.

Clausing (51) showed that the plane strain ductility decreased more than the uniaxial true strain to failure with increasing yield stress in steels of yield stresses in the range from 750 to 1700 MPa, or the ratio plane strain ductility/uniaxial true strain to failure dropped with increasing yield strength. See Fig. 2.19.

If localised shear failure processes occur at the crack tip, the limiting strain is considerably smaller than the uniform true strain to failure. This type of failure has been observed in a number of high yield strength materials (48, 49).

Further, steels tend to have lower work hardening rate with increasing yield stress, the extent of the plastic zone around the crack tip is smaller and the amount of eventual growth of voids may be limited. If the voids grow extensively, just very close to the crack tip, the limiting strain may be localised shear between the blunted crack and a nearest void.

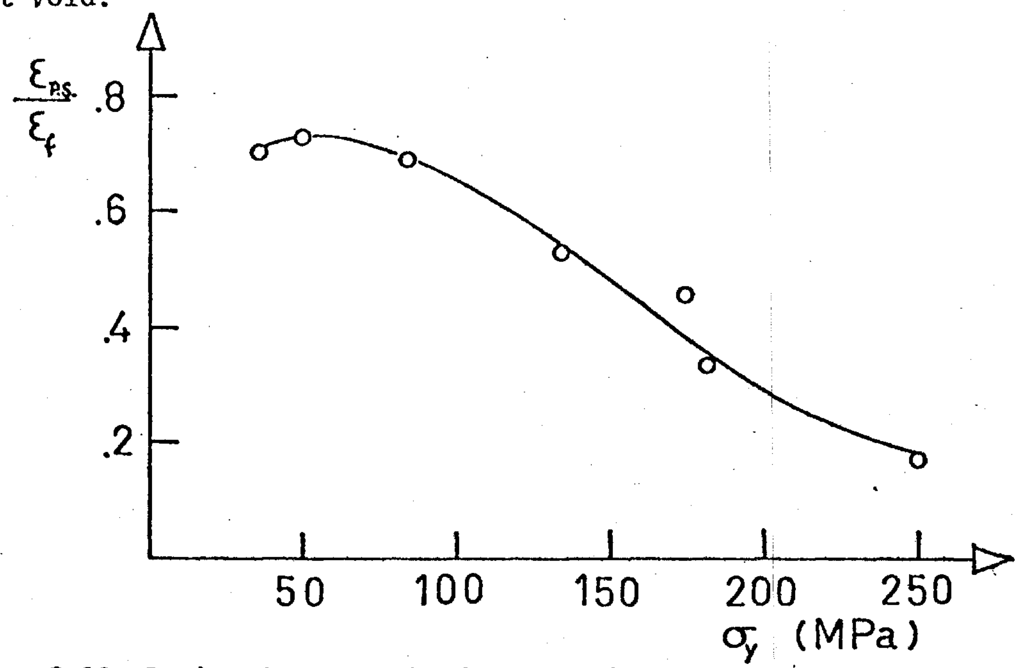

Fig. 2.19 Ratio plane strain ductility/uniax true strain to failure as a function of yield stress.

In addition, the estimated gauge length l may be related directly to the microstructure, for example, to the spacing between second phase particles. In an analysis by Smith and Knott (10) where the critical C.O.D.$_i$ and the ductility in terms of ε_f were measured, the calculated gauge length in equation (1-9) correlated very well with the interparticle spacing of the non metallic inclusions.

Also Rice and Johnson (11) developed a correlation between the critical C.O.D. and the inclusion spacing. Their model is based on a slip line field theory, where void growth will occur when the void sites are enveloped by the highly strained region close to the crack tip, the process zone, and the correlation between C.O.D. and inclusion spacing, X_o, was found as

$$C.O.D._i \sim 1.0 \text{ to } 2.7\ X_o \tag{2-39}$$

where the coefficient is determined by the true strain to failure. However, Green and Knott (52) applied the same type of analysis in work hardening materials and concluded $C.O.D._i$ to be in the range .5 to 2.5 X_o depending on the initial void radius. Further, expression (2-39) reflects the size of the process zone.

As voids grow in the highly strained region close to the crack tip. Thomason (45) developed a void growth and coalescence model where an array of initially square holes in the matrix were assumed.

During the deformation, the ligaments between the voids are elongated, the voids grow, and at a critical stage internal necking occurs in the ligament between the blunted crack tip and a nearest void. The ligaments are deformed similar to a plane strain tensile sample and the limiting strain is related to the volume fraction as

$$\varepsilon \propto V_f^{-\frac{1}{2}} \tag{2-40}$$

In Thomason's model where plane strain of the matrix is assumed, the transverse void growth is small compared with the extensional growth. Further, he suggested that the growth occurred very close to the crack tip, and a confirmation of this assumption was found in a high sulphur mild steel. If the ductile fracture is initiated away from the crack tip, the model has to be modified due to any effects of the stress state.

A similar analysis of void growth is given by Brown and Embury (46) where the true strain to failure, ε_f, is related to the volume fraction, V_f of second phase particles and shows the same tendency of dependence between ε_f and V_f as in Thomason's model.

Further, Green and Knott (52) applied the dependence of strain to failure and volume fraction to relate the critical opening displacement to the volume fraction, when an expression of the type (1-9) was assumed.

As the interparticle spacing (gauge length) was inverse proportional to the volume fraction, the critical opening displacement seemed to be a function of the interparticle spacing or the volume fraction only, given as

$$C.O.D._i \approx \beta X_o \ln X_o \qquad (2\text{-}41)$$

where β is assumed a constant value and X_o is the interparticle spacing.

However, the void growth and coalescence may depend on the shape and distribution of void sites which may affect the local stress and strain field, and must be included in a further detailed study of the limiting processes in the process zone at the crack tip prior to crack extension.

One of the important metallurgical objectives of this thesis was to examine the nature of the events occuring in the process zone and to attempt to relate the influence of various microstructural constituents to the levels of stress and strain attained in the process zone. The approach cannot be too rigorous because it involves the specification of various limiting processes, e.g. void nucleation at inclusions or carbides, or the onset of localisation of the deformation process.

In order to correlate the fracture resistance in terms of G_c and the microstructural parameters of the material, one must examine the individual terms involved in equation (1-5) given as

$$G_c = \sigma \times \delta_{crit} \tag{1-5}$$

Of importance here is to quantify the meaning of a critical stress σ in terms of the deformation history of the process zone and to describe the opening displacement δ_{crit} in terms of a strain required for some defined physical process, and the volume of material (related to the gauge length) over which these critical strains are exceeded.

Thus in the latter part of this thesis a semi quantitative model is developed for the description of the process zone in both 4340 and H.S.L.A. steels and in some simpler plain carbon steels with well described microstructures.

CHAPTER 3

MATERIALS AND EXPERIMENTAL TECHNIQUES

This chapter describes the composition and structure of the materials used in this study, and the test methods used in the small scale fracture toughness testing.

3.1 Materials

Two types of steel were utilized in the present work. These were

1) A low carbon controlled rolled H.S.L.A. (High strength low alloy) structural steel $\sigma_y \sim 500$ MPa.

2) Samples of AISI 4340 quenched and tempered steel which were tempered at different tempering temperatures to produce a variation of the yield stress level.

3.1.1 H.S.L.A. steels

Increasing interest for steels of enhanced yield strength combined with high fracture resistance both to brittle, cleavage, and ductile tearing has led to the development of the high strength low alloy structural steels which are being utilized for bridges, structures and for arctic pipelines.

The structural steels used in this study were controlled rolled. The strength of such steels is achieved from a combination of grain refinement, plus precipitation strengthening (53), and the basic microstructures may be either polygonal or acicular ferrite. However, as shown in Fig. 3.1, non ferritic phases such as martensite/austenite constituents and carbide aggregates may also be produced, and these may strongly affect the fracture behaviour and properties. The cementite precipitates may appear along the grain boundaries of the ferrite, while the presence of the martensite austenite constituents (M/A) may depend on the mode of ferrite nucleation and morphological development. If the ferrite is nucleated at the elongated prior austenite grain boundaries, the final structure appears to be banded with the M/A phase oriented parallel to the rolling direction. See Fig. 3.1-3.4. The fracture resistance measured in terms of the maximum Charpy V-notch energy or the CVN shelf energy is observed to be strongly dependent on the amount and distribution of both the M/A phase and the non metallic inclusions, and those differences may be reflected in the fracture mechanics parameters.

The basic compositions and hot rolling schedule of the H.S.L.A. steels are given in Table 3.1.

During the hot rolling process, the sulphides, mainly MnS, are deformed to a platelike or stringerlike shape which may affect the directionality of the mechanical properties. Thus one of the steels was treated with Ce, in order to control the shape and character of the sulphide inclusions. Previous work indicates that the toughness, in terms of the CVN shelf value, is considerably increased in the transverse direction where rare earth elements are added (54). Although the sulphides become more globular due to rare earth treatment, there may be

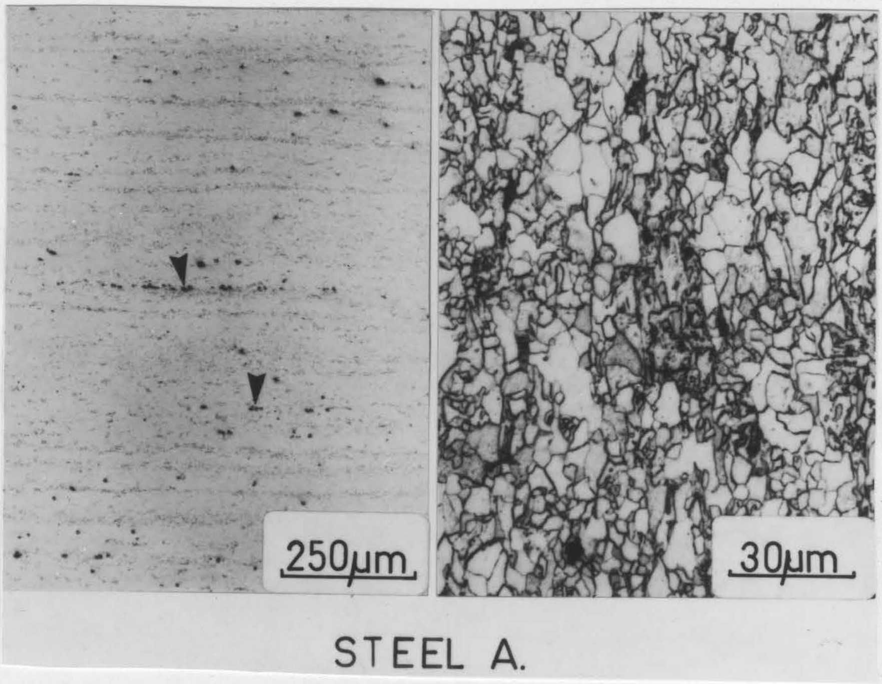

Fig. 3.1 Micro structure of Steel A.

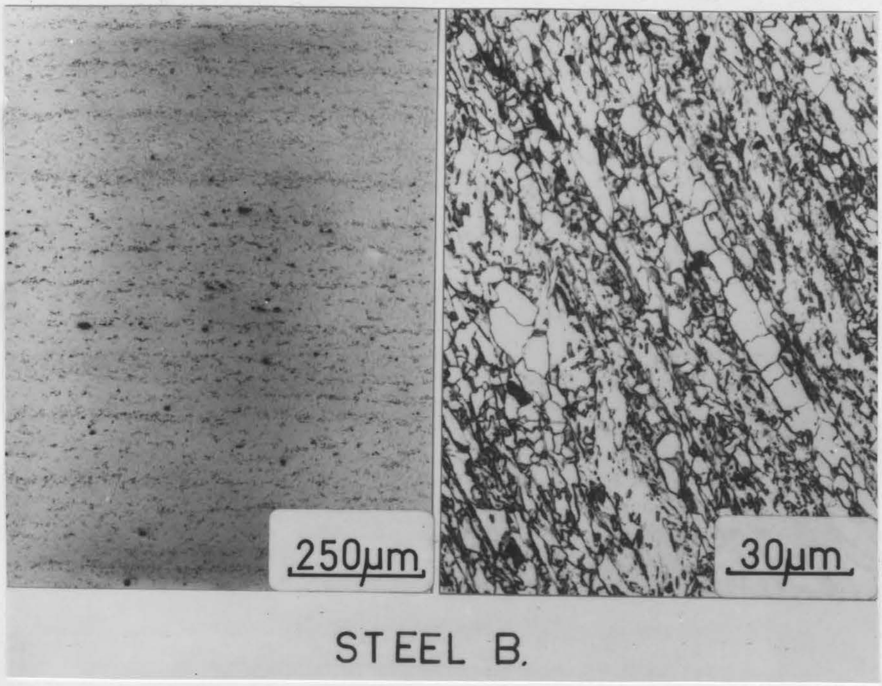

Fig. 3.2 Micro structure of Steel B.

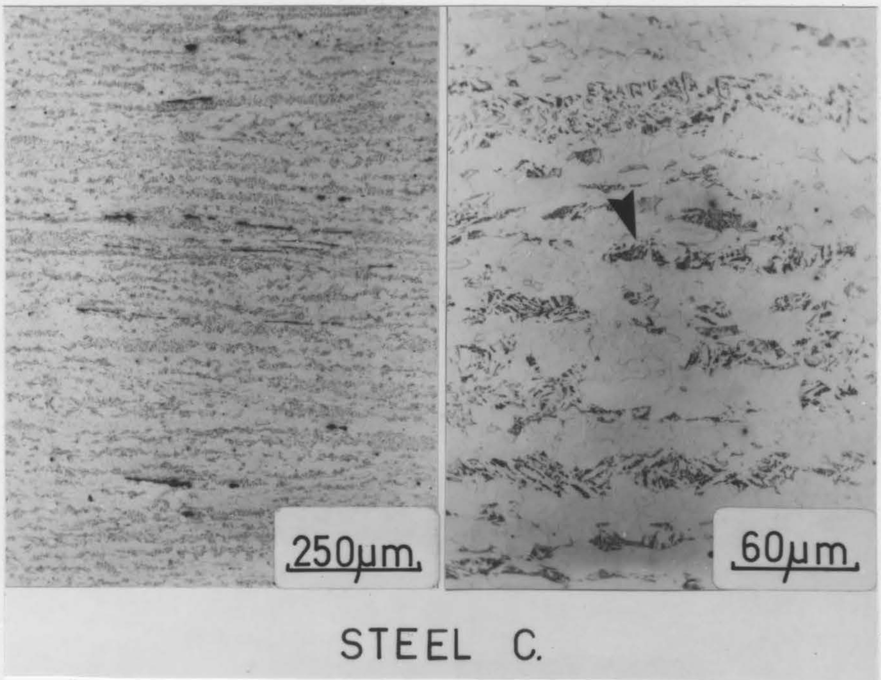

Fig. 3.3 Micro structure of Steel C.

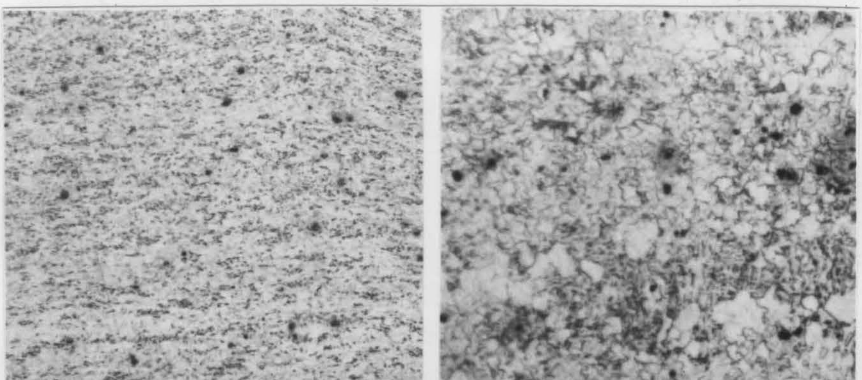

Fig. 3.4 Micro structure of Steel D.

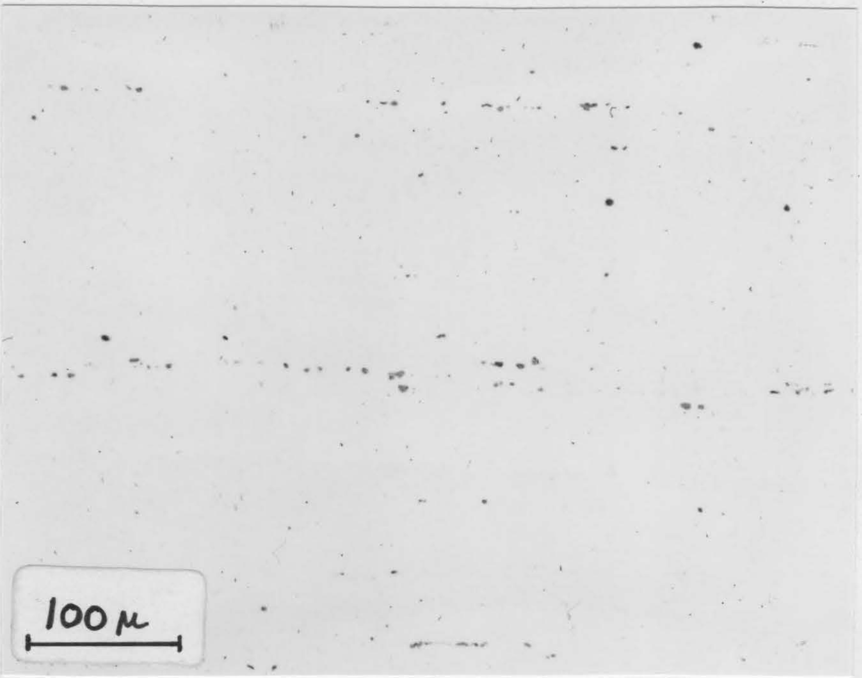

Fig. 3.5 Clusters of globular sulphides.

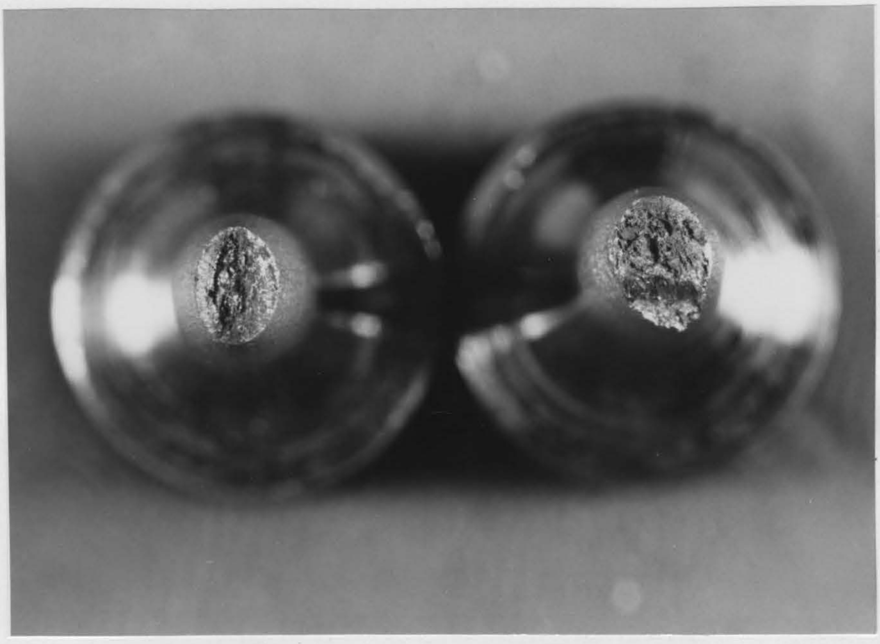

Fig. 3.6 Fracture surface of tensile samples of steel D of the H.S.L.A. steels in the longitudinal and transverse direction.

	C	P	S	Mn	Si	Nb	Mo	Al	Ce	Ni	Rolling Practice
STEEL A	0.05	0.006	0.017	1.92	0.07	0.06	0.32	0.32	0.03	0.022	Reheat temperature 1130°C 75% reduction below 840°C
STEEL B	0.05	0.009	0.007	1.98	0.30	0.06	0.55	0.04	0.004	0.22	Reheat temperature 1140°C 55% reduction below 840°C
STEEL C	0.05	0.003	0.018	2.08	0.23	0.06	0.41	-	-	0.24	Reheat temperature 1175°C 55% reduction below 790°C
STEEL D	.06	-	.009	1.76	.25	.056	.44	-	-	-	Reheat temperature 1175°C 50% reduction below 800°C

Table 3.1 Composition and Rolling Practice

	Tensile orientation	σ_y (MPa)	σ_{UTS} (MPa)	Fracture strain
Steel A	L	476	613	1.1
	T	461	589	1.2
Steel B	L	507	709	0.9
	T	500	639	0.8
Steel C	L	506	732	NA
	T	465	685	0.6
Steel D	L	465	775	1.1
	T	495	775	1.05

Table 3.2 Tensile Properties at Room Temperature of H.S.L.A.

regions containing numerous globular sulphides produced as shown in Fig. 3.5.

The presence of elongated sulphides may affect the fracture behaviour of an initially round tensile specimen as shown for steel D. See Fig. 3.6. The tensile fracture surface has an ellipsoidal form due to decohesion of the matrix sulphides interface. The tensile properties of the four H.S.L.A. steels are summarized in Table 3.2.

3.1.2 Quenched and tempered AISI 4340

4340 is a low alloy carbon steel often preferred for components where high strength, high hardenability, and uniformity of structure, are desired (55). It is a typical quenched and tempered steel, which is austenitized, then quenched to martensite (oil quench) followed by subsequent tempering to increase the ductility of the material and lower the yield strength. By varying the tempering temperature the yield strength can be changed for the same base material.

In this work the austenitizing treatment was kept constant to avoid any of the controversial effects due to variations in retained austenite reported previously in the literature (56). To avoid decarburizing during austenitizing, the samples were sealed in quartz tubes containing inert gas atmosphere, and the tubes were broken at the time of quenching to have as fast cooling as possible. The holding time for the austenitizing of the 10 x 10 mm cross section bend specimens was 20 min. The subsequent tempering was done in saltbaths for one hour followed by air cooling. Basic composition heat treatment and tensile data are summarized in Table 3.3, and microstructure of lowest and highest tempering temperature shown in Fig. 3.7 and 3.8.

Composition

Vol. %	C	Mn	Si	P	S	Cr	Ni	Mo	Cb
min.	.38	.65	.2				1.65	.2-	.056
max.	-.43	-.85	-.35	.04	.04	.7	-2.0	.3	

Heat treatment and tensile properties

Austenitized at 870°C for 25 min, oil quench, tempered at various temperatures	Tempering temp. (°C)	260	370	450	540	605	650	680
	Yield stress σ_y(MPa)	1560	1500	1380	1140	1030	820	805
	True strain to failure, ε_f	.29	.31	.38	.49	.56	.61	.76

Table 3.3 AISI 4340

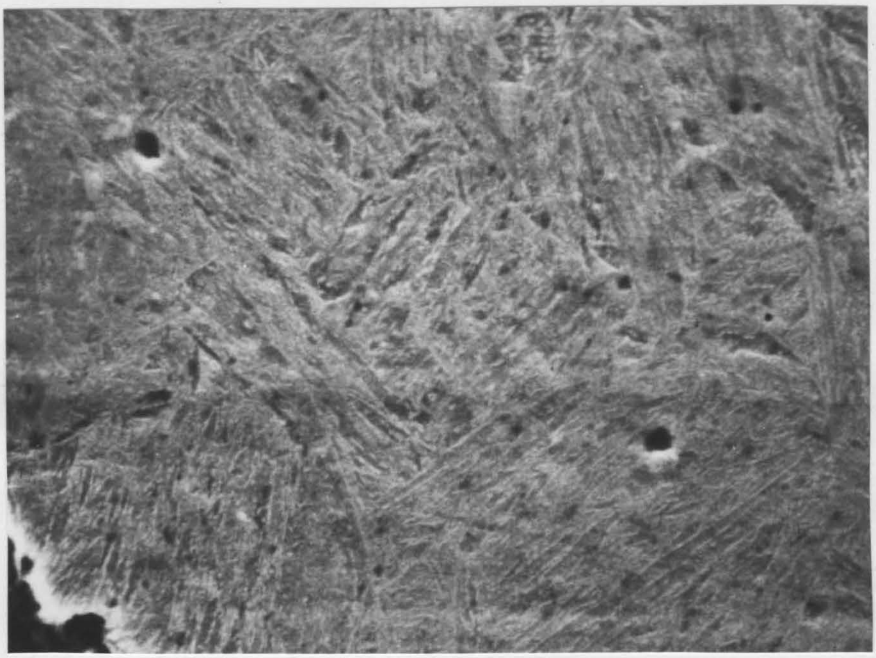

Fig. 3.7 Micro structure of 4340, tempering temp. 260°C.

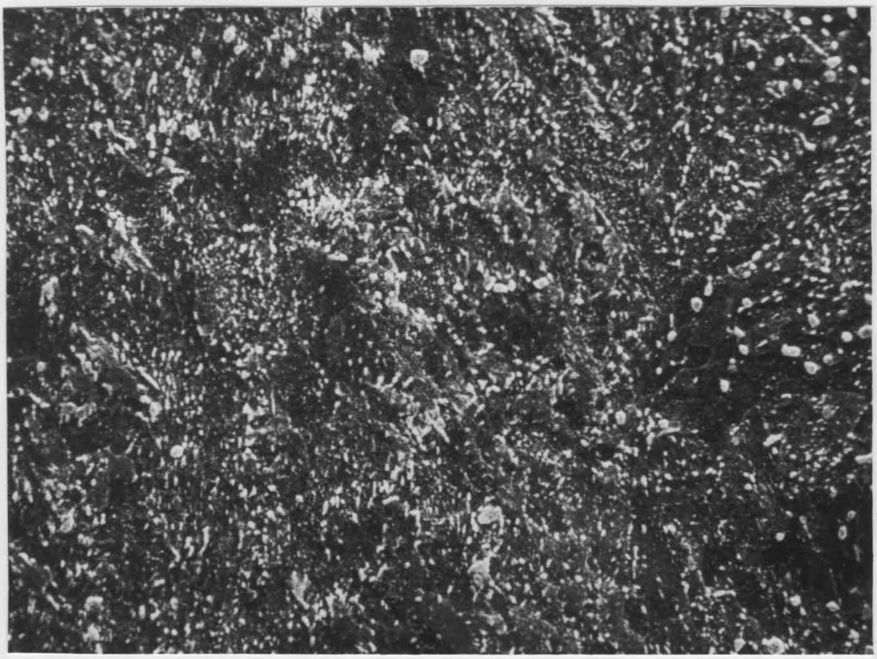

Fig. 3.8 Micro structure of 4340, tempering temp. 680°C.

3.2 Experimental Methods

3.2.1 Test samples

Bend type specimens were used for the small scale fracture toughness testing where the basic size was chosen to be the standard Charpy V-Notch impact specimen with cross section of 10 x 10 mm, initial notch depth 2 mm and notch angle 45°.

To determine the effects of notch geometry in the small scale fracture mechanics tests, a variety of slot widths or root radii were produced to examine the range from samples with sharp precracking to slot width with $2r \sim 550$ μm.

The slots were made at the bottom of the machined notch sufficiently deep to have parallel sides and a clearly defined end radius. (See Fig. 3.9.) Tungsten wires of different diameters and a silicone carbide abrasive were used to prepare the notch of different radii.

In order to examine influence of sample geometry on the data, both C.O.D. and J-integral samples of different widths, thicknesses, and notch depth to sample width ratios were tested. In addition, C.O.D. measurements were done in samples of different notch angle. The maximum thickness of the samples was limited by the dimension of the bending rig used, and the maximum allowable load during testing was limited by the load capacity of the Instron machine.

The dimensions of the samples for the C.O.D. and J-integral testing are given in Table 3.4.

3.2.2 Design of the testing device

A four point bending rig of the type shown in Fig. 3.10 was used, which could easily be modified to a three point bending rig when necessary. The rig was designed to be mounted below the crosshead of the Instron, for testing at lower temperatures by immersion in baths of suitable liquids, see Fig. 3.11.

With a four point bending rig, a constant bending moment occurs between the two central load points. Thus identical stress fields are obtained at both notches in a double notch sample if the two notches are initially identical in depth and notch geometry.

3.2.3 Techniques used to determine fracture parameters

3.2.3.1 C.O.D.

In obtaining the C.O.D. values two techniques were used both of which appear to give consistent results and have relatively simple test procedures.

The two methods are:

1) Crack profile replicating technique*
2) Clip gauge method.

Both techniques are described in section 2.3.2.2.

3.2.3.2 J-integral

Development of a new simple test method for determining J-integral values

As the J-integral is considered as a fracture criterion and the data can be obtained in test samples which undergo extensive amount of plastic deformation, see section 2.3.3, several methods have previously been developed for determining J_{Ic}, the magnitude of the J-integral at crack initiation in plane strain conditions. These were reviewed in Chapter 2. However, even if the testing is based on the analysis of

*Kerr Citricone Silicone Rubber (Wash and Accelerator) was used. Available in Dental Supply Stores.

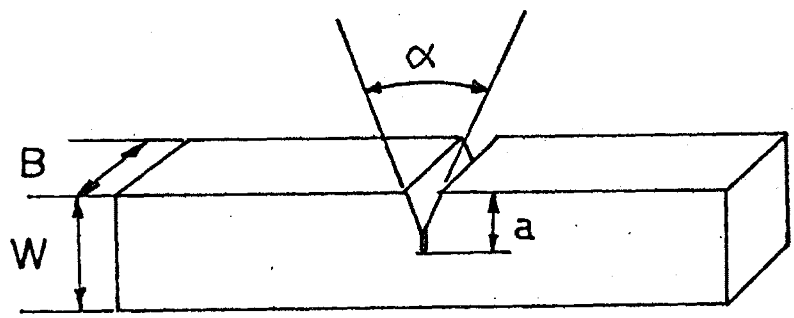

Fig. 3.9 Small scale bend sample.

Test type	$W_{(mm)}$	$B_{(mm)}$	$a_{(mm)}$	α	. -
C.O.D.	10	2-18	2.1-5.1	30-150°	four point bend
J_{Ic}	10-19.1	10-19.1	2.1-10	45°	three and four point b.

Table 3.4 Dimensions of the samples used.

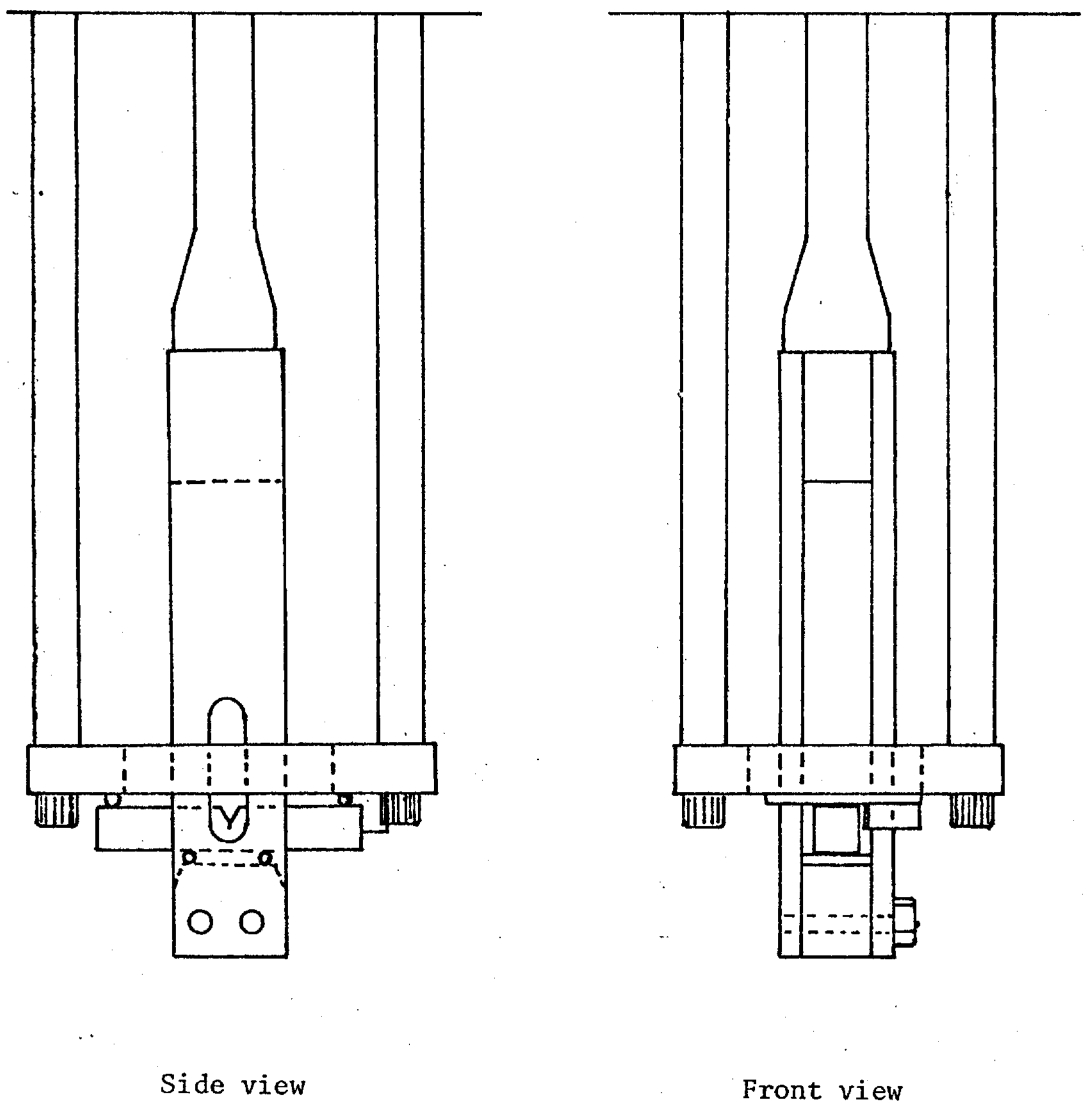

Fig. 3.10 Bending rig used during this study.

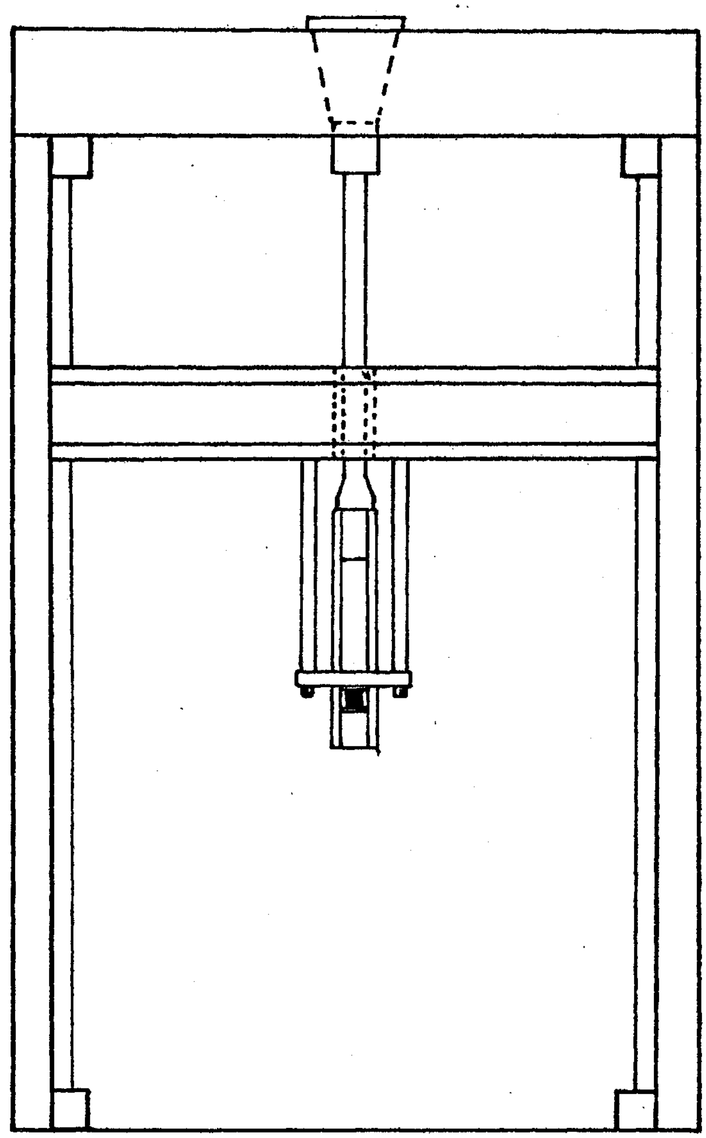

Fig. 3.11 The rig mounted on the cross head of the Instron machine.

Rice, of deeply notched bend type specimens where equation (1-8) is utilized, the currently available test methods require either the use of several samples or somewhat sophisticated electronic equipment for detection of crack initiation in a single specimen technique.

A much simpler method of detecting crack initiation was developed during the present work by utilizing the method of replication of the crack tip using silicone rubber developed by Robinson and Tetelman for measuring critical C.O.D. values. See section 2.3.2.2 The technique is outlined in Fig. 3.12. The method utilizes a single edge notch sample tested in bending. The crack tip can be replicated in the on load condition at any point, and the point of initial crack extension delineated from the replica profile. The J-integral in terms of J_{Ic} is then determined from equation (1-8) such as

$$J_{Ic} = \frac{2U}{Bb} \qquad (1\text{-}8)$$

U is the work done, the area under the load/load point displacement curve up to crack initiation, due to the presence of the crack only where the elastic energy for an unnotched test sample up to the load at crack initiation is subtracted.

During the curing of the silicone rubber, which takes 5-10 min., the load relaxes approximately 3% but this should not affect the determination of the point of crack initiation. The technique has the additional benefit that the replica profile yields a direct measure of C.O.D. at crack initiation.

As the value of J_{Ic} is equal to the energy release rate at crack initiation, G_{Ic}, even when a large amount of plastic deformation

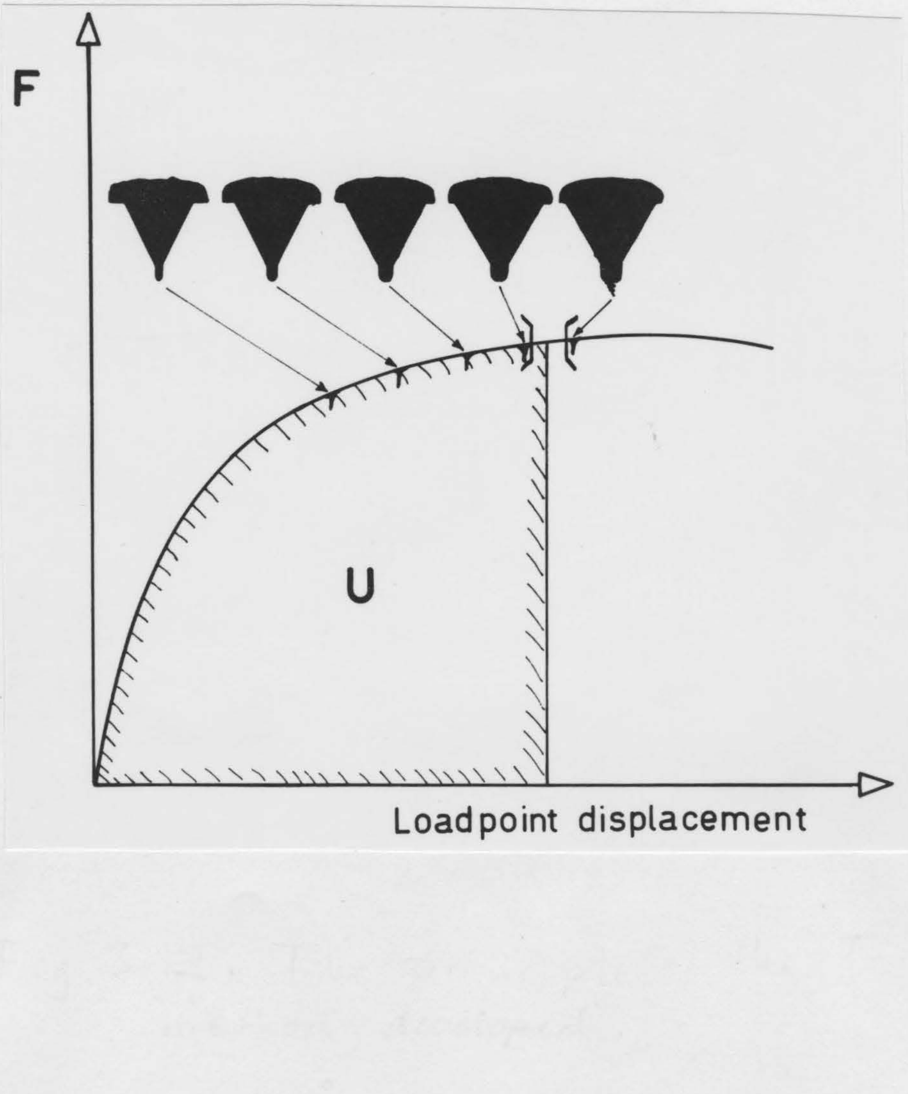

Fig. 3.12 The principle of the J-integral test method developed.

occurs before crack initiation, the plane strain stress intensity factor can be derived from the obtained values of J_{Ic} using relations such as

$$J_{Ic} = G_{Ic} = \frac{K_{Ic}^{2}(1-\nu^{2})}{E} \rightarrow K_{Ic} = [J_{Ic}\frac{E}{1-\nu^{2}}]^{\frac{1}{2}} \tag{3-1}$$

Thus in theory the data for J_{Ic} may be used for design problems and not only as a comparative material parameter.

The load point displacement was measured directly by use of a simple extensometer mounted at the base plate of the bending rig. See Fig. 3.13. The displacement measured at point A in Fig. 3.13 represents the displacement between the load points, and the load/load point displacement curve obtained. It will then exclude any eventual effects due to the stiffness of the machine between the bending rig and the load cell.

Further, to prevent plastic deformation at the load points, small blocks of very high strength material with large radius of curvature were used at the load points. See Fig. 3.13. Thus the potential energy input will be consumed in the crack tip region only.

3.2.4 Experimental errors

Dimensional instability in the silicone rubber was investigated. However, the contraction during curing was observed to be less than 1% at room temperature and this effect can thus be ignored.

As the profile of the extended crack is not uniform, at least four sections of the total crack profile from the plane strain region were examined to obtain the average C.O.D. value at crack initiation.

Where a clip gauge technique is used for measuring C.O.D. values, a consistent calibration curve must be obtained where the actual rota-

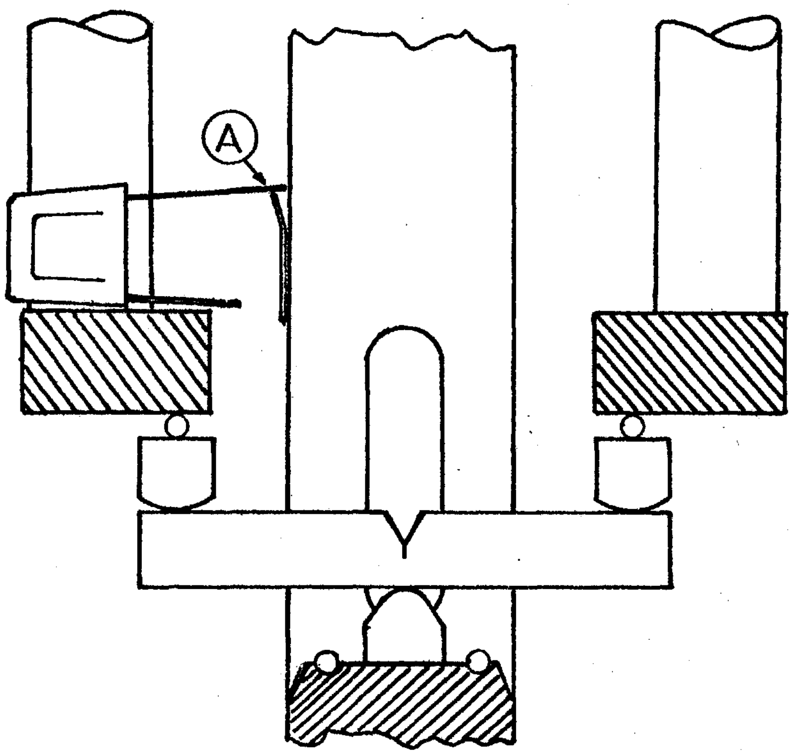

Fig. 3.13 Details of the bending rig. Load point displacement measured at point A.

tional factor r can be determined directly for a given clip gauge displacement V_g. See Fig. 3.14. As there is a limited amount of calibration data available, the data of r along the solid line drawn may in some cases deviate from the actual value of r, which leads to a different value of the critical C.O.D.

In terms of the validity of the magnitude of J_{Ic}, the actual value obtained depends on the distance between two subsequent replicated profiles made (See Fig. 3.15), since the work done, U, at crack initiation is determined as the area under the load/load point displacement curve up to the mid point between the last profile without the existence of an extended crack, and the first where the extended crack has appeared.

3.2.5 Metallographic procedures

The samples were polished down to .3μ, then etched. In this work both picral and nital etchants were used, and a combination of these seemed to give clearly visible microstructure. The picral etchant was first utilized with a final short time etch with nital. Both optical microscope and scanning electron microscope were used in obtaining the microstructures.

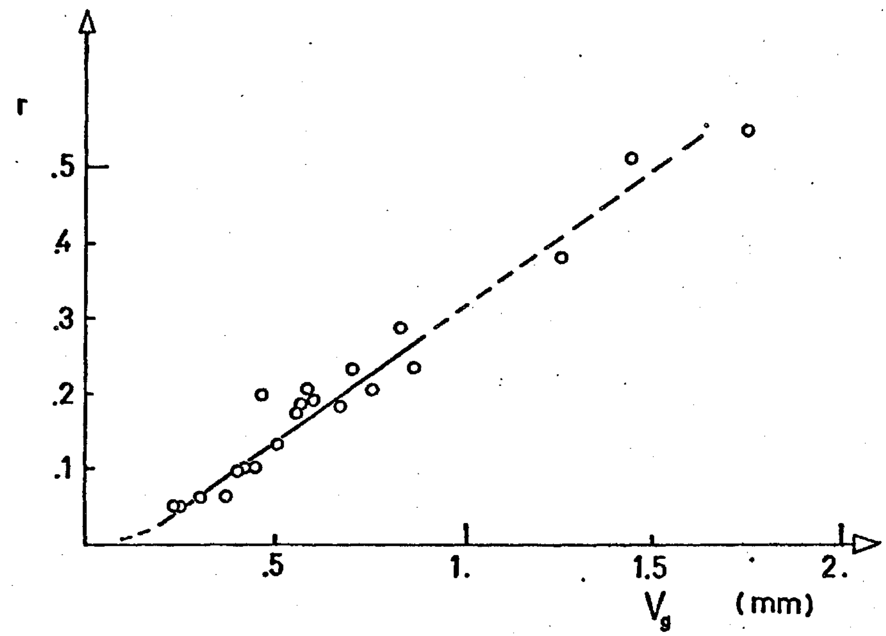

Fig. 3.14 Calibration curve r versus clip gauge displacement, V_g.

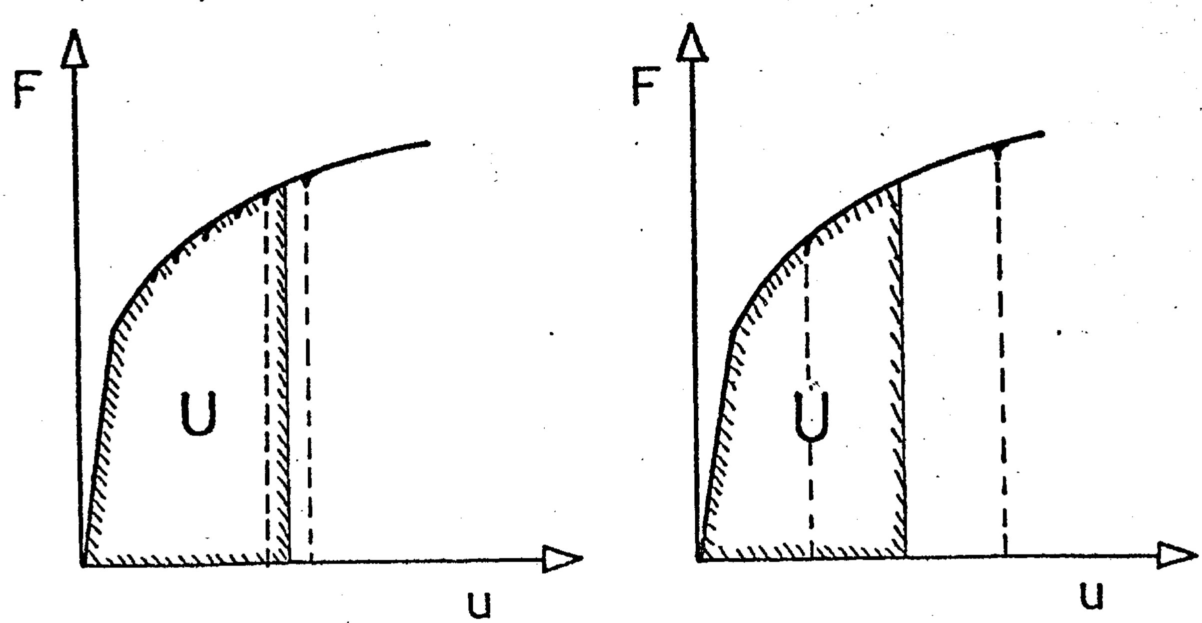

Fig. 3.15 The effect of no. of replicated profiles on the accuracy of the work done U up to crack initiation.

CHAPTER 4

RESULTS

As stated earlier in the thesis, the objectives of the present work included the development of small scale fracture toughness tests to obtain C.O.D. and J-integral data, the correlation of these data with more conventional tests, and the explanation of the toughness in terms of microstructural parameters.

Thus for clarity the chapter is divided into four subsections. The C.O.D. data obtained are presented in section 4.1, J-integral results in section 4.2, correlations with other toughness parameters in section 4.3, and the observations of the detailed microstructures of the crack tip regions for the different steels are described in section 4.4.

4.1 C.O.D. data*

In order to establish the utility of C.O.D. data, it is first necessary to determine the influence of sample geometry on the C.O.D. values. Thus in this study both the effect of notch root geometry and sample geometry were considered. One of the H.S.L.A. steels, steel D, was used for this part of the work using notches oriented in the T-L direction. See Fig. 4.1. The estimated material parameter is the C.O.D. at crack initiation obtained from an initially sharp crack, which in fully yielded samples, generally do not coincide with the C.O.D. at maximum load or instability. See Fig. 4.2.

*Obtained chart curves on the Instron, see Appendix I.

4.1.1 Effects of Geometry

4.1.1.1 Notch root geometry

The C.O.D. data at crack initiation vary with slot width as shown in Fig. 4.3. Above a certain slot width, the C.O.D.$_i$ value increases with increasing slot width. However, below the critical slot width, $2r_c$, the C.O.D.$_i$ seem to be independent of the geometry of the notch. This minimum value appears to be the critical material parameter. A sample containing a notch with $r < r_c$ will produce a C.O.D.$_i$ value which represents infinite sharp cracks, e.g. internal flaws in the material and is identical to that obtained for a sample containing a precrack sharpened by fatigue.

4.1.1.2 Influence of sample geometry

The following effects on C.O.D. were considered.

1) Thickness of specimen

Using samples with notch radius $r < r_c$, the C.O.D. values at crack initiation were measured as a function of sample thickness when the remained sample geometry was kept constant. See Fig. 4.4. The value at crack initiation is constant for sample thickness greater than about 5 mm thickness. Below the thickness of 5 mm, the C.O.D.$_i$ increases due to the change in stress and strain states. The data at maximum load or instability, however, show a more marked dependence on the thickness.

2) Angle of notch

From a slip line field theory (57), the plastic zone size in a non hardening material may be changed as the total included notch angle α is changed and which may affect the critical C.O.D. values. But within a range $30° \leq \alpha \leq 90°$, the initial C.O.D. for $r < r_c$ is constant. The 150° notch acts in a manner analogous to an unnotched beam where the

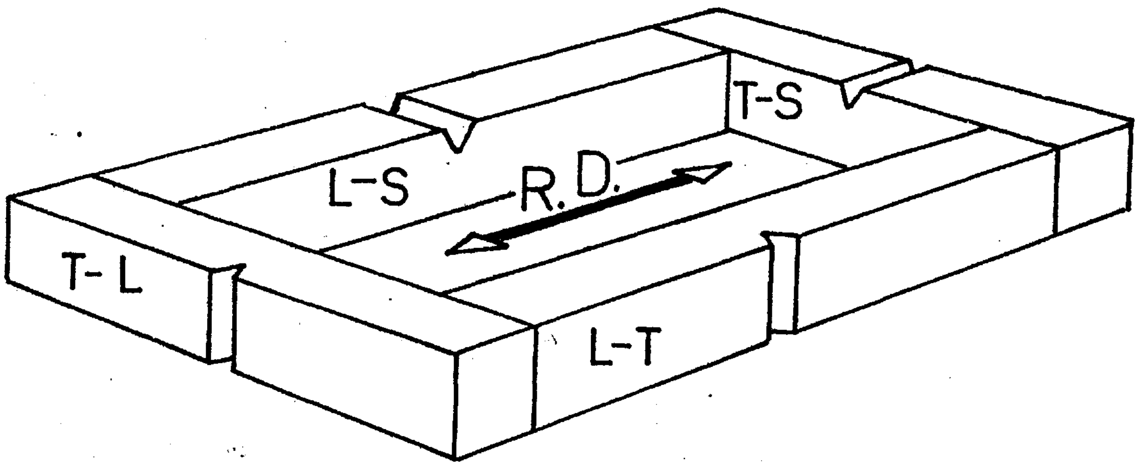

Fig. 4.1 The different orientations of the small scale test samples with respect to the rolling direction.

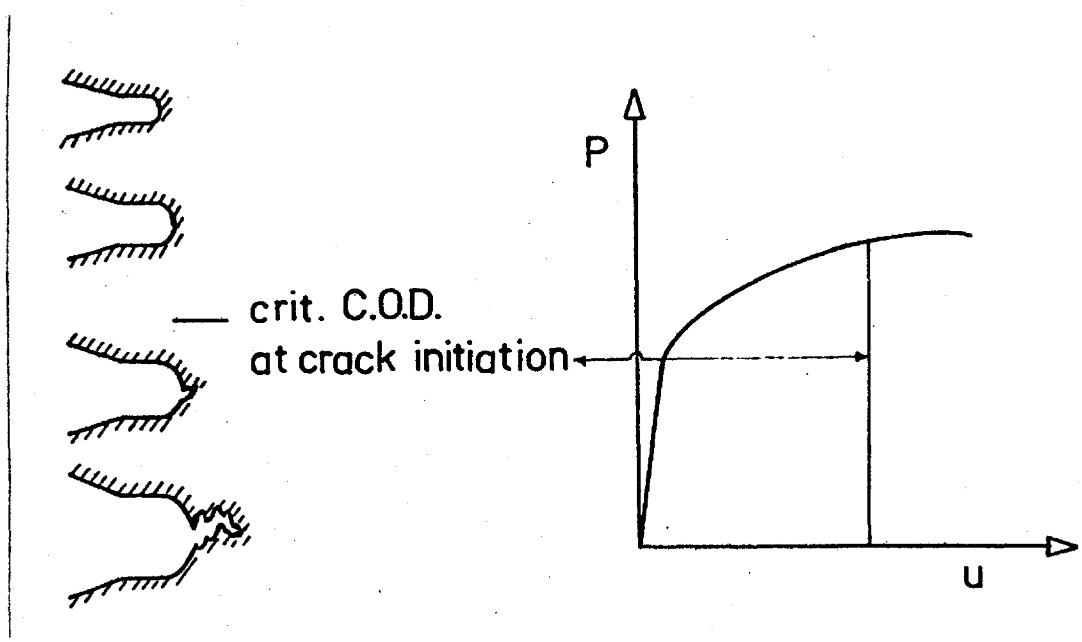

Fig. 4.2 The opening displacement at crack initiation in a general yielded test sample.

crack initiates at the corners instead of the mid region of the sample. Plane stress occurs and the minimum C.O.D.$_i$ value is higher. See Fig. 4.5. The notch depth to width ratio was .2 and all samples tested showed spread of yielding back to the upper surface of the sample.

3. Effect of the notch depth/width ratio

Deeper notches in specimens of fixed dimensions will reduce the size of the plastic zone around the notch because of the constraint of the surrounding material. In the samples tested for a given notch depth of 2 mm, general yielding occurs even up to the top surface. However, the results show that the C.O.D. data for samples with $r < r_c$ at crack initiation is independent of the notch depth, i.e. independent of the size of the plastic zone (See Fig. 4.6), while the opening displacement at maximum load varies with the sample geometry and reflects the size of the plastic zone.

4.1.2 Results of the materials tested

1) H.S.L.A.

The four different structural steels described in section 3.1 are investigated. One of the steels, steel A, is Cerium treated, and the specimens are machined in the transverse direction to the rolling with the crack propagation parallel to the rolling direction, i.e. T-L direction.

All the steels show the same behaviour with respect to the slot width, where the critical minimum C.O.D. value of steel A is nearly twice the one for steel C and D. See Fig. 4.7. Although there are only two data points available for steel B, these suggest that this steel

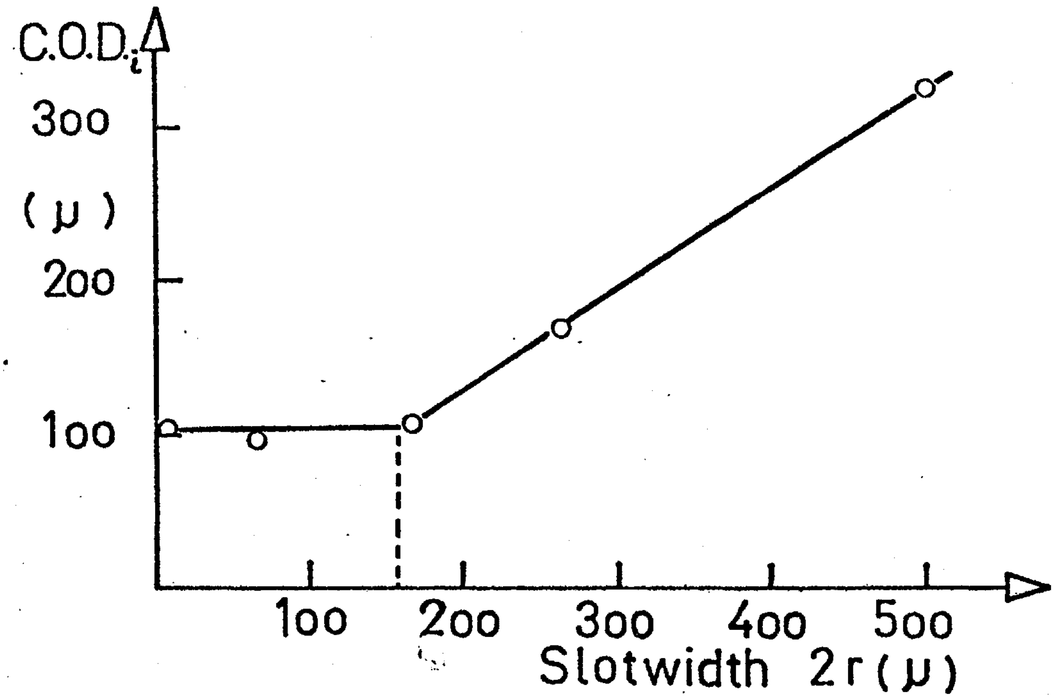

Fig. 4.3 C.O.D.$_i$ versus slot width, 2r.

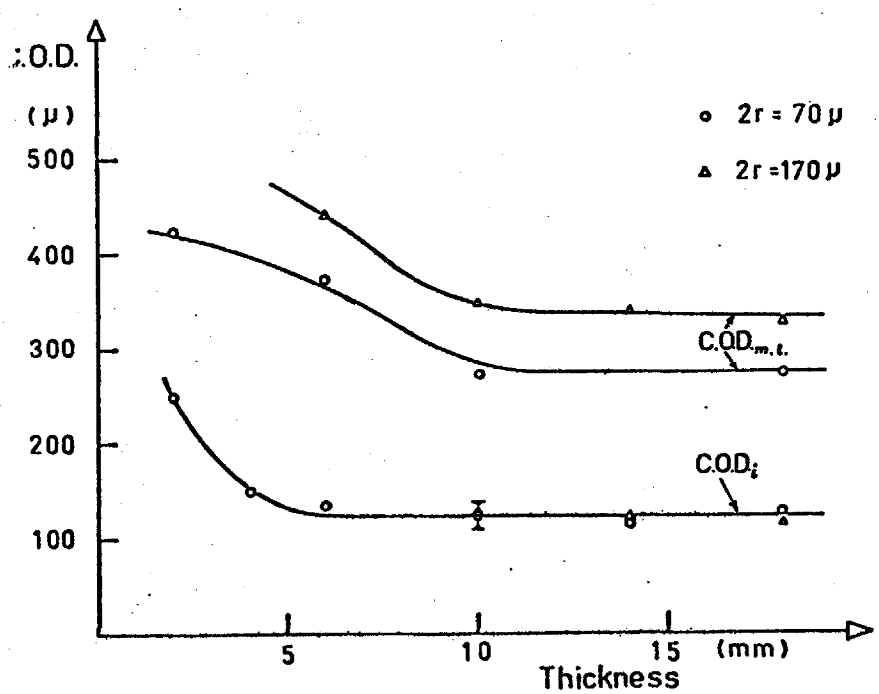

Fig. 4.4 Effect of thickness on C.O.D. data where remained sample geometry is fixed.

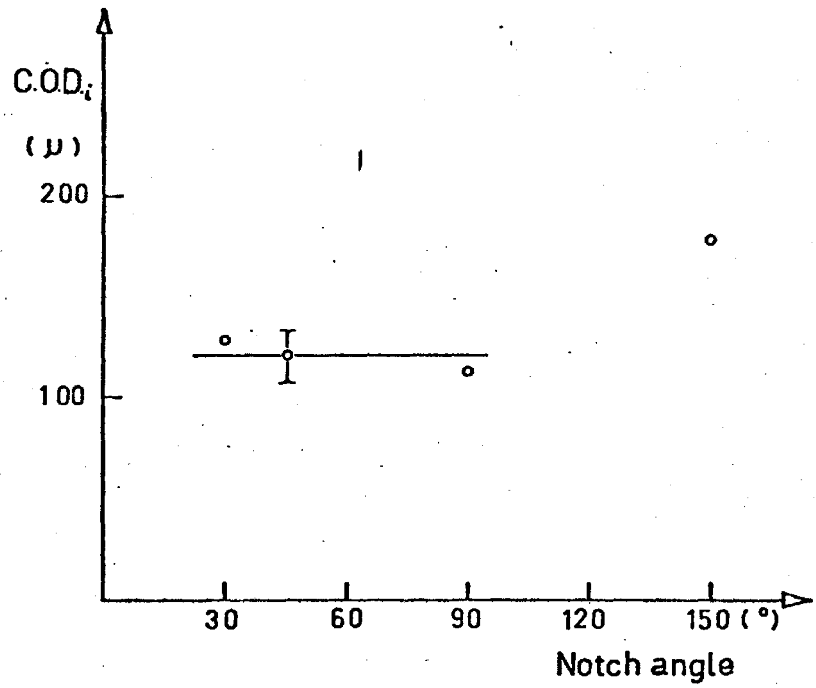

Fig. 4.5 Notch angle, α, versus minimum values of C.O.D. at crack initiation.

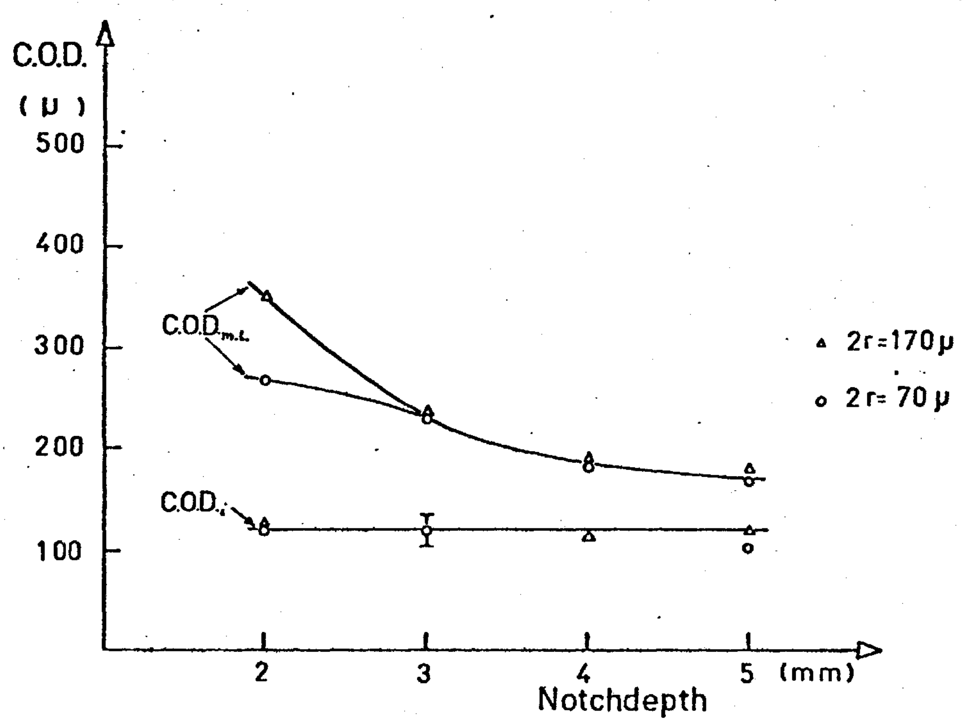

Fig. 4.6 Influence of the ratio notch depth/sample width.

will have approximately the same behaviour as the other H.S.L.A. steels, shown by the broken line in Fig. 4.7. Further, the slope of the curves where the critical C.O.D.$_i$ values are dependent on the notch root radius, increases with increasing toughness or minimum C.O.D.$_i$ value.

In addition, the effect of directionality, and thus inclusion geometry in steel D, is shown in Fig. 4.8 and Table 4.1. The critical value at crack initiation ($r < r_c$) in the L-T direction, is nearly twice the one obtained in the T-L direction. The two "crack arrest" orientations (i.e. orientation where delamination tends to arrest the crack) have approximately the same initial C.O.D. value as in the T-L direction. However, further crack advance is very slow, and the sample oriented in the L-S direction did not break during the test but showed extensive delamination parallel to the rolling plane. See Fig. 4.9. It acted almost as a laminated unnotched highly ductile beam.

2) AISI 4340

The critical opening displacement was measured in samples of 4340 tempered at various temperatures to give yield stresses in the range 805-1560 MPa. In the study of the behaviour of the 4340 samples, both clip gauge method and crack profile were used and shown to give consistent values.

Fig. 4.10 shows that the C.O.D. initiation values decreases with increasing yield stress in an almost linear manner.

The C.O.D. data at instability or maximum load conditions are only slightly higher than at crack initiation except at the lowest yield stresses. The C.O.D. at maximum load for the lower yield stress materials

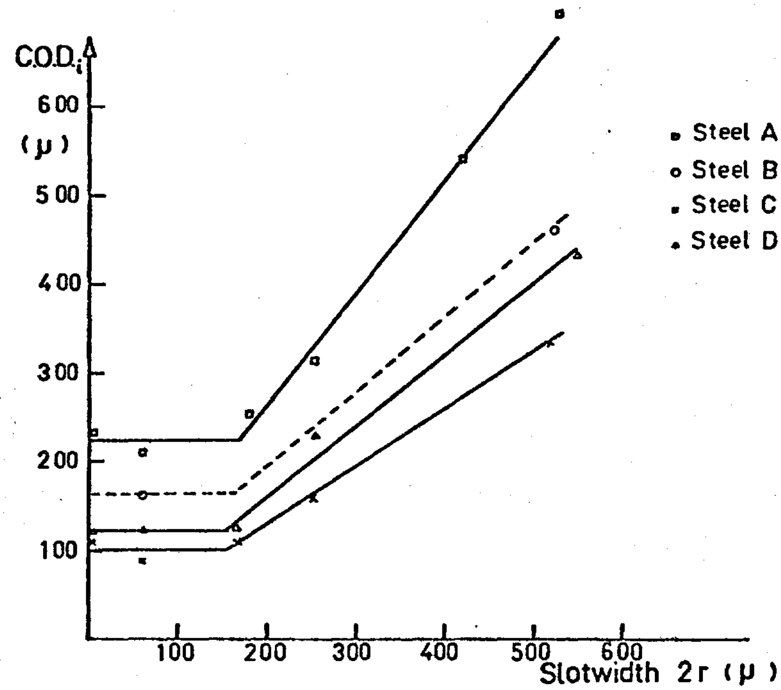

Fig. 4.7 C.O.D.$_i$ versus slot width of four H.S.L.A. steels, samples oriented as in the T-L direction.

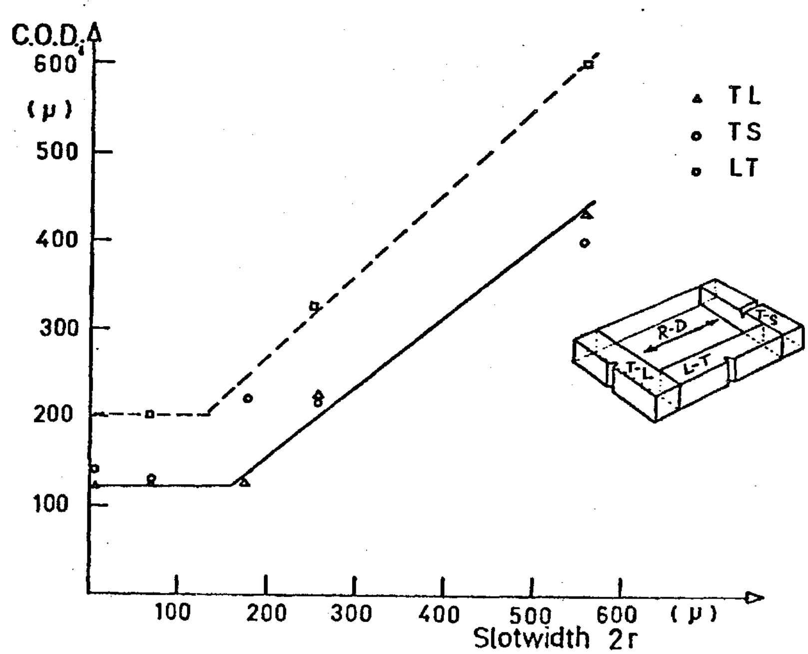

Fig. 4.8 Effect of directionality on the C.O.D.$_i$ data in steel D of the H.S.L.A. steels.

	T-L	L-T	T-S	L-S
$C.O.D._i$ (μ)	110	200	135	120

Table 4.1 Minimum values of $C.O.D._i$ in four directions of H.S.L.A., steel D.

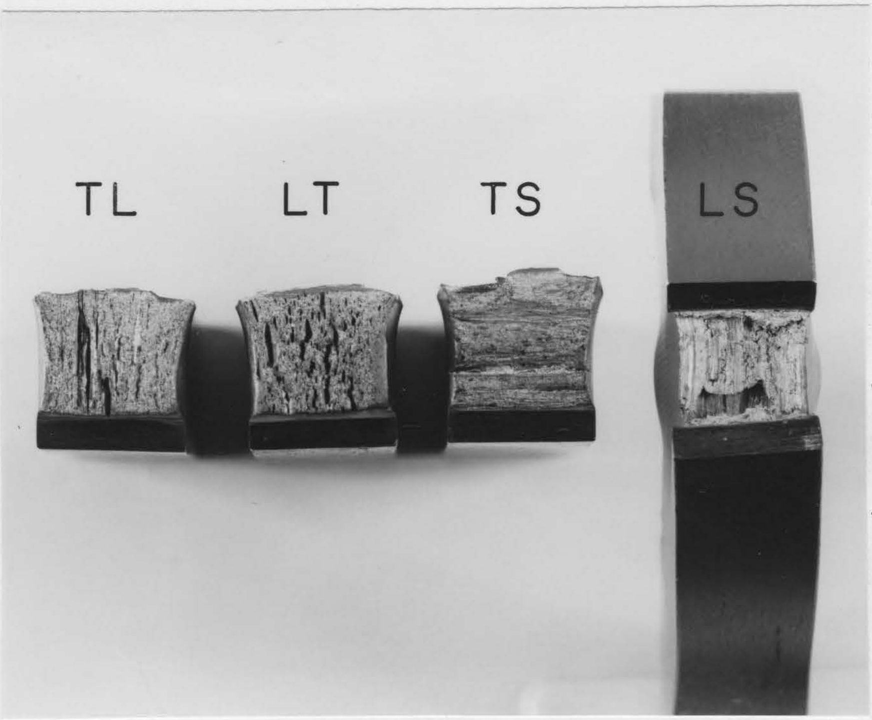

Fig. 4.9 Fracture surface of samples of steel D oriented in four directions.

are increased due to the higher ductility of the material, where a certain amount of stable crack growth is obtained before the attainment of the maximum load condition.

At three tempering temperatures the C.O.D. at initiation was measured as a function of slot width or root radius, where the critical slot width was found to be in the range 100-150 μ. Also the gradient of the C.O.D. versus slot width relationship was observed to increase with increasing tempering temperature, i.e. with decreasing yield stress. See Fig. 4.11.

4.2 Results of J-integral testing

In order to evaluate the test method developed in this study, tests were made to establish the influence of sample and notch geometry on the data obtained. Tests were conducted on samples of steel D of the H.S.L.A. steels and on 4340 tempered to various yield stress levels to determine the range of conditions under which valid J_{Ic} results could be obtained. The range of yield stresses is of interest in regard to the development of small scale fracture tests and their correlation with more conventional large scale test techniques.

Tests were conducted on samples with notches of various root radii shown in Fig. 4.12 which indicates that below a root radius of 75 μ, the value of J_{Ic} is independent of notch root geometry. This is similar to the influence of notch root radius reported by Knott and co-workers (10, 58) on C.O.D. and K_{Ic} values. Further tests on samples of different notch depths and sample width W revealed, as shown in Fig. 4.13, that the recorded values of J_{Ic} were constant for values of $a/W \gtrsim .41$.

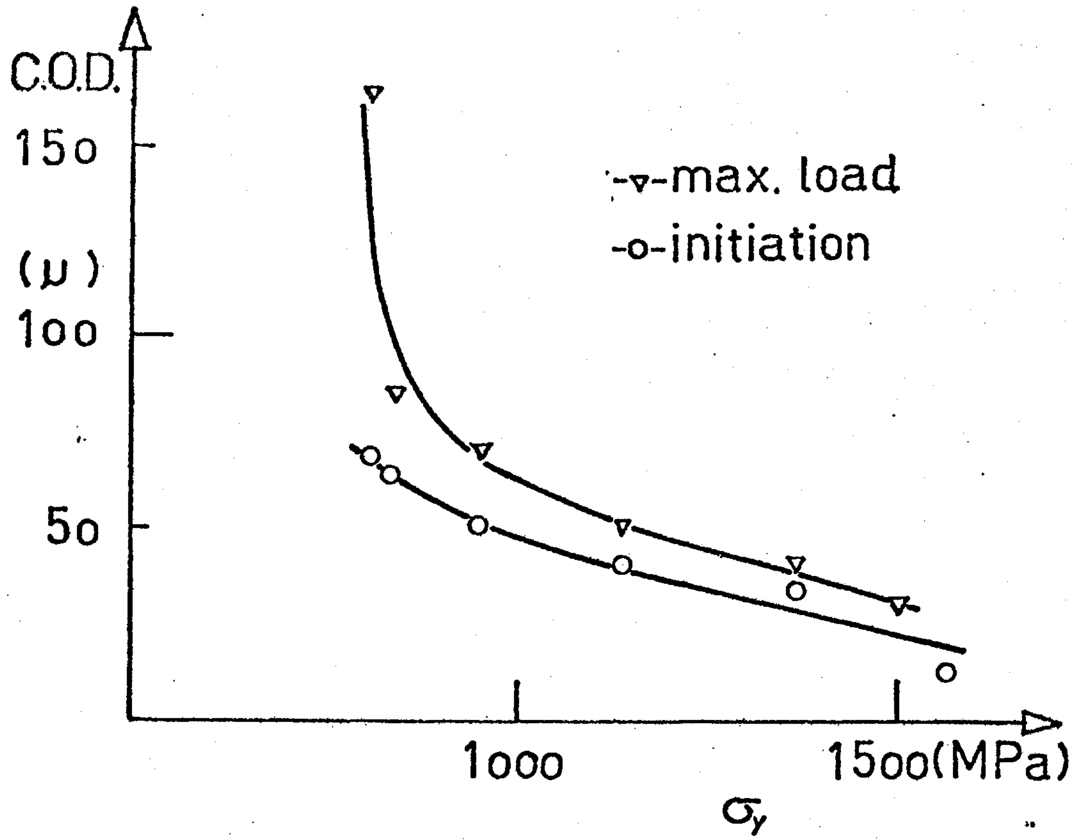

Fig. 4.10 The magnitude of C.O.D. as a function of yield stress in 4340 steel.

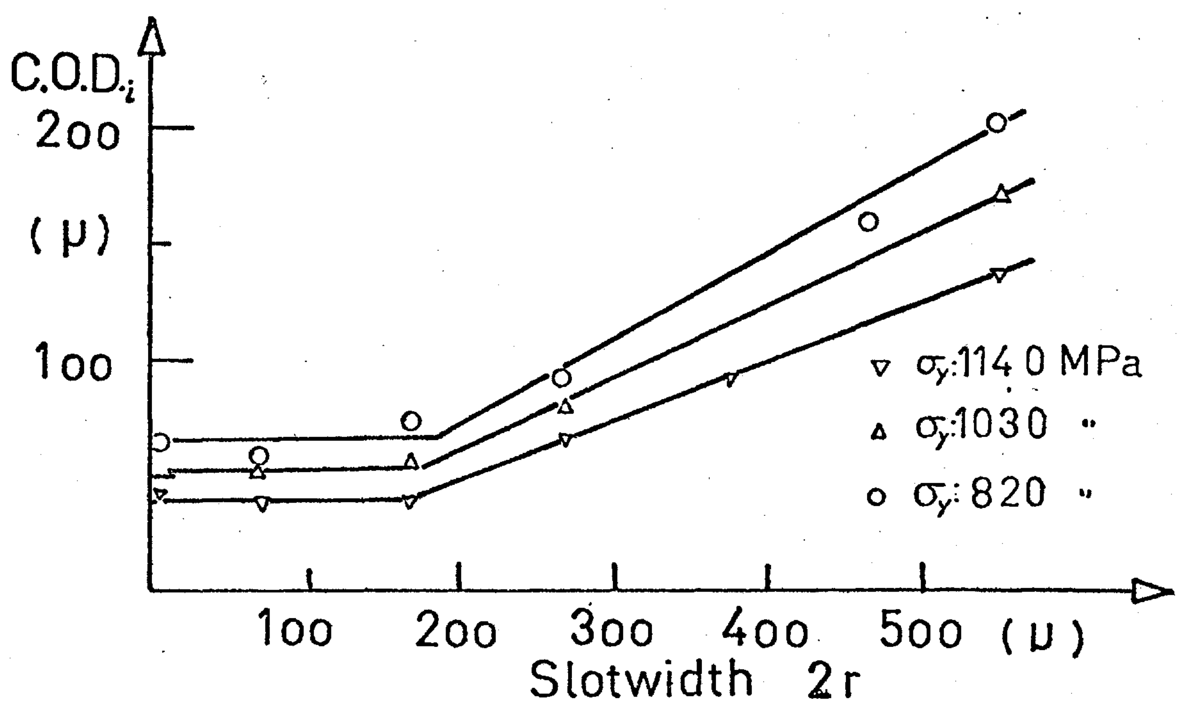

Fig. 4.11 C.O.D.$_i$ versus slot width for samples of 4340 tempered at three different temperatures.

Samples of 4340 in the form of notched bars 10 x 10 mm in cross section and with $a/W = .51$ were quenched and tempered to various yield strengths and tested to determine the values of J_{Ic}. The results are summarized in Table 4.2 together with values of K_{Ic} derived from equation (3-1). The results from the present work are compared with existing values in the literature in Table 4.2 and it can be seen that excellent agreement is achieved over the yield stress range 805-1560 MPa.

Finally, in order to determine the applicability of the simple method for determining J_{Ic} for the structural steels, tests were conducted on steel D of the H.S.L.A. steels. The estimated size requirements for J_{Ic} testing can be expressed as in equation (2-33) such as

$$B,\ b,\ a \geq \alpha \frac{J_{Ic}}{\sigma_{flow}} \text{ where } \alpha \sim 50$$

Thus a series of samples of various widths (W) and thicknesses (B) were tested using a notch depth to sample width ratio of $a/W = .51$.

The results are shown in Table 4.3 and indicate that consistent values of J_{Ic} can be obtained for low yield strength structural steels in small scale testing. In addition, J_{Ic} was obtained both in three point and four point bending and there is no difference in the values. See Table 4.3.

To see the size difference between the specimens used for J_{Ic} testing and the corresponding minimum size requirements of standard K_{Ic} fullscale ASTM samples, the data are compared in Table 4.4. These data shows the advantage of using J_{Ic} as a failure criterion especially in the higher toughness region and when a single specimen test is applied.

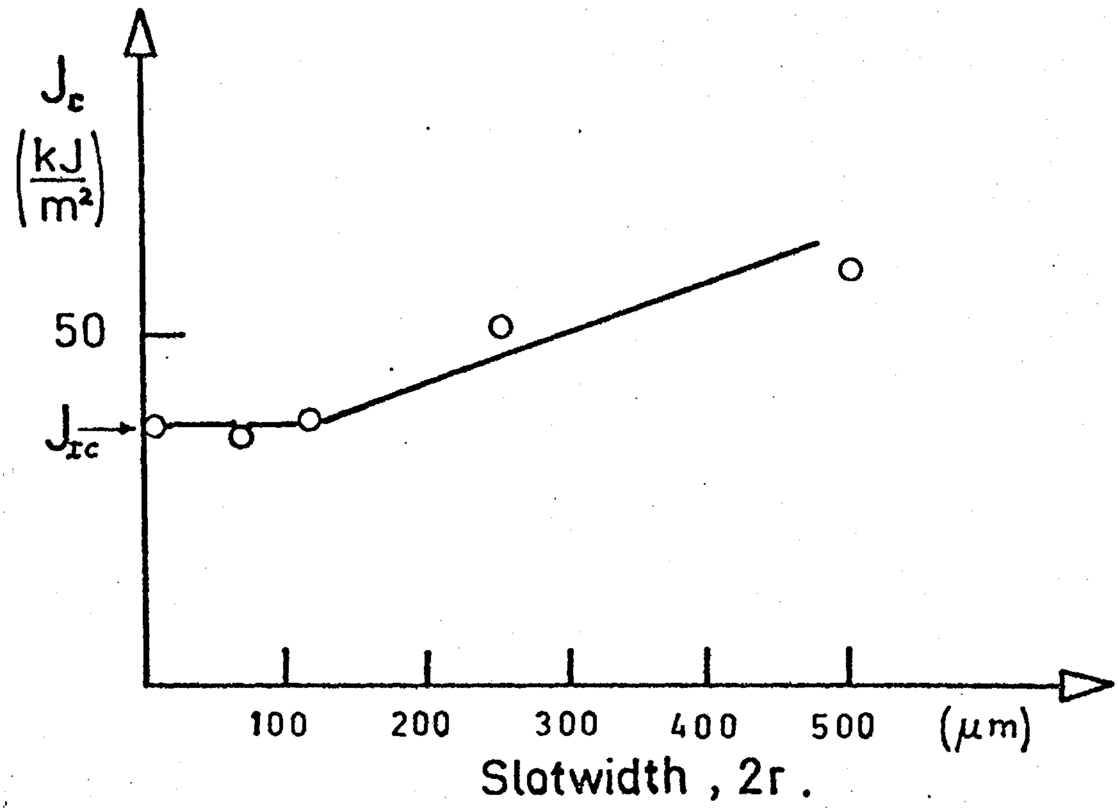

Fig. 4.12 Influence of slot width on the measured J_{Ic} values. The data was obtained from samples of 4340 tempered at 540°C.

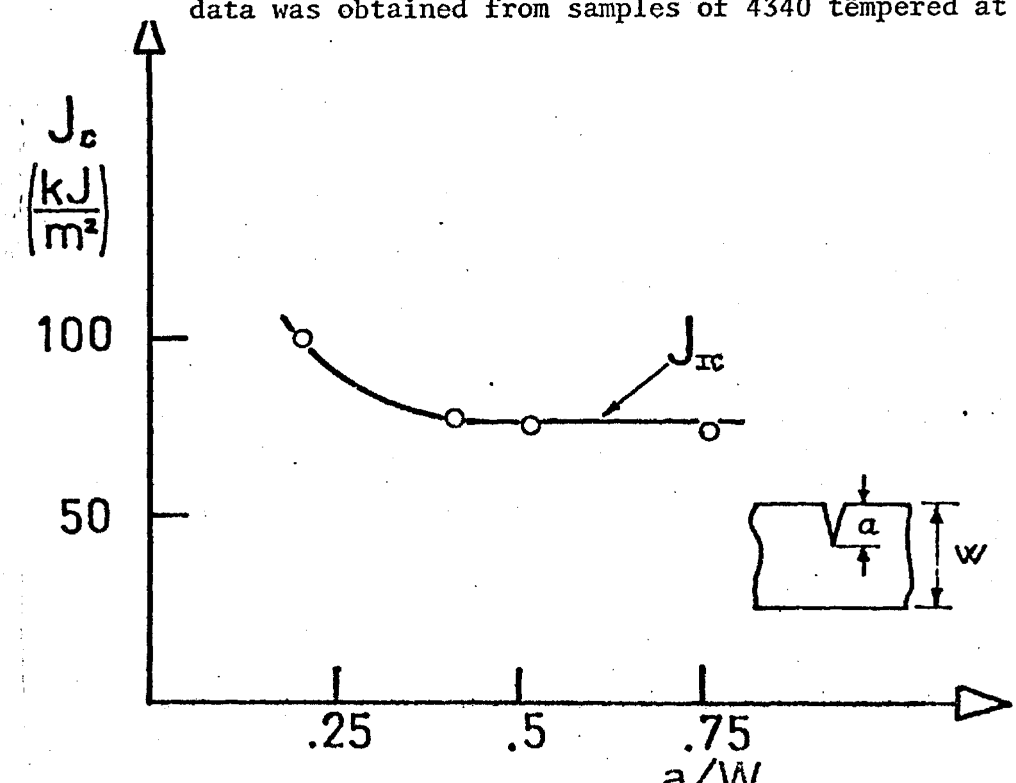

Fig. 4.13 Results showing the influence of the ratio of notch depth to sample width on the measured J_{Ic} values. The data was obtained in steel D of the H.S.L.A. steels.

Tempering Temp.	260°C	450°C	540°C	605°C	650°C	680°C
σ_y (MPa)	1560	1380	1140	1030	820	805
J_{Ic} (kJ/m^2)	15.5	23	37	44.2	59	64
K_{Ic} derived from J_{Ic} by eqn. 3 ($MNm^{-3/2}$)	59.5	74	95	101	115	120
K_{Ic} from literature ($MNm^{-3/2}$)	45 - 60 (1-2)	80 (3-4)	107 (5)	110 - 125 (2)	125 (6) *	130 (6) *

*Derived from C.O.D.$_i$ measurements.

Table 4.2

1) Fracture toughness testing and its applications, ASTM Special Technical Publication No. 381.

2) R.W. Herzberg, Deformation and fracture mechanics of engineering materials.

3) J.N. Robinson and C.W. Tuck, Eng. Fracture Mech., vol. 4, pp. 377-392, 1972.

4) G.E. Pellisier, Eng. Fracture Mech., vol. 1, pp. 55-75, 1968.

5) Standard ASTM.

6) J.N. Robinson and A.S. Tetėlman, Technical Report No. 11, UCLA-ENG-7360, Aug. 1973. University of California, Los Angeles, California, School of Eng. and Applied Science.

	3 point bend specimen				4 point bend
Width, W (mm)	10	19.1	19.1	19.1	10
Thickness, T (mm)	10	10	14	19.1	10
J_{Ic} (kJ/m^2)	78	78	83	82	79

Table 4.3 Influence of specimen geometry of bend specimen of H.S.L.A. tested in T-L direction. The T-L direction is such that the sample is cut perpendicular to the rolling direction and notched so that the crack propogates in the rolling direction.

	4340						H.S.L.A.
σ_y(MPa)	1560	1380	1140	1030	820	805	∿500
Min size B,b, for std K_{Ic} (mm)	3.6	7.35	18.5	24.6	46.5	52.5	180
Size of B,b, J_{Ic} samples tested (mm)	4.9	4.9	4.9	4.9	4.9	4.9	3.5-8
Ratio $\frac{b_K}{b_J}$	.75	1.5	3.75	5.0	9.5	10.75	22-50

Table 4-4

4.3 Correlations with other toughness parameters

As the most widely used toughness test is the Charpy V-notch impact, steel D of the structural steels was tested to obtain the characteristic Charpy curves in four different directions, shown in Fig. 4.14, and the maximum shelf values are compared with the corresponding data for minimum C.O.D.$_i$ in Table 4.5. The C.O.D. data for the two directions that did not show the crack arrest phenomena were then plotted in a diagram with the existing literature data of C.O.D.$_i$ in correspondence with the maximum shelf level CVN values in Fig. 4.15. The data are in excellent agreement with the existing literature values. However, some of the literature C.O.D. data are derived from the existing K_{Ic} values for some higher strength materials where it is assumed $G_{Ic} \sim 1.1 \times \sigma_y \times$ C.O.D.$_i$, and the data obtained may not be the correct C.O.D.$_i$ values.

4.4. Microstructures of the crack tip regions

In order to try to relate the microstructural features with the obtained data during small scale testing, the samples were sectioned and polished to show the eventual crack initiation and propagation in the material. The Figures 4.16-18 show the processes at three different tempering temperatures in 4340, Fig. 4.20-23 similarly the crack tip regions in four different directions for the tested H.S.L.A. steels. Fig. 4.24 and 4.25 show the crack tip regions in the T-L and L-S samples at higher magnification and Fig. 4.19 at high magnification of voids occurring at carbides in 4340 at 680°C tempering temperature. Fig. 4.26 and 4.27 show the sulphide morphology of steel D of the H.S.L.A. steels.

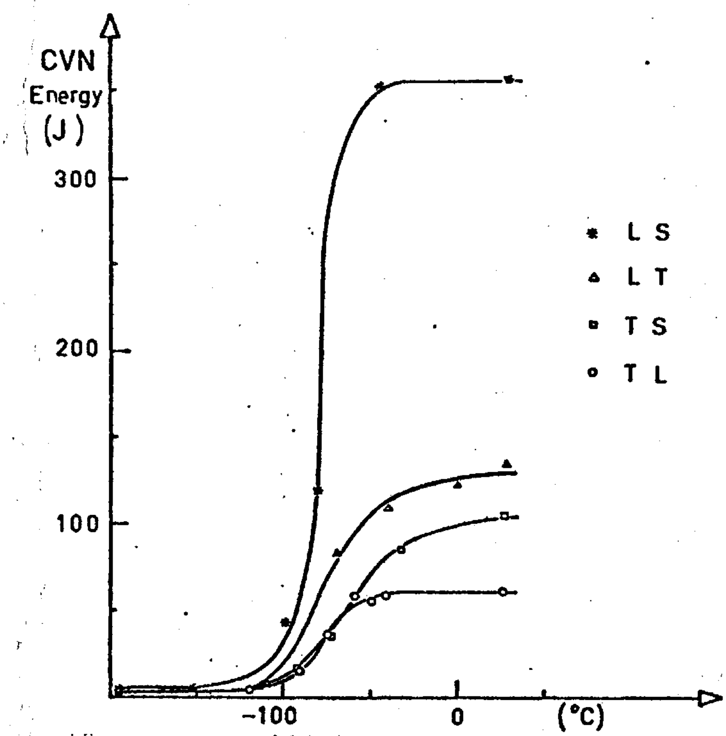

Fig. 4.14 Charpy V-notch impact data versus temperature for samples machined in four different orientations relative to the rolling direction.

	T-L	L-T	T-S	L-S
$C.O.D._i$ (μ)	110	200	135	120
CVN_{max}(J)	62	135	105	355

Table 4.5

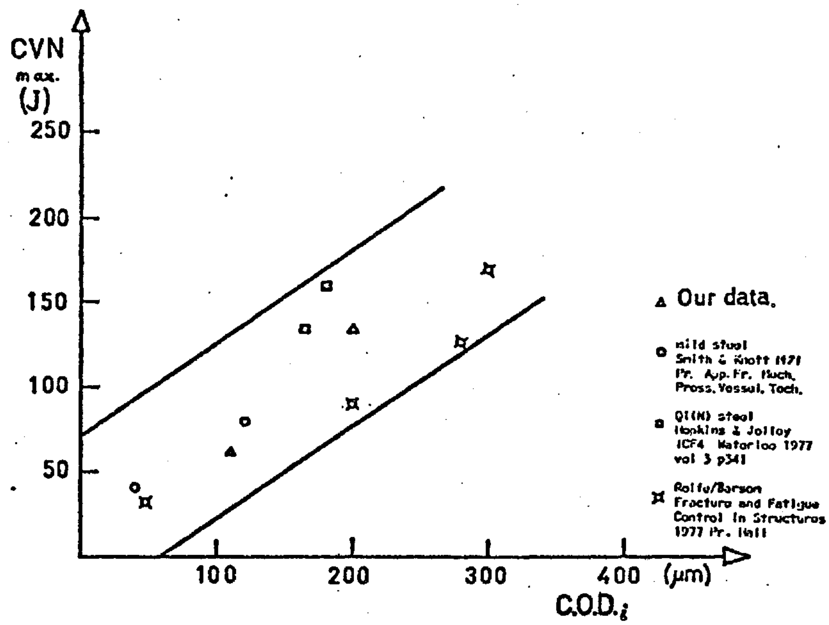

Fig. 4.15 Results of C.O.D.$_i$ versus CVN max value in steel D compared with existing literature data.

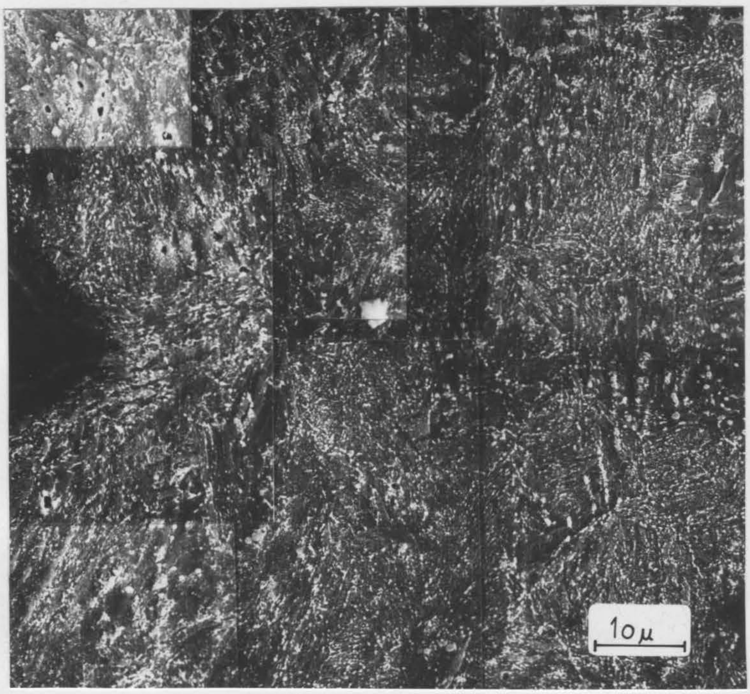

Fig. 4.16 4340 crack tip region, 680°C tempering temperature.

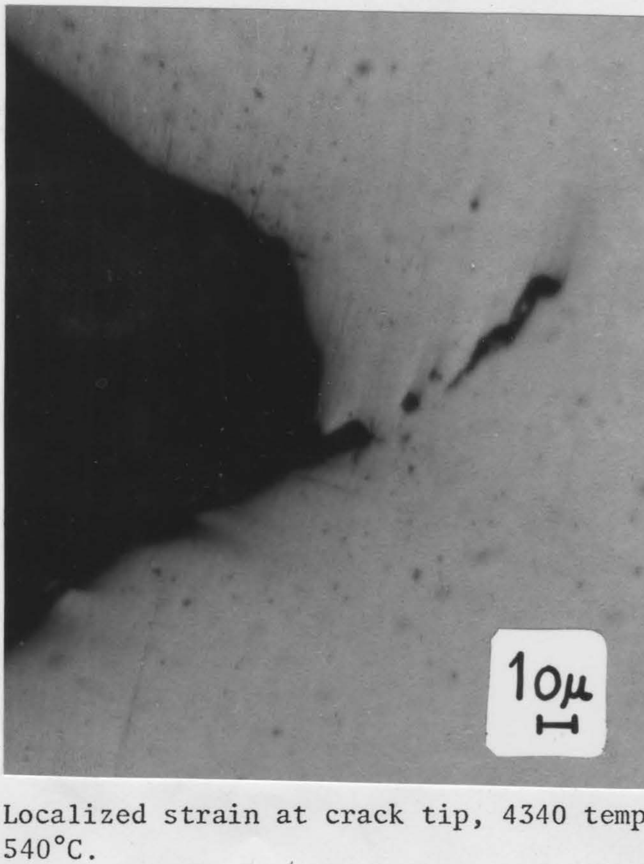

Fig. 4.17 Localized strain at crack tip, 4340 tempered at 540°C.

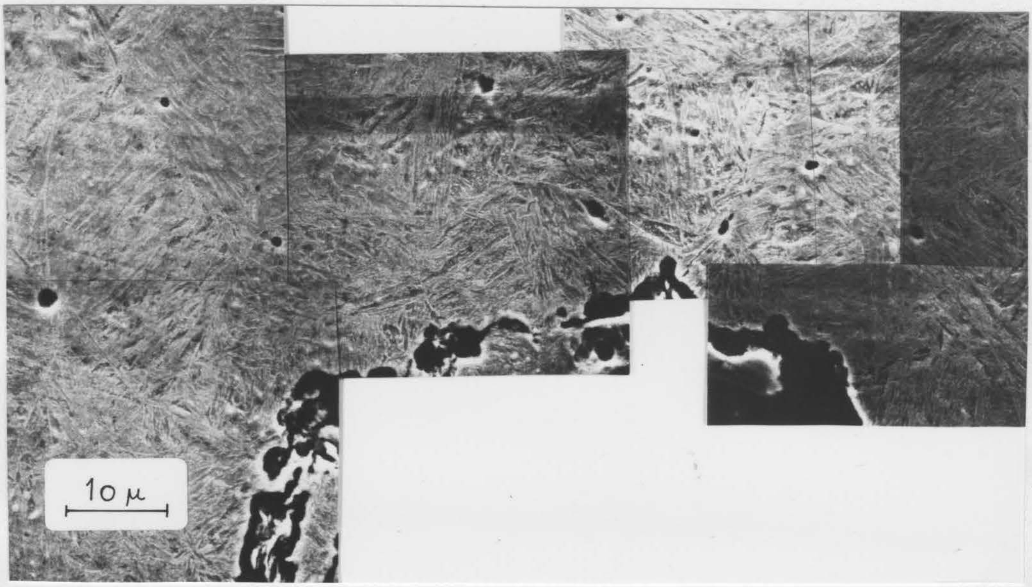

Fig. 4.18 Crack tip region in 4340, tempered at 370°C.

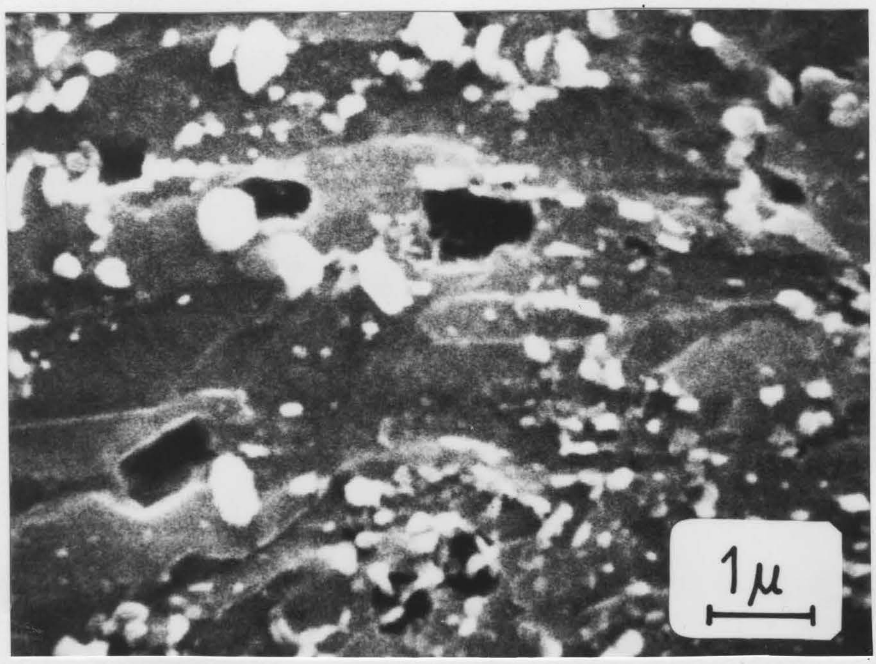

Fig. 4.19 Voids at carbides in 4340, tempered at 680°C.

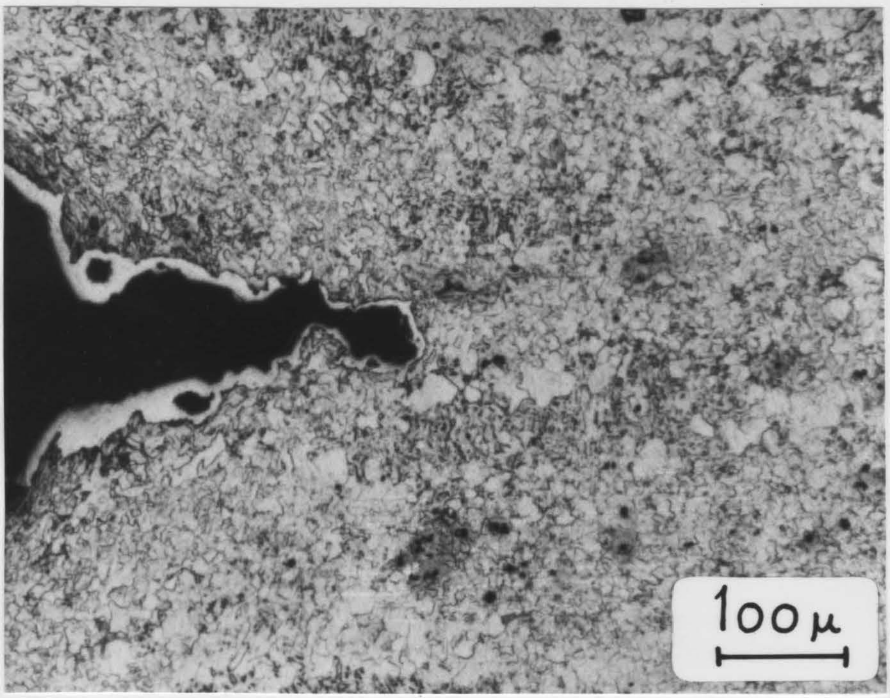

Fig. 4.20 Crack tip region of H.S.L.A., steel D, in the T-L direction.

Fig. 4.21 Crack tip region of steel D in the L-T direction.

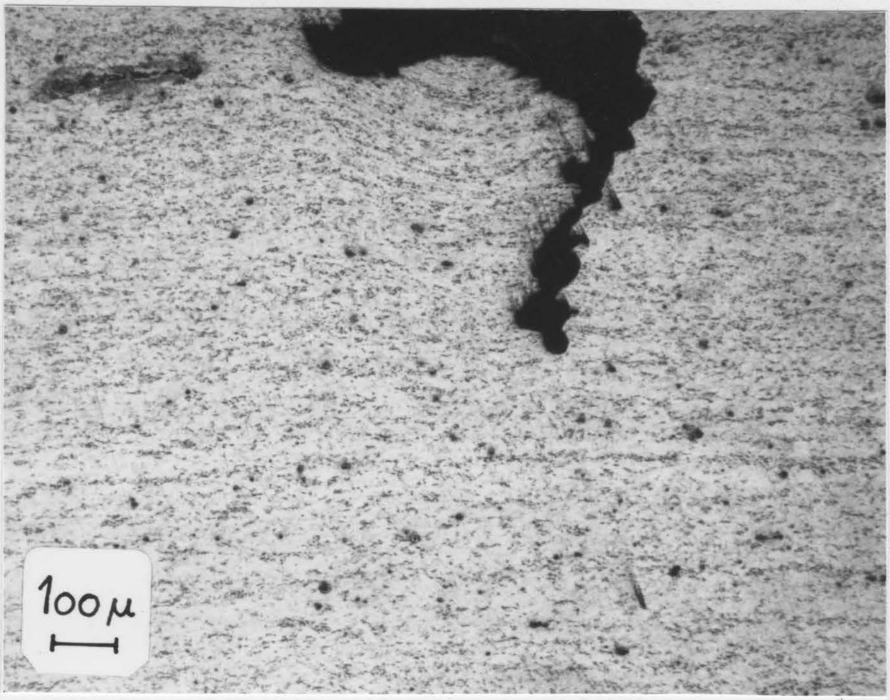

Fig. 4.22 Crack tip region of steel D in the T-S direction.

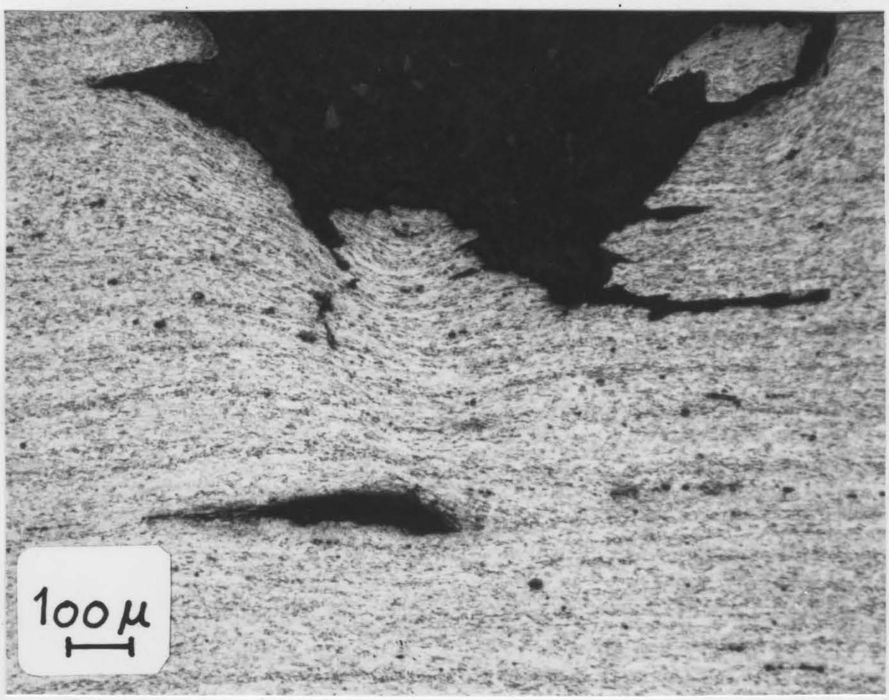

Fig. 4.23 Crack tip region of steel D in the L-S direction.

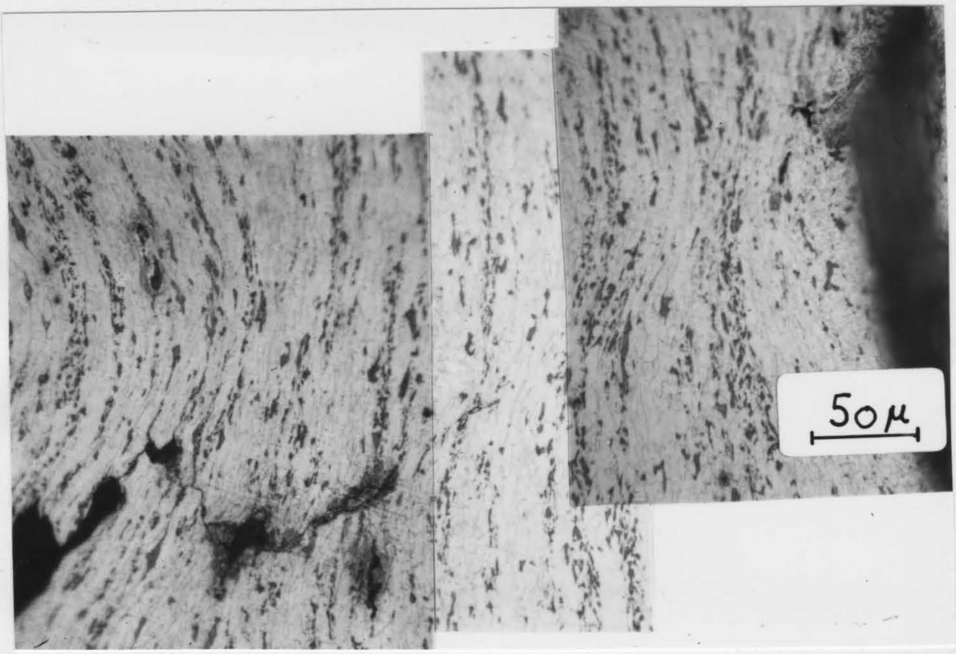

Fig. 4.24 Localized strain at the crack tip of steel D in the L-S direction.

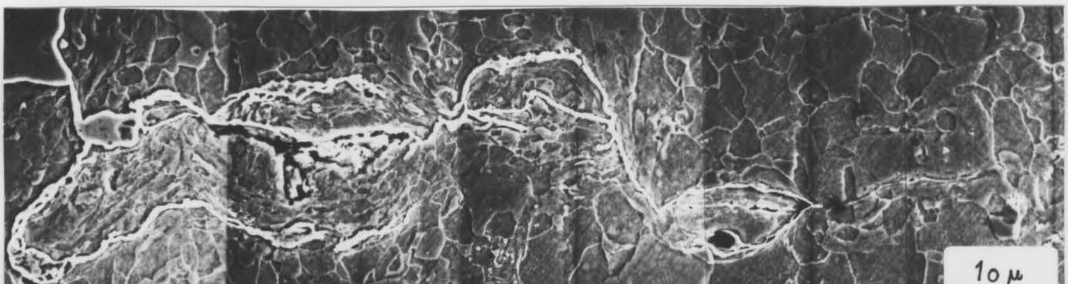

Fig. 4.25 Region at crack tip of steel D in the T-L direction, higher magnification.

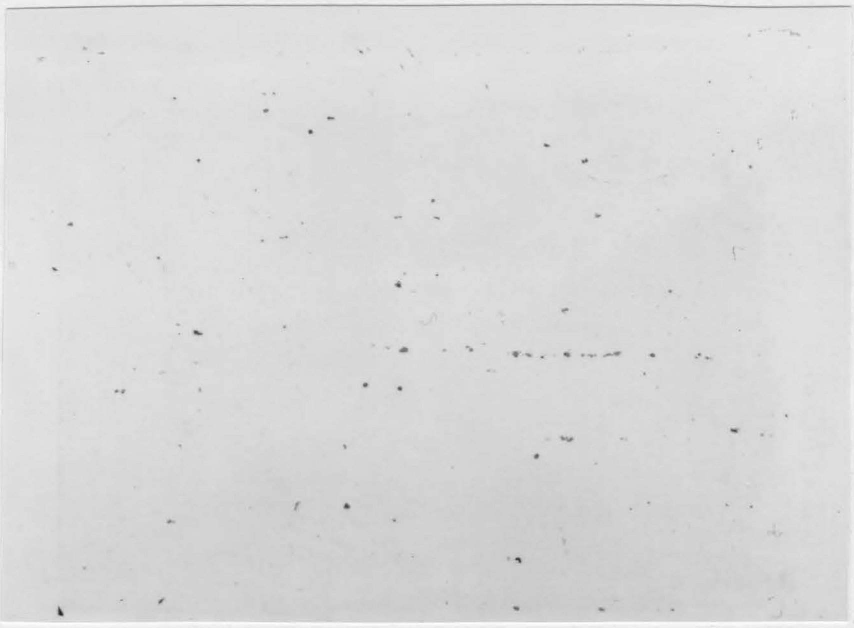

Fig. 4.26 Sulphide distribution in a plane transverse to the rolling direction in steel D.

Fig. 4.27 Sulphide morphology in a plane parallel to rolling plane in steel D.

CHAPTER 5

DISCUSSION

This chapter will include a discussion of the evaluation of the techniques used in the present work, the data obtained from small scale fracture tests and a more detailed discussion concerning the correlation between microstructural features of the materials, and the fracture resistance in terms of the magnitude of the critical opening displacements.

5.1 Testing Techniques

The technique of replicating the crack profile appears to give very consistent results and is an easy way of measuring the opening displacement at the crack tip. However, it requires that there are two parallel sides of the slot at the bottom of a notch in order to measure the displacement. Further, the curing time of the silicone rubber must not be too long and this limits the temperature range over which the technique can be applied.

The percentage of accelerator can be adjusted in the two component rubber to achieve a curing time around 5-10 min. at room temperature.

The clip gauge technique was used for the higher strength 4340 to obtain the C.O.D. values and gave consistent values provided a calibration curve between the actual clip gauge displacement and the rotational constant r was established. Using an estimated value of .3 or .39 for three and four point bending may give a considerable error in the calculated

C.O.D. data. If the silicone rubber was utilized for this calibration, very few samples are needed in order to establish the calibration curve.

Further, the clip gauge technique has considerable advantage at lower test temperatures which may lead to difficulties curing the silicone rubber at that temperature. If the resistance curve of a material is of interest, the clip gauge technique is of great utility since several samples have to be deformed to different amounts of stable crack growth to obtain the critical value at crack initiation.

However, the crack profile technique which is applicable to cases where stable crack growth occurs before instability may be applied to a broader range of test conditions, if samples with deeper notches relative to the total sample width are used. This was done for the data obtained of 4340 tempered at the lower tempering temperatures. The reasoning behind this extension is that in such samples less energy is stored in the sample before instability and crack arrest occurs after some fast crack propagation even in the high strength steels.

By using the silicone rubber at that stage, the C.O.D. at crack initiation can still be obtained since the sides of the original slot are almost parallel and the width of the extended crack can be subtracted from the measured total width.

Also samples with deeper notches are suitable for the single specimen J-integral testing as described in section 3.2. Thus the crack profile technique can be utilized to some extent in samples of materials with almost no stable crack growth before maximum load capacity. Hence it is apparent that the silicone rubber technique is useful in materials with a range of yield stresses, if the testing or at least the casting of the rubber is done at a temperature where the curing time is not too long.

In terms of the utilization of the single specimen test technique developed for measuring J_{Ic}, this is a real simplification in the method of obtaining J_{Ic} compared with getting J_{Ic} either from a single specimen technique or a compliance technique which requires several samples as reviewed in section 3.

The technique by Clarke et. al (23), which is currently being extensively used, requires at least 10% unloading and reloading to obtain a line which represents the stiffness. The change in slope of the loading lines is assumed to represent the point of crack initiation and the reduction in stiffness is assumed to arise only from the reduction in area of the uncracked remained ligament. This may be a questionable assumption in materials which undergo considerable amount of plastic deformation where elastic back stresses may occur, which influence the form of the unloading and reloading behaviour. With the test technique described in this work, this problem is avoided since the replication of the crack is done in the on-load condition.

During the testing, care was taken about uncertainties such as energy consumption in the form of plastic deformation at the load points. Further, the load point displacement is measured directly on the testing rig and any eventual elastic elongation on the rig between the real load points and the measurement point may be ignored. This can be assumed since the rig is designed for higher elastically allowable loads than the maximum load for the load cell which again is about three to ten times the maximum load obtained in the J-integral samples tested. In addition, the measurement point on the rig is very close to the actual load points compared with the dimensions of the total rig. Thus it is assumed that the measured load point displacement represents the actual load point displacements.

The real advantage of this single specimen technique is that two characteristic fracture mechanics parameters are obtained, both the C.O.D.$_i$ and J_{Ic}, and the plane strain stress intensity factor K_{Ic} may be calculated indirectly from the measured J_{Ic} value.

Similar to the C.O.D. testing technique where the silicone rubber is utilized, the testing has to be done under conditions in which stable crack growth occurs and possibility of hardening the silicone rubber within a reasonable time.

5.2 Discussion of Data Obtained

5.2.1 Effects of geometry

As shown in the Figs. 4.4-6 where the minimum C.O.D.$_i$ value is measured as a function of sample geometry, these data indicate that the value at crack initiation is independent of the geometry and the size of the total plastic zone. Thus it can be concluded that the minimum value of C.O.D.$_i$ is a material parameter only as long as plane strain conditions are obtained. These data are in agreement with the suggestion by Cottrell and Wells (8,9) that the C.O.D., under certain conditions, is a characteristic material parameter. Further the effect of thickness on C.O.D.$_i$ is in accordance with the observations by Smith and Knott (10) that below a certain thickness the magnitude of C.O.D.$_i$ increased as the stress state changed towards plane stress with decreasing thickness.

Also Griffis showed (59) that above some minimum value of the thickness, the C.O.D.$_i$ data were independent of the sample thickness.

In terms of the data obtained from the J_{Ic} testing, the derived K_{Ic} values are in very good agreement with the existing literature data for standard K_{Ic}. However much of the present data was obtained from single sample tests, and thus no statistical comparison with existing data can be made. However for the data obtained for steel D of the H.S.L.A. steels, a number of samples with different geometry were tested, and the data from these tests shows little scatter, providing the proposed requirement to notch depth is achieved. No standard K_{Ic} values from room temperature testing were available for the H.S.L.A. steel, but the obtained J_{Ic} value is in agreement with the magnitude of the corresponding C.O.D.$_i$ values in the literature.

Where the J_{Ic} is measured as a function of sample geometry in steel D of the H.S.L.A. steels, the same value is obtained in a sample with cross section as a standard Charpy V-notch impact sample, as the values obtained in the samples which fulfill the estimated size requirements for J-integral testing when the proportionality factor α is 50. If this factor is set to 25 even the tests of samples of 10 x 10 mm cross section and notch depth 5.2 mm are large enough. Since there is uncertainty about the magnitude of this constant, these data may give some indication that the lower estimated value of α is sufficient. All the J_{Ic} data for 4340 are obtained in samples of 10 x 10 mm cross section.

From the data obtained in the deeply notched bend specimens it seem to give consistent values in the toughness range tested with samples of the size of 10 x 10 mm cross section. Since the design parameter K_{Ic}

can be derived (with certain assumptions) from the obtained J_{Ic} values, it shows the advantage of the J_{Ic} as a failure criterion compared with the standard K_{Ic}-testing. See Table 4.4. Therefore a simple single specimen test method for obtaining J_{Ic} should greatly extend the use of small scale fracture mechanics tests.

In addition, data obtained in small scale fracture mechanics tests may better represent local toughness as in welds and heat affected zones than a standard K_{Ic} test value in cases of very high toughness, where the minimum size requirement for the standard K_{Ic} test sample is of order larger than the local region of interest.

5.2.2 Metallurgical factors on the data obtained

The obtained values of C.O.D.$_i$ for samples of different orientation, with respect to the rolling direction, strongly depend on the directionality of the test samples, which may be expected. Since the non metallic inclusions in general are neither isotropic in shape, nor homogenious in distribution, it is reasonable that the C.O.D.$_i$ values in the L-T direction are twice the values of the T-L direction. Both the minimum C.O.D.$_i$ value and the slope of the curves differ with test direction. These variations with direction are also in agreement with the values obtained by Smith and Knott (10) in a free machining steel.

However, the other two directions tested gave approximately the same value of C.O.D.$_i$ min. as the lowest obtained in the T-L direction. The maximum value of the Charpy V-notch impact data are increased, especially for the L-S direction, while crack propagation is very slow in the two "crack arrest" directions and the C.O.D.$_{max}$ is high. The reasoning for this effect may be that the laminated layers which are normal to the moving crack direction reach a critical localized strain at crack initiation, but the crack propagation measured in the CVN-impact test leads to more delamination as the crack progress. This is verified in the Figs. 4.22, 4.23 and 4.24, where a highly strained shear band is visible between a blunted crack and a delaminated void.

The C.O.D. data may also depend on the inclusion content and prior metallurgical history of the material. Four different H.S.L.A. steels (see section 4), were tested and both the minimum C.O.D.$_i$ value and the slope of the C.O.D.$_i$ versus 2r increase substantially in the steel in which the sulphide shape control was produced by Ce-treatment. A lower sulphur content also increases the C.O.D. data as shown for steel B. Thus desulphurization or sulphide shape control of the material will strongly affect the fracture resistance, and this is reflected in the magnitudes of the critical opening displacements.

The data obtained for the C.O.D. in 4340 tempered to give different yield stresses, give values of C.O.D. which increase with increasing ductility of the material. The data obtained are in excellent agreement with existing data in the literature (18), which both reflects the effect of ductility and the consistency of the thickness used.

The obtained J_{Ic} values also increased with the increasing ductility, which is in accordance with the observed changes in C.O.D. and K_{Ic}.

5.3 Critical Events Controlling the Fracture Toughness

5.3.1 Discussion of the effects of yield strength and stress state on the ductility

In the attempt to relate the C.O.D. value with the ductility of the material it is important to consider the physical processes which occur in fracture and how they may be affected by both the yield stress level of the material and the stress state.

In ductile failure there may be a nucleation, growth and coalescence of voids before final failure. The nucleation and growth processes have been analyzed by a number of authors (47)(60)(61) and the critical failure strain may be given such as

$$\varepsilon_f = \ln (\varepsilon_n + \varepsilon_g + 1) \tag{5-1}$$

where ε_n is the nucleation strain, ε_g is the growth strain, both engineering strains.

First one may consider the effect of the stress state on the nucleation strain. At the particle-matrix interface a certain radial stress occurs which may reach a critical value to nucleate a void at the particle. Weiss (62) has expressed this in the form

$$\sigma_{rr} = \sigma_{rr}(\text{crit}) = Y(\bar{\varepsilon}) + \sigma_m \tag{5-2}$$

where $\sigma_{rr}(\text{crit})$ is the critical radial stress at nucleation, $Y(\bar{\varepsilon})$ the equivalent flow stress, and σ_m the hydrostatic tension.

At a given critical interfacial decohesion strength it is readily seen from equation (5-2) that increasing the magnitude of the hydrostatic tension decreases the strain needed to achieve void nucleation. Thus the hydrostatic tension has a strong effect on the onset of void nucleation.

In terms of the growth of voids, an analysis by Brown (61) based on Rice and Tracey's growth model gives an expression of the growth strain such as

$$\varepsilon_g = \frac{\sqrt{\frac{\pi}{V_f 6}} - \sqrt{\frac{2}{3}}}{2 + .56 \sinh \frac{\sigma_m^\infty}{2\tau_o}} \tag{5-3}$$

where V_f is the volume fraction of second phase particles, σ_m^∞ the applied hydrostatic tension, and τ_o is the yield stress in shear. Therefore also the growth strain is dependent on both the yield strength of the material and the hydrostatic tension.

In a very simple form the critical failure strain may then be written such as

$$\varepsilon_f = A(\sigma_y, \sigma_m = 0) - B\left(\frac{\sigma_m(\sigma_y)}{\sigma_y}\right) \tag{5-4}$$

where $A(\sigma_y, \sigma_m = 0)$ is a function representing a strain which is dependent on the yield strength only, while $B(\frac{\sigma_m(\sigma_y)}{\sigma_y})$ is a function representing a strain depending on the hydrostatic tension, σ_m, and may also depend on the yield strength σ_y. As the yield stress increases $A(\sigma_y, \sigma_m = 0)$ in general decreases. If the hydrostatic tension $\sigma_m(\sigma_y)$ is fixed, or at least the ratio $(\frac{\sigma_m}{\sigma_y})$ is constant, the macroscopic critical strain ε_f decreases with increasing yield strength.

However, if the hydrostatic tension is increased, the magnitude of $B(\frac{\sigma_m(\sigma_y)}{\sigma_y})$ increases and the critical strain ε_f decreases. It may be shown schematically in a sketch as in Fig. 5.1. Thus if the ratio of the critical strain ε_{f2} at a high hydrostatic tension and the critical strain ε_{f1} for a deformation path with low hydrostatic tension is plotted as a function of the yield strength, the ratio will most likely decrease as the yield strength increases. See Fig. 5.2.

Utilizing equation (5-4) it will show a significant difference in macroscopic critical strain in a uniaxial tensile test and a plane strain tension test since the hydrostatic component is different in the two conditions. As the hydrostatic component is larger for a plane strain tension sample, the corresponding critical strain decreases compared with the uniaxial tensile strain to failure.

Clausing showed this effect of the ratio of plane strain ductility and the true strain to failure in tension as a function of the yield stress, and the data obtained are similar to Fig. 5.2. See Fig. 5.3.

At a crack tip a large hydrostatic tension is obtained close to the tip region, (See Fig. 5.4) schematically drawn for a non work hardening material in plane strain where $\sigma_m = \sigma_3 = \frac{1}{2}(\sigma_1 + \sigma_2)$. Therefore if the fracture events are determined in the region ahead of the crack it is probable that the critical strain at fracture in a notched sample is of order a critical strain where a high hydrostatic component occurs and not necessarily simply the uniaxial tensile test value at failure. This is discussed in more detail in the following section.

5.3.2 The concept of the process zone

In order to explain why the fracture resistance of a material can be expressed in terms of a critical opening displacement at initiation of crack extension for an initially sharp crack, one must consider what microstructural feature that may determine the magnitude of the critical C.O.D. The opening displacement at the crack tip may be expressed in the form

$$\text{C.O.D.}_i = \varepsilon_c \times 1 \qquad (1\text{-}9)$$

Thus the C.O.D.$_i$ is related to the product of two parameters, a critical strain and a characteristic gauge length both of which may be determined

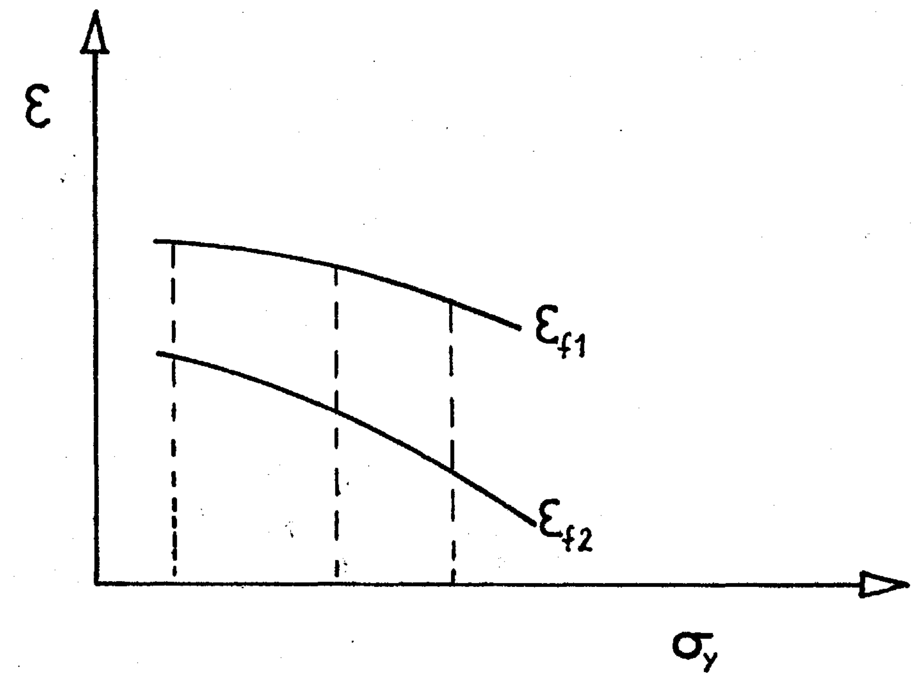

Fig. 5.1 A principal sketch of the effects of yield strength and hydrostatic tension on the critical strain to failure.

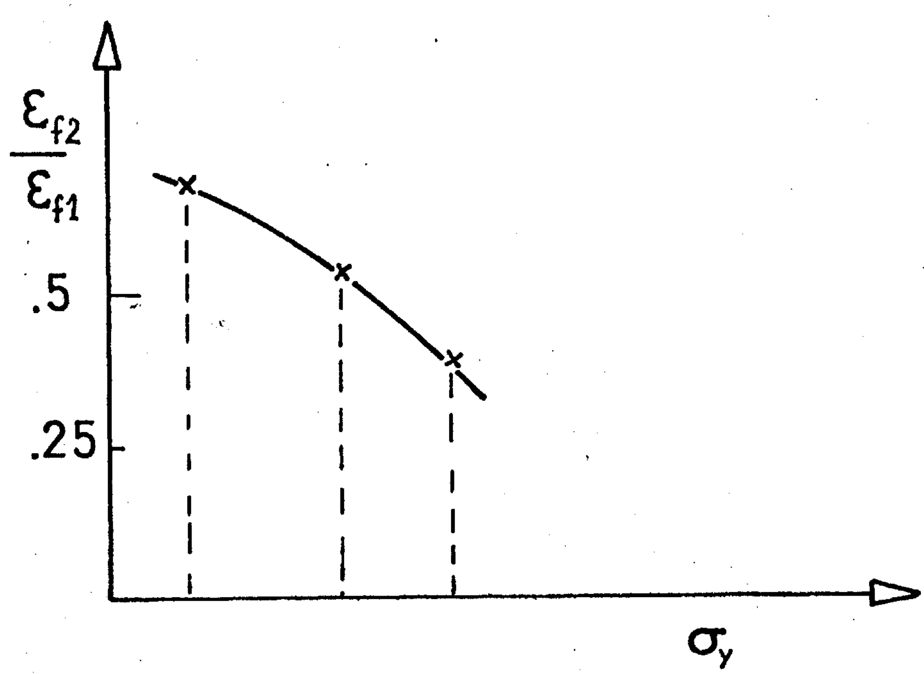

Fig. 5.2 The ratio of a critical strain at high hydrostatic tension ε_{f2}, and a critical strain at low hydrostatic tension ε_{f1} as a function of yield strength.

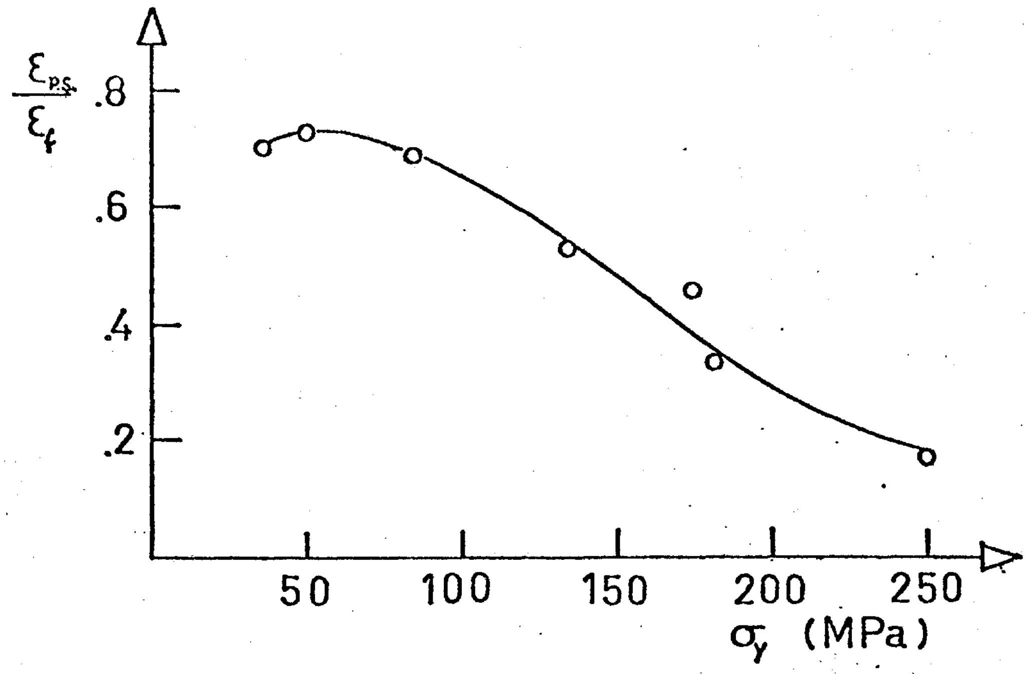

Fig. 5.3 Ratio of plane strain ductility and uniaxial true strain to failure versus yield stress.

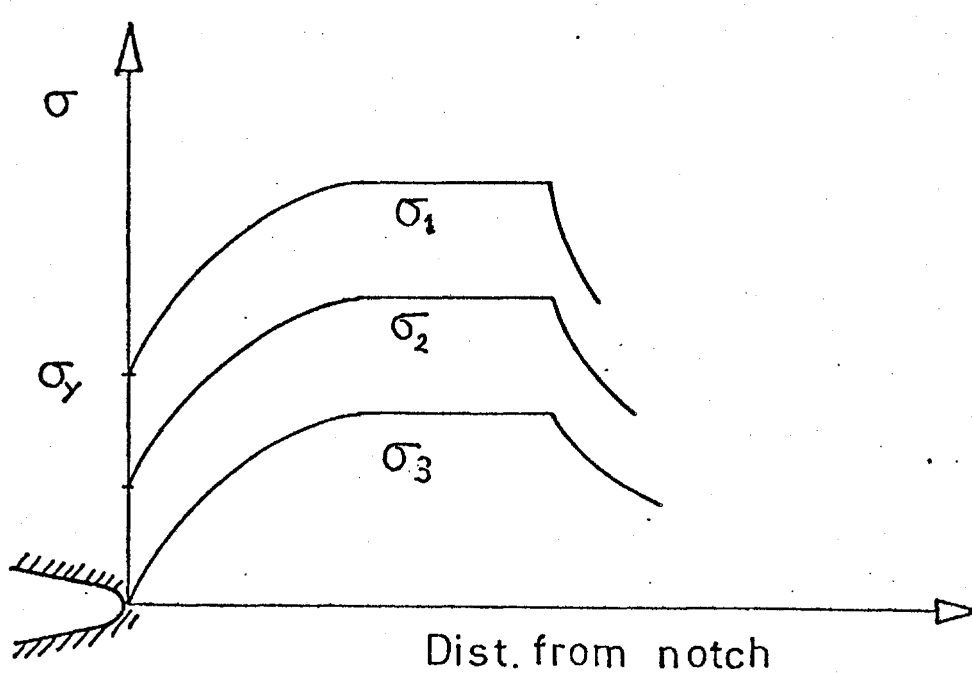

Fig. 5.4 Stress state ahead of a crack in plane strain conditions in a non work hardening material.

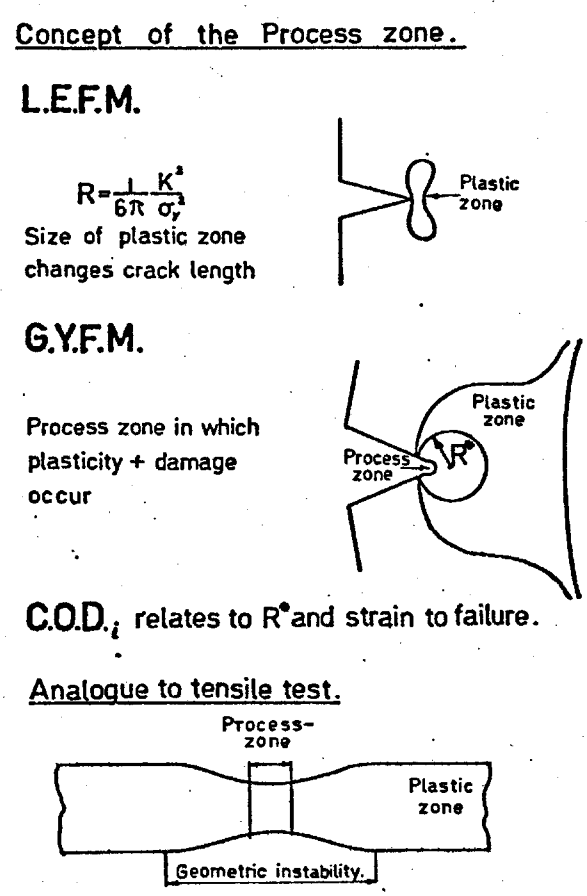

Fig. 5.5 The process zone.

by microstructural parameters.

As shown previously the C.O.D.$_i$ is independent of the total plastic zone size. Thus one can consider that the events controlling C.O.D.$_i$ must occur in a process zone near the crack tip of which the size, or the volume, does not scale with the extent of the plastic zone. This concept is illustrated schematically in Fig. 5.5 and an analogue can be drawn to the concept of the neck in a tensile sample. The material in the neck is not brought to the onset of failure but the failure events occur in a volume which is independent of the total sample length.

However, the problem of delineating the events which control C.O.D. by the magnitude of ε_f and l is complicated by the variations in the magnitude of the strain and stress state which occurs in the vicinity of the crack tip. These are illustrated in Fig. 5.4 and 5.6. One must ask then what is the critical strain that determines the fracture resistance? It is conceivable that the strain may be the nucleation strain at the non metallic inclusions, the nucleation strain at a secondary phase, the plane strain ductility, a critical shear strain or simply the uniaxial true strain to failure.

As can be seen in Fig. 5.4, the hydrostatic stress varies in the region close to the crack tip. Thus it is of importance to consider the stress state under which the critical strain is defined.

According to Smith and Knott (10) the critical strain in a free machining steel was approximately equal the uniaxial strain to failure. However, there is strong evidence for at least higher strength steels that the critical strain is of the order of the plane strain ductility (49,50).

As discussed in section 5.3.1 the plane strain ductility decreases more than the uniaxial true strain to failure with increasing yield strength. Also the stress state in a plane strain tension sample is quite similar to the crack tip region in a fracture toughness sample, with a high value of the hydrostatic tension compared with a uniaxial tensile sample. Thus a materials fracture resistance, in terms of a critical C.O.D. may be determined by the plane strain ductility rather than the uniaxial true strain to failure, compared with the values of the C.O.D.

In this context it may be of interest to examine the curves obtained for C.O.D.$_i$ versus slot width, as shown for the H.S.L.A. steels and for three yield stress levels of 4340. See Fig. 5.7. The slope of the part of the curve which is slot width dependent is simply some kind of a strain (displacement/initial slot width or gauge length). Is it then reasonable that the slope represents the critical fracture resistance strain?

The slope decreases as the ductility in terms of uniaxial true strain to failure decreases. In the more ductile materials, here the H.S.L.A. steels, the magnitude of the slope is close to the value of the uniaxial true strain to failure or another critical strain of the same order at that yield stress level. While at higher yield strengths in the 4340 steel, the magnitude of the slope is substantially lower than ε_f.

In order to determine what kind of critical strain the slope represents, the ratio of the true strain of the slope and the uniaxial true strain to failure is plotted as a function of the yield

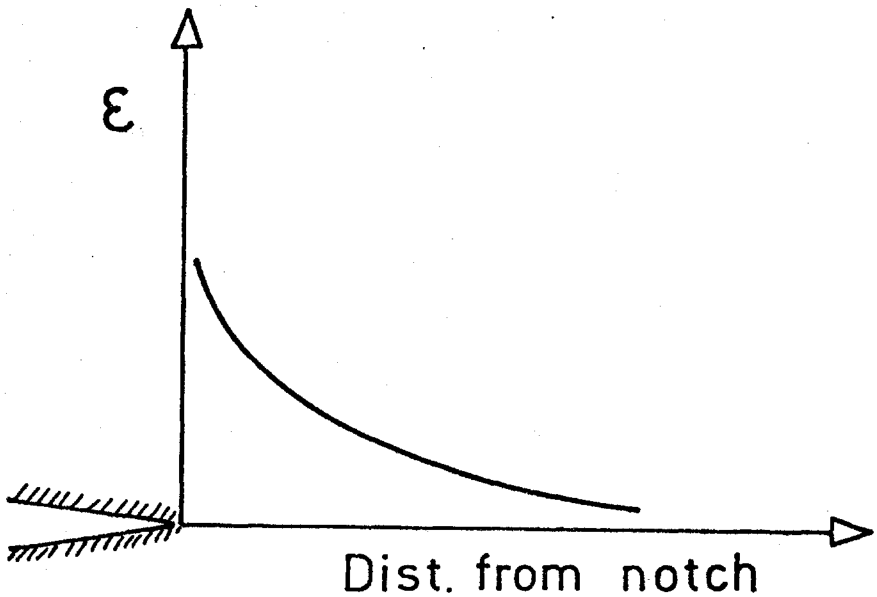

Fig. 5.6 Distribution of strain ahead of the crack tip.

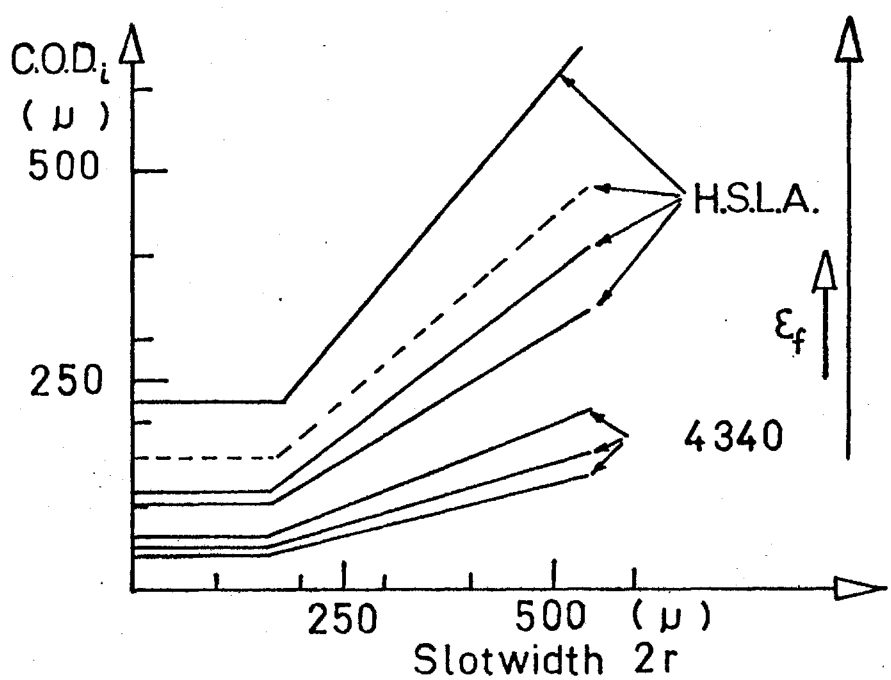

Fig. 5.7 C.O.D. vs slot width showing the change in slope with ductility.

stress. See Fig. 5.8 where

$$\varepsilon_{slope} = \ln \left(1 + \frac{C.O.D._i}{2r}\right) \qquad (5\text{-}5)$$

Of importance is that the data show the same tendency as Clausings data; that the ratio of the strains decreases with increasing yield stress. Further, the magnitude of the ratio of $\varepsilon_{slope}/\varepsilon_f$ is approximately the same as the value of the ratio $\varepsilon_{Pl.strain}/\varepsilon_f$ in Clausings curve. Thus if the strain which represents the slope of the curves C.O.D.$_i$ versus slot width is the critical strain at crack initiation, this may be the plane strain ductility or at least in magnitude close to the plane strain ductility.

As a check of the critical strain to failure the strain ahead of a crack tip was determined by a hardness measurement method and the data are shown in Fig. 5.9.

Although there are uncertainties using this method, the crack tip value of the strain was much lower than the uniaxial true strain to failure. Then the ratio of the crack tip strain and the uniaxial strain to failure was calculated and the value was very close to the curve from the data of Clausing at the yield stress level examined. Again the critical strain seem to be of the order of the plane strain ductility.

In plane strain tension there is a tendency to get localized deformation in bands in the final stage before failure. This localization may also occur at a crack tip and is more dominant at higher yield strengths when the ductility in terms of uniaxial strain to failure is lower. See Figs. 4.16-18.

Therefore, in the ductile range where the magnitude of the

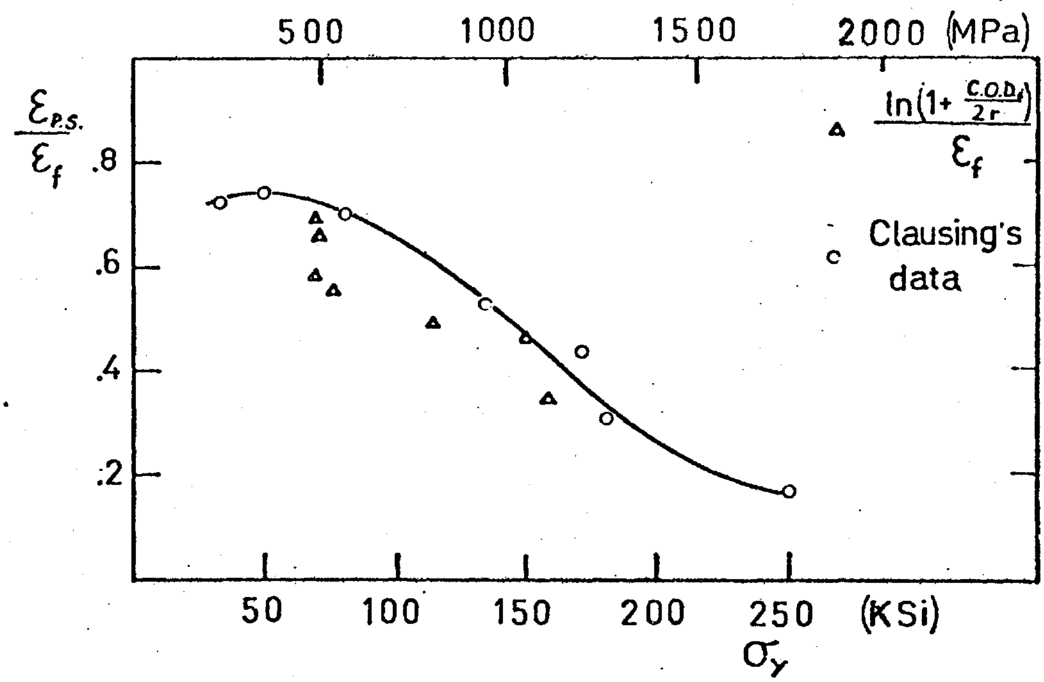

Fig. 5.8 The ratio $\varepsilon_{slope}/\varepsilon_f$ as a function of yield stress compared with the ratio $\varepsilon_{Pl.strain}$ versus yield stress.

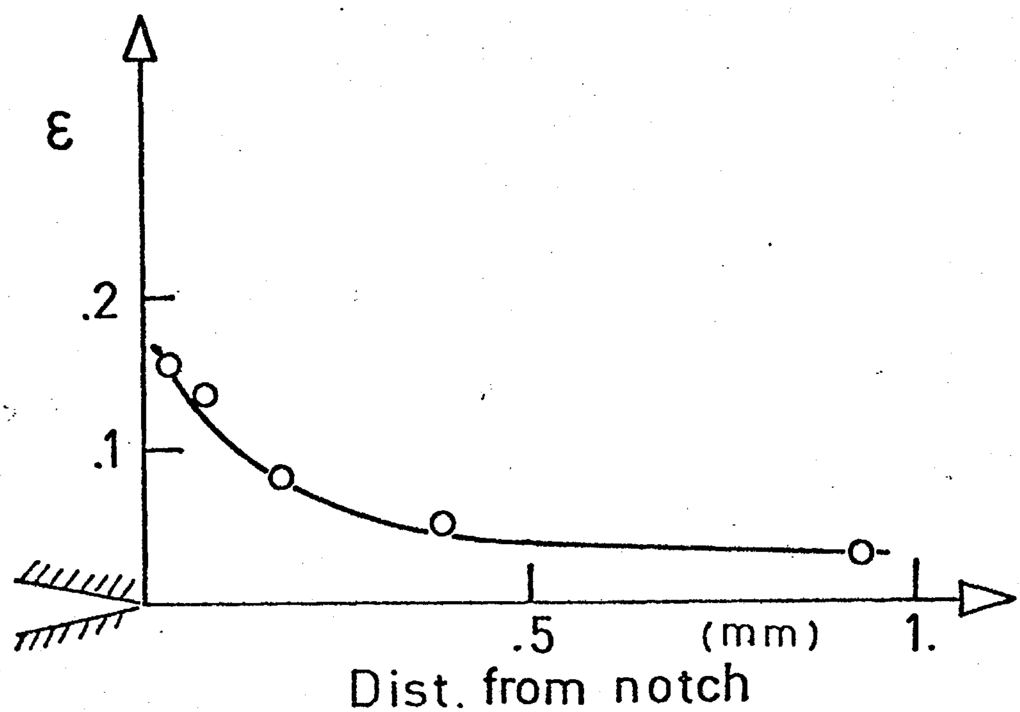

Fig. 5.9 Strain ahead of crack tip obtained by hardness measurements.

fracture resistance is assumed to be determined by a critical strain, the critical strain is most likely to be the plane strain ductility.

However, the estimated gauge length in equation (1-9) has to be determined in order to relate the fracture toughness to the microstructural features. For this study, spheroidized plain carbon steel with four different carbon contents was examined in which the micro structure is well known. All the four steels had relatively low yield stress in combination with a high ductility and high toughness in terms of the maximum shelf value of the CVN-impact test. The data are given in Table 5.1 together with the corresponding values for C.O.D.$_i$ and J_{Ic}. The microstructures of the crack tip regions are given in the Figs. 5.10-16.

For the 1015 steel, the value for the critical opening displacement may not represent the characteristic opening displacement since plane strain conditions were not obtained. In addition, the micro structure in the 1015 steel showed a banded structure with regions containing almost no carbides which may affect the data obtained.

For the 1090, 1045 and 1035 steels, both the C.O.D.$_i$ and J_{Ic} values increased with decreasing carbon content which is in accord with the change in tensile ductility.

Since the plain carbon steels tested have very high ductility combined with low yield stress and if the plane strain ductility is assumed as the limiting strain involved at crack initiation, the estimated strain in equation (1-9) may be of the order of the uniaxial true strain to failure.

Measuring the minimum value of the critical opening displacement,

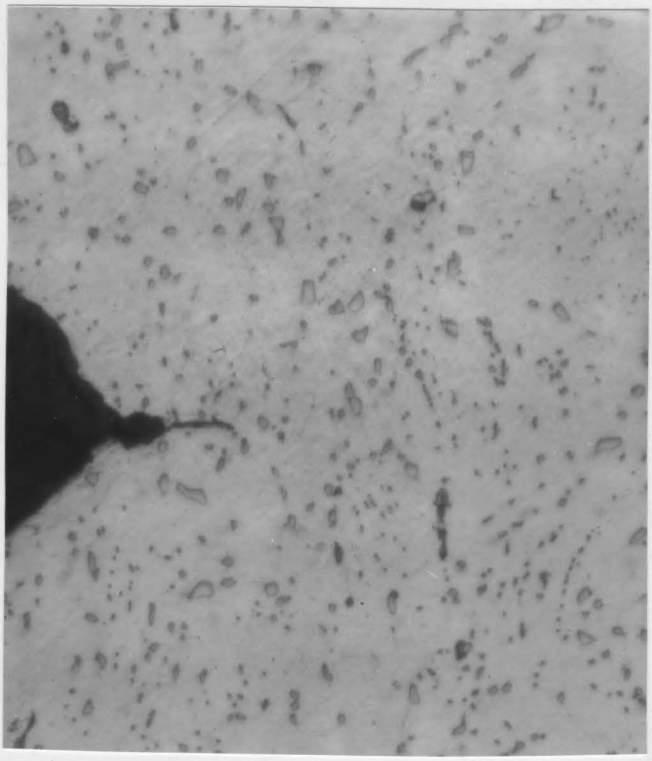

Fig. 5.10 Crack tip region of 1015 steel.

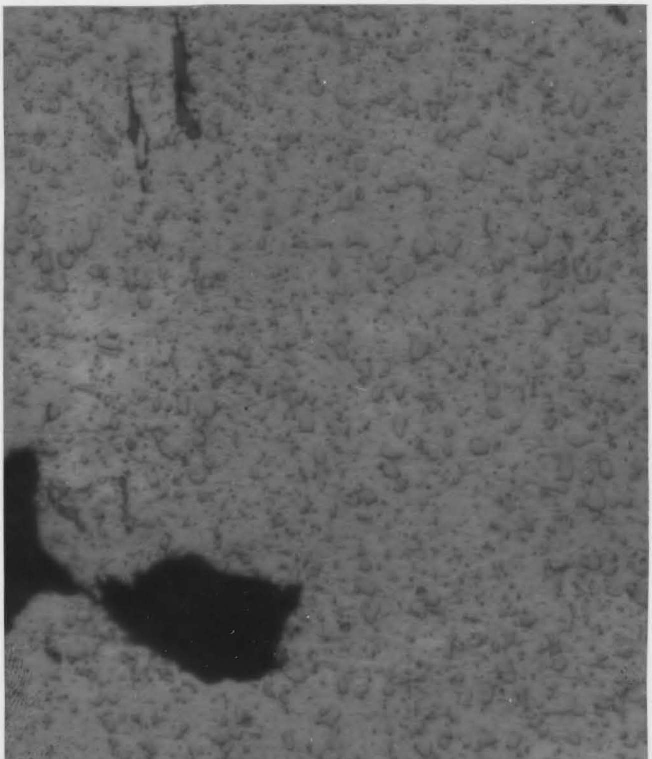

Fig. 5.11 Crack tip region of 1035 steel.

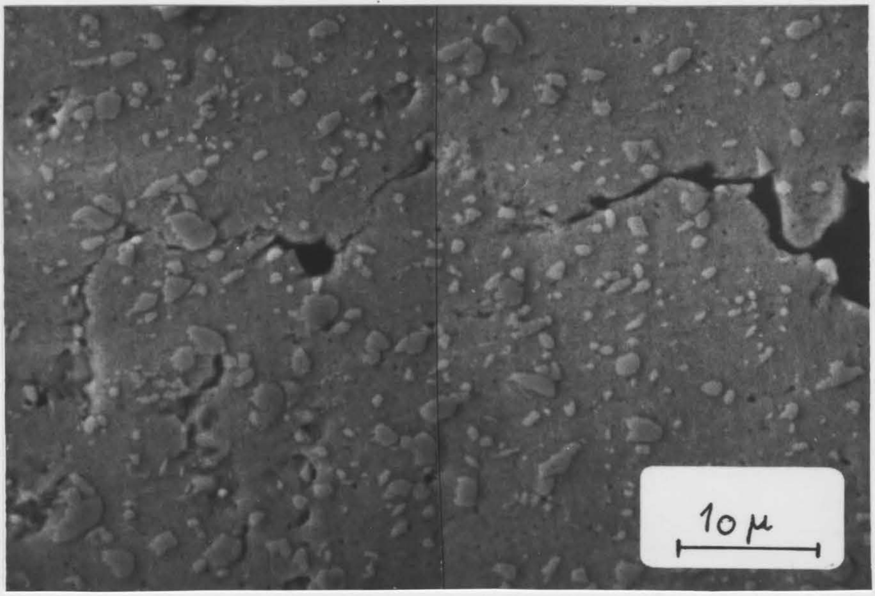

Fig. 5.12 Crack tip region of 1045 steel.

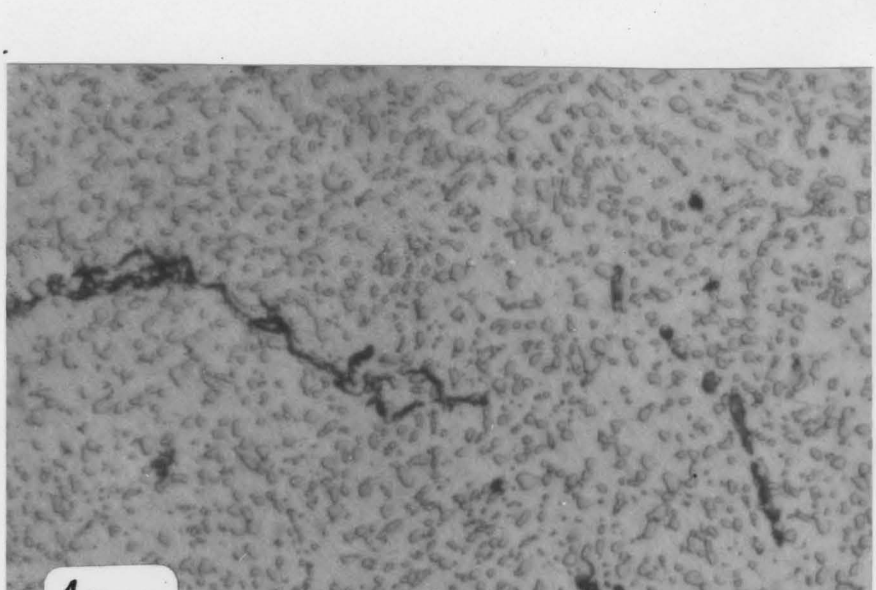

Fig. 5.13 Crack tip region of 1090 steel.

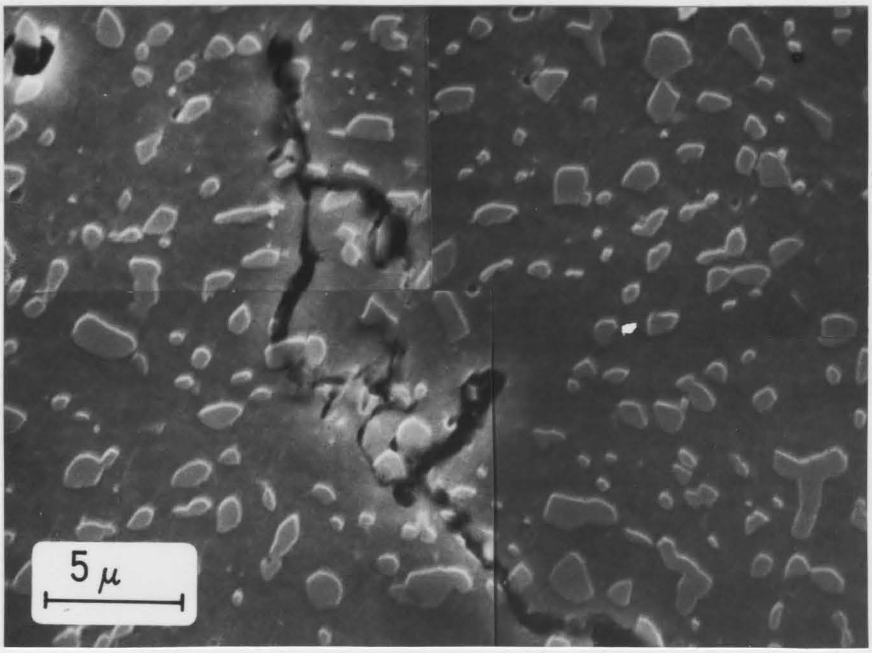

Fig. 5.14 Higher magnification of steel 1090.

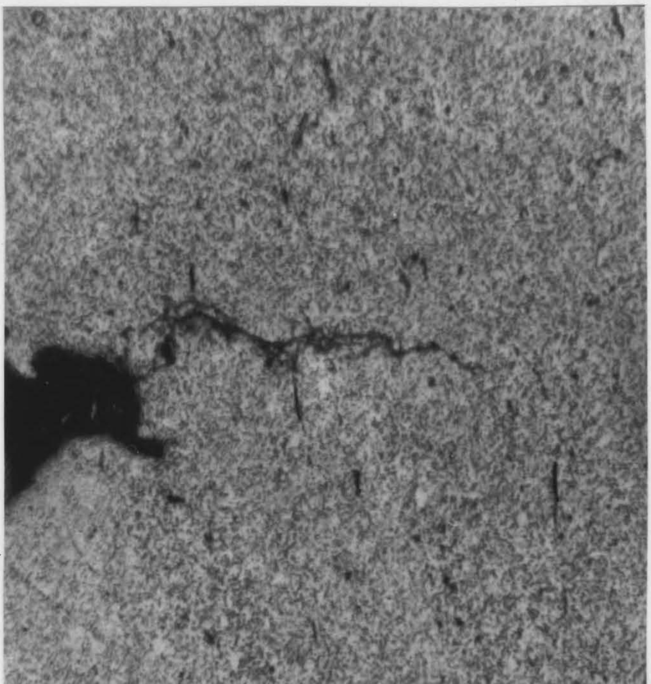

Fig. 5.15 Lower magnification of steel 1090.

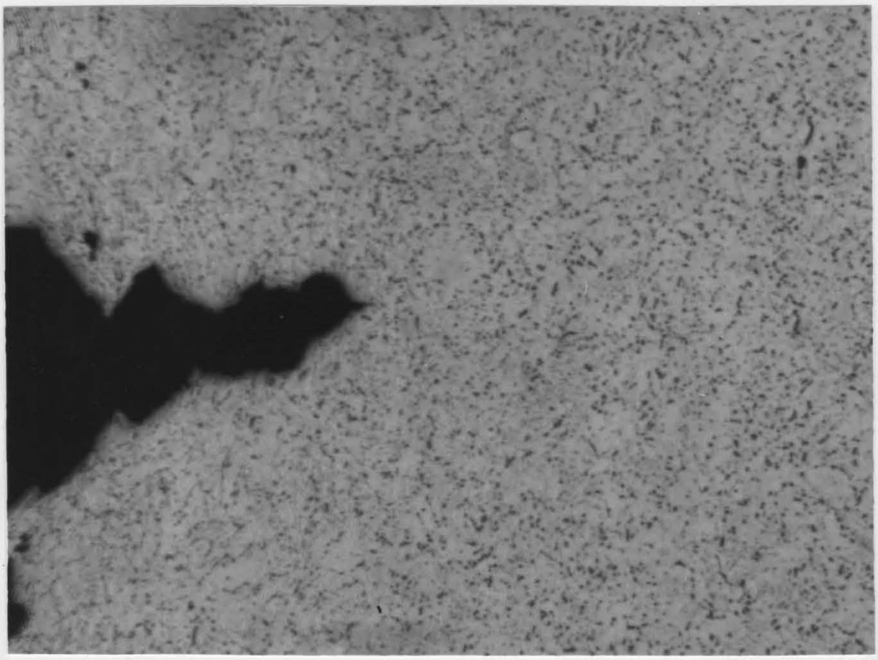

Fig. 5.16 Lower magnification of steel 1015.

the characteristic gauge length can readily be calculated, which is given for the different steels in Table 5.1. In the three carbon steels where a plane strain C.O.D.$_i$ value is measured, all have approximately the same characteristic gauge length. This value cannot be representative for the carbide spacing since there are two orders of magnitude between the calculated gauge length and the carbide spacing. However, the spacing between the non metallic inclusions is very close to the calculated values in three of the plain carbon steels ($\bar{l}_{\text{non met incl}} \sim 140\ \mu$).

Calculating the gauge length in the same manner for the 4340 and H.S.L.A. steels in the T-L direction leads to values of almost the same magnitude, 189-226 μ except steel A and the L-T direction for steel D. See Table 5-2.

The sulphide morphology of steel D of the H.S.L.A. steels is shown in Fig. 4.26 and 4.27 where the spacing between the bands of sulphides is approximately 150 μ, which may indicate that the gauge length here is more represented by the spacing between the bands of the sulphides than the interparticle spacing between the smaller sulphides.

In terms of the effect of directionality in steel D of the H.S.L.A. steels, the gauge length was determined for the two crack arrest directions and found to be of the same order as the T-L direction. However, in the L-T direction the critical gauge length was approximately twice that in the other three directions. Any well defined "length" in the micro structure scaling with the calculated gauge length, in the L-T direction, cannot be obtained from the data available.

Although the data in the L-T direction for steel D cannot be correlated readily with the microstructural data, the characteristic

TABLE 5.1

	1015	1035	1045	1090
ε_f	1.4	1.03	.91	.63
$J_{Ic}(\frac{kJ}{m^2})$	-	123	102	65
C.O.D.$_i$ (μ)	∿ 800	160	130	90
$l = \frac{C.O.D._i}{\varepsilon_f}$	-	155	143	143

TABLE 5.2

	4340			H.S.L.A.					
				Steel A	Steel C	Steel D			
				T-L	T-L	T-L	L-T	T-S	L-S
σ_y (MPa)	1130	1030	820	461	465	495	465	495	465
ε_{slope}	.175	.26	.3	.8	.5	.58	.63	-	-
ε_f	.49	.56	.61	1.2	.7	1.05	1.1	1.05	1.1
C.O.D.$_i$ (μ)	40	50	65	225	100	110	200	135	120
$l = \frac{C.O.D._i}{\varepsilon_{slope}}$ (μ)	226	195	210	280	200	189	315	-	-

length in general seem to scale with the spacing between the large non metallic inclusions or the spacing between the bands of smaller sulphides.

Thus the minimum value of the crack tip opening displacement of a crack initiation can be expressed such as

$$C.O.D._i = \varepsilon_{Pl.strain} \times \bar{l}_{non\ met\ incl}$$

where $\varepsilon_{Pl.strain}$ = plane strain ductility, = spacing between large inclusions or bands of inclusions.

Therefore the fracture toughness in terms of $C.O.D._i$ may be controlled by either desulphurization or sulphide shape control where the non metallic inclusions are dominated by the sulphides.

If the volume fraction of the non metallic inclusions is kept constant, while the size decreases, the interparticle spacing or the spacing between the bands of inclusions decreases and thus the characteristic gauge length decreases leading to a lower fracture toughness. This effect of the size of the non metallic inclusions is in agreement with the literature (63,64) increasing the spacing between the non metallic inclusions at a given volume fraction (larger inclusions) increases the fracture toughness K_{Ic}. Thus, if the spacing between the inclusions represents the characteristic gauge length, coarsening the non metallic inclusions may lead to a higher fracture resistance. However, increasing the size of the carbides at a given carbon content, larger spacing, decrease the fracture toughness (65).

In terms of the ductility, increasing volume fraction of carbides in the plain carbon steels decrease the uniaxial tensile ductility, and the corresponding $C.O.D._i$ values. See Table 5.2 Also the fracture toughness measured as K_{Ic} is found in the literature (65) to decrease as the volume fraction of the carbides increase. Therefore the ductility involved in the expression for the critical opening displacement will decrease with increasing volume fraction of carbides, assuming the characteristic gauge length is constant as shown in Table 5.2.

As a conclusion, the spacing of the large non metallic inclusions, or the spacing between the clusters of the sulphides, seem to determine the characteristic gauge length or the size of the process zone, while the carbide content will affect the ductility term involved in the expression for the opening displacement.

CHAPTER 6

SUMMARY

In this section the main conclusions are summarized. In addition, suggestions for future work are included.

6.1 Conclusion

This study has led to the following conclusions:

- The minimum value of the crack tip opening displacement at initiation of crack extension in plane strain conditions is a characteristic of the material only, independent of the sample geometry and the extent of the plastic zone.
- Development of a very simple single specimen method for J-integral testing from which both J_{Ic} and $C.O.D._i$ are obtained directly, and the plane strain stress intensity factor K_{Ic} calculated indirectly from the measured J_{Ic}-value.
- The fracture resistance expressed in terms of $C.O.D._i$ can be directly related to the materials plane strain ductility and the interparticle spacing, or distance between bands, of the non metallic inclusions such as

$$C.O.D._i = \varepsilon_{Pl.strain} \times \bar{l}$$

6.2 Suggestions for Future Work

In the attempt to extend the use of small scale testing in the area of fracture mechanics, it is of importance to examine the following suggestions:

- Utilization of small scale fracture mechanics testing at higher yield strength levels. i.e. higher strength materials at room temperature and testing over a range of temperatures down to cleavage behaviour.
- Any possibility for development of a simple single specimen J-integral test method for determination of a resistance curve. J versus stable crack growth Δa.
- More detailed studies of the magnitude of the fracture resistance in correlation with the ductility, stress level, and stress state, and the limiting processes occuring at the crack tip, including the transition from any eventual critical strain to a critical stress behaviour prior to fracture with lowering the test temperature.
- Utilization of small scale samples for obtaining C.O.D.$_i$ and J_{Ic} for the local toughness as in welds, heat affected zones and irradiated materials.

REFERENCES

1. Westergaard, H.M., J. Appl. Mechanics, A, 49 (June, 1939).
2. Orrowan, E., Trans. Inst. Engrs. Shipbuilders Scotland, 89, 165 (1945).
3. Irwin, G.R., 9th Inter. Congr. Appl. Mech., VIII, Paper 101(II), University of Brussels, 245 (1957).
4. Burdekin, F.M. and Stone, D.E.W., Journal of Strain Analysis, Vol. 1, No. 2, p. 145, 1966.
5. Rice, J.R., Brown University, ARPA SD-86 Report, E 39.
6. Knott, J.F., Fundamentals of Fracture Mechanics, Butterworths, p. 126, 1973.
7. Rolfe, S.T. and Barson, Fracture and Fatigue Control in Structures, Prentice Hall, Inc., 1977.
8. Cottrell, A.H., Proceedings Roy. Soc. A., Vol. 285, Plate 1, pp. 10-21.
9. Wells, A.A., Crack Propagation Symposium Proceedings, Cranfield College of Aeronautics 1, 210 (1961).
10. Smith, R.F. and Knott, J.F., Practical Appl. of Fracture Mechanics to Pressure Vessel Technology, C9/71, pp. 65-75.
11. Rice, J.R. and Johnson, M.A., Inelastic Behaviour of Solids, M. Kauminen, et al., McGraw Hill, pp. 641-672, 1970.
12. Levy, N., et al., Int. J. Fracture Mech., 7, pp. 143-156, 1971.
13. Rice, J.R., J. Appl. Mech. (Trans. ASME), 35, 379 (June, 1968).

14. Begley, J.A. and Landes, J.D., ASTM STP 514, pp. 1-20, 1972.

15. Rice, J.R., Fracture, H. Liebowitz, Ed., Vol. 2, Academic Press, New York, pp. 191-311, 1968.

16. Theocaris, P.S., J. Strain Analysis, Vol. 9, p. 197, 1974.

17. Clark, G. and Knott, J.F., J. Mech. Phys. Solids, Vol. 11, p. 179, 1975.

18. Robinson, J.N. and Tetelman, A.S., Technical Report No. 11, Univ. of California, Los Angeles, UCLA-ENG-76360, (August, 1973).

19. "Methods for C.O.D. Testing", British Standards Institution, Draft for Development 19, (London, 1972).

20. Rice, J.R., Paris, P.C. and Merkle, J.G., Progress in Flaw Growth and Fracture Toughness Testing, ASTM, STP 536, pp. 231-245, 1973.

21. Landes, J.D. and Begley, J.A., Mechanics of Crack Growth, ASTM, STP 536, pp. 170-186, 1973.

22. Clarke, G.A., et al., Mechanics of Crack Growth, ASTM, STP 560, pp. 27-42.

23. Knott, J.F. and Cottrell, A.H., JISI, Vol. 201, p. 249, 1963.

24. Wells, A.A., Br. Weld J., p. 563 (November, 1963).

25. Brock, D., 3rd Int. Congress on Fracture, Munich, Paper 3, 422 (1973).

26. Ritchie, R., Garrett and Knott, Int. J. Fracture Mechanics, Vol. 11, p. 79, 1971.

27. Johnson, H.H., Materials Research and Standards <u>5</u>, p. 442, 1965.

28. Hopkins, P. and Jolley, G., 4th Int. Conf. Fracture, Waterloo, Canada, Vol. 3, p. 325, 1977.

29. Clark, G. and Knott, J.F., Metal Science, p. 531 (November, 1977).

30. Knott, J.F., Sec. Int. Conference on Fracture, Brighton, 1969.

31. Chipperfield, et al., Third Int. Conference on Fracture, Munich (April, 1973).

32. Landes, J.D. and Begley, J.A., ASTM, STP 514, pp. 24-39.

33. Rice, J.R. and Rosengren, G.F., J. Mech. Phys. Solids, Vol. 16, pp. 1-12, 1968.

34. Hutchinson, J.W., J. Mech. Phys. Solids, Vol. 16, pp. 13-31, 1968.

35. Bucci, R.J., et al., ASTM, STP 514, pp. 40-69, 1972.

36. Clarke, G.A., Recommended Procedure for J_{Ic}-determination, Westinghouse Research Lab, Pittsburgh, Pennsylvania (March, 1977).

37. Landes, J.D. and Begley, J.A., Westinghouse Research Lab, Report 76-1E7 JINTFP3, (May 1976).

38. Harrison, J.D., at E 24 Committee Meetings, ASTM Committee Week, Florida (March, 1976).

39. Paris, P.C., ASTM, STP 514, p. 21, 1972.

40. Barson, J.M. and Rolfe, S.T., ASTM, STP 466, pp. 281-302, 1970.

41. Rolfe, S.T. and Novak, S.R., ASTM, STP 463, pp. 124-159, 1970.

42. Maxey, W.A., et al., The Fifth National Symposium on Fracture Mechanics, University of Illinois, 1971.

43. Robinson, J.N., Int. J. of Fracture, Vol. 12, p. 723, 1976.

44. Dugdale, D.S., J. Mech. Phys. Solids, Vol. 18 (No. 2), p. 100, 1960.

45. Thomasson, P.F., Prospects of Fracture Mechanics, Ed. G.C. Sih et al., Nordhoff International Publishing, Delft, Netherlands, 1974.

46. Brown, L.M. and Embury, J.D., Microstructure and Design of Alloys, Inst. Met., Paper 33, 1973.

47. McClintock, F.A., J. Appl. Mechanics, p. 363, (June, 1968).

48. Tanaka, K. and Spretnak, J.W., Met. Trans., AIME, Vol. 4, p. 443, 1973.

49. Hahn, G.T., Barnes, C. and Rosenfield, A.R., ARL TR-0194, Battelle, Columbus, Ohio, 1974.

50. McClintock, F.A., et al., Int. J. Fracture Mechanics, Vol. 2, No. 4, p. 614, 1966.

51. Clausing, D.P., Int. J. Fracture Mechanics, Vol. 6, p. 71, 1970.

52. Green, G. and Knott, J.F., J. Eng. Materials Technology, p. 37 (January, 1976).

53. Civallero, M.A., et al., Micro alloying 75, Session 2B, p. 8.

54. Hertzberg, R.W. and Goodenow, R.A., Micro alloying 75, No. 3, p. 8.

55. Aerospace Structural Metals Handbook, Vol. 1, Syracuse Press, 1963.

56. Metals Handbook, Vol. 8, American Society for Metals, 1973.

57. Green, A.P. and Hundy, B.B., J. Mech. Phys. Solids, Vol. 4, 128, (1956).

58. Chipperfield, C.G. and Knott, J.F., Metals Technology, Vol. 2, p. 45, 1975.

59. Griffis, C.A., Journal of Pressure Vessel Technology, Trans ASME, p. 278 (November, 1975).

60. Rice, J.R. and Tracey, D.M., J. Mech. Phys. Solids, Vol. 17, p. 201, 1969.

61. Brown, L.M., Discussion Paper, Cavendish Laboratory Cambridge, "Initiation and growth of voids by plastic flow near second phase particles".

62. Weiss, V., et al., ASTM, STP 605, Properties Related to Fracture Toughness.

63. Birkle, A.J., et al., Trans ASM, Vol. 59, p. 982 (1966).

64. Cox, T.B. and Low, J.R., Met. Trans, Vol. 5, p. 1457, 1974.

65. Rawal, S.P. and Gurland, J., Tech. Rep. No. 41, U.S. Energy Research and Development Commission (February, 1976).

Appendix I

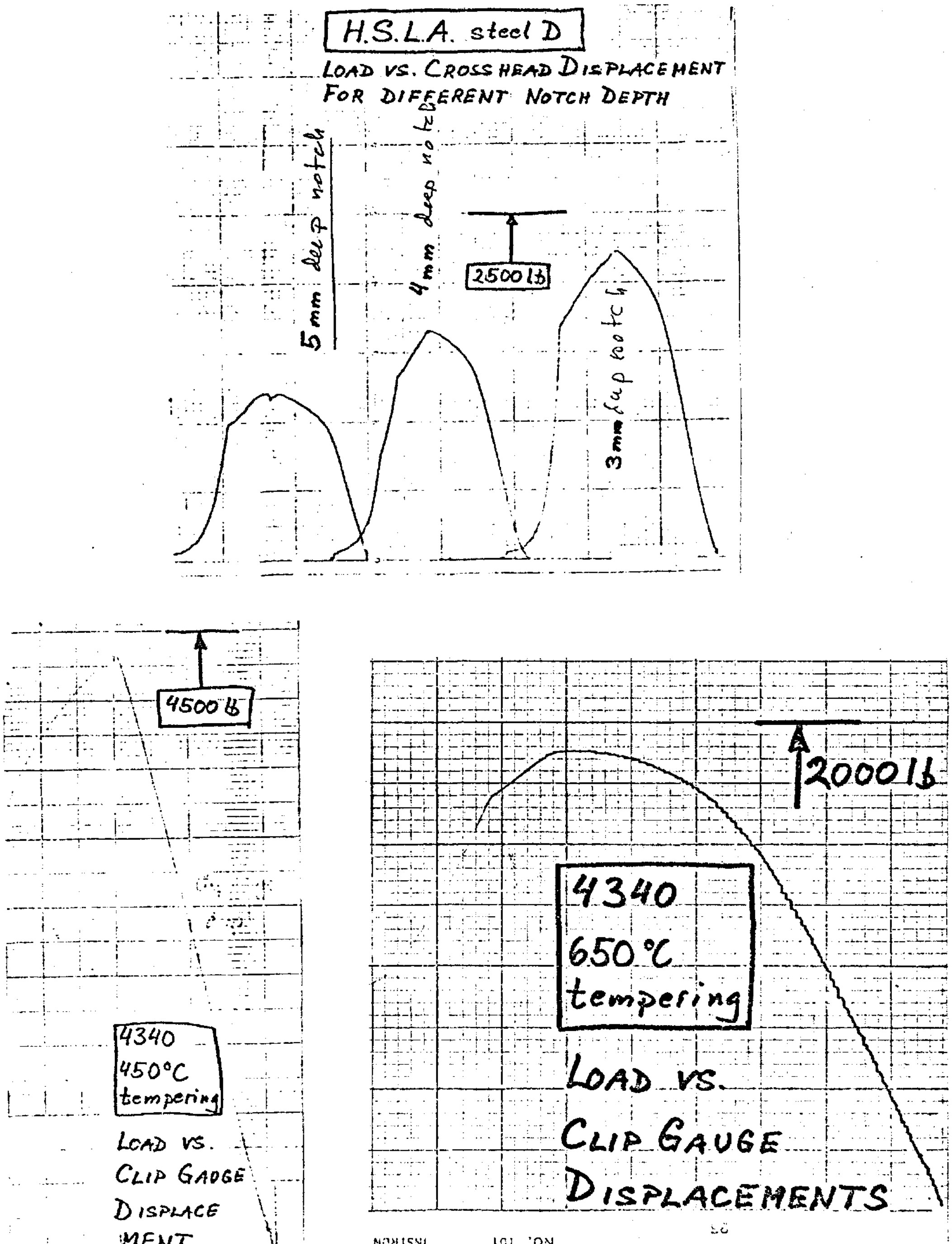

Fig. A1 Chart curves from testing on the Instron Machine.